

Weak annihilation and new physics in charmless $B \rightarrow MM$ decays

Christoph Bobeth

*Technische Universität München, Institute for Advanced Study,
Lichtenbergstraße 2a, D-85748 Garching, Germany*

Martin Gorbahn

Department of Mathematical Sciences, University of Liverpool, L69 3BX Liverpool, United Kingdom

Stefan Vickers

*Technische Universität München, Excellence Cluster Universe,
Boltzmannstraße 2, D-85748 Garching, Germany*

(Dated: July 12, 2021)

We use currently available data of nonleptonic charmless 2-body $B \rightarrow MM$ decays ($MM = PP, PV, VV$) that are mediated by $b \rightarrow (d, s)$ QCD- and QED-penguin operators to study weak annihilation and new-physics effects in the framework of QCD factorization. In particular we introduce one weak annihilation parameter for decays related by ($u \leftrightarrow d$) quark interchange and test this universality assumption. Within the standard model, the data supports this assumption with the only exceptions in the $B \rightarrow K\pi$ system, which exhibits the well-known “ $\Delta\mathcal{A}_{CP}$ puzzle”, and some tensions in $B \rightarrow K^*\phi$. Beyond the standard model, we simultaneously determine weak-annihilation and new-physics parameters from data, employing model-independent scenarios that address the “ $\Delta\mathcal{A}_{CP}$ puzzle”, such as QED-penguins and $b \rightarrow s \bar{u}u$ current-current operators. We discuss also possibilities that allow further tests of our assumption once improved measurements from LHCb and Belle II become available.

I. INTRODUCTION

Nonleptonic charmless 2-body decays $B \rightarrow MM$, with final state mesons $MM = (PP, PV, VV)$, form a large class of decays that allow to test in principle the underlying tree and penguin topologies at the parton level, as predicted by the standard model (SM). Further, the subclass of QCD- and QED-penguin dominated decays are sensitive to new physics (NP) beyond the SM, as any other $b \rightarrow (d, s)$ flavor-changing neutral-current (FCNC) process, which makes them valuable probes of the according short-distance couplings.

The major obstacle to constraining the short-distance couplings with data is the evaluation of hadronic matrix elements in 2-body B -meson decays beyond naive factorization. In view of this, strategies have been developed to construct tests of the weak phases of the Cabibbo-Kobayashi-Maskawa (CKM) quark-mixing matrix of the SM where the hadronic matrix elements are determined from data, usually involving additional assumptions of $SU(2)$ and/or $SU(3)$ flavor symmetries. Although this allows to test the consistency of weak phases extracted in tree- and loop-induced processes in the framework of the SM, no other detailed information can be obtained on particular short-distance couplings of the involved QCD- and QED-penguin operators.

In this respect, systematic expansions in the heavy bottom quark mass, m_b , yield at leading order in $1/m_b$ a simplified representation of hadronic 2-body matrix elements in terms of rather well known heavy-to-light form factors and distribution amplitudes (DA) of the involved mesons. These approaches, QCD factorization (QCDF) [1–6], soft-collinear effective theory (SCET) [7–10] or per-

turbative QCD (pQCD) [11–14], provide predictions at leading order in $1/m_b$ that allow in principle to test short-distance couplings with data.

Weak annihilation (WA) contributions are formally of subleading order in $1/m_b$, but an additional chiral enhancement makes them phenomenologically relevant for a consistent description of experimental data in the SM and scenarios beyond. In QCDF and SCET, they are plagued by nonfactorizable divergences, which are present in endpoint regions of convolutions of meson DAs. In QCDF, these divergences are frequently parameterized by a phenomenological complex parameter [3] and hence are model-dependent. In particular, the associated strong phase governs the size of CP asymmetries. In practice this leads to large theoretical uncertainties in the prediction of observables [5, 15]. Although branching fractions and CP asymmetries are sensitive to new physics effects, the model-dependence and the arising uncertainties due to the involved strong phases raise the question how reliable information can be extracted on the short-distance couplings.

Here we determine the model-dependence in the framework of QCDF from data, admitting one phenomenological parameter for decays $B \rightarrow M_a M_b$ that are related by ($u \leftrightarrow d$) quark exchange. The theoretical uncertainties of all other input parameters (see App. A) are treated as uncorrelated and have been included into the likelihood as explained in App. B. We use data of mostly QCD-penguin dominated $B_{u,d}$ decays into $PP = K\pi, K\eta^{(\prime)}, KK$ or $PV = K\rho, K\phi, K\omega, K^*\pi, K^*\eta^{(\prime)}$ or $VV = K^*\rho, K^*\phi, K^*\omega, K^*K^*$, and further B_s decays into $PP = \pi\pi, KK, K\pi$ or $VV = \phi\phi, K^*\phi, K^*K^*$ final states. We determine also the relative magnitude of sub-

leading WA amplitudes compared to the relevant leading order amplitudes. The results within the context of the SM are presented in Sec. IV. Given the current data, a simultaneous fit of the WA parameters and the short-distance couplings is pursued in Sec. V for generic NP extensions of the SM in order to explore the constraining power of these decays. Before presenting our results of the fit, we review the observables and collect the experimental input of charmless 2-body decays in Sec. II. The relevant details of QCDF and the definition of the phenomenological parameter are summarized in Sec. III. Various appendices collect additional material on numerical input in App. A and the statistical treatment of experimental and theoretical uncertainties as well as determination of pull values and p values in App. B.

II. $B \rightarrow MM$ OBSERVABLES AND DATA

The 2-body decays of B mesons into final states $f = PP, PV, V_h V_h$ with light charmless pseudo-scalar (P) and/or vector (V_h) mesons with polarization mode $h = L, \perp, \parallel$ provide various observables in time-integrated, time-dependent, and also angular analyses. These are reviewed in the first part of this section, whereas in the second part the according available experimental data is listed that has been used in the fits.

A. Observables

The most important observables for decays of charged B_u mesons into a final state f are the CP-averaged branching fraction and the (direct) CP-asymmetry

$$\begin{aligned}\bar{\mathcal{B}}[B_u \rightarrow f] &= \frac{\tau_{B_u}}{2} (\Gamma[\bar{B}_u \rightarrow \bar{f}] + \Gamma[B_u \rightarrow f]) , \\ \mathcal{A}_{\text{CP}}[B_u \rightarrow f] &= \frac{\Gamma[\bar{B}_u \rightarrow \bar{f}] - \Gamma[B_u \rightarrow f]}{\Gamma[\bar{B}_u \rightarrow \bar{f}] + \Gamma[B_u \rightarrow f]} .\end{aligned}\quad (\text{II.1})$$

Concerning decays of neutral B_D mesons ($D = d, s$) into a common final state f for both flavor eigenstates \bar{B}_D and B_D , the simplest measurements are untagged rates. The decay is governed by the decay rates $R_f^{\text{H,L}} \equiv \Gamma[B_D^{\text{H,L}} \rightarrow f]$ of the heavy and light mass eigenstates $B_D^{\text{H,L}}$, which yield the averaged and time-integrated branching fraction

$$\begin{aligned}\bar{\mathcal{B}}[B_D \rightarrow f] &= \frac{1}{2} \int dt \left(R_f^{\text{L}} e^{-\Gamma_D^{\text{L}} t} + R_f^{\text{H}} e^{-\Gamma_D^{\text{H}} t} \right) \\ &= \frac{1}{2} \left(\frac{R_f^{\text{L}}}{\Gamma_D^{\text{L}}} + \frac{R_f^{\text{H}}}{\Gamma_D^{\text{H}}} \right) ,\end{aligned}\quad (\text{II.2})$$

with their respective lifetimes $\Gamma_D^{\text{H,L}}$ in the two exponentials. The mass eigenstates are related to the flavor eigenstates $|B_D^{\text{L}}\rangle = p|B_D\rangle + q|\bar{B}_D\rangle$ and $|B_D^{\text{H}}\rangle = p|B_D\rangle - q|\bar{B}_D\rangle$

defining q and p . On the other hand, theoretical predictions are made for the flavor eigenstates, implying $t = 0$,

$$\mathcal{B}[B_D \rightarrow f] = \frac{\frac{1}{2} (\Gamma[\bar{B}_D \rightarrow f] + \Gamma[B_D \rightarrow f])}{\frac{1}{2} (\Gamma_D^{\text{L}} + \Gamma_D^{\text{H}})} \quad (\text{II.3})$$

with the average lifetime $\tau_{B_D} = (\Gamma_D)^{-1} \equiv 2/(\Gamma_D^{\text{L}} + \Gamma_D^{\text{H}})$. Both branching fractions are related via [16]

$$\bar{\mathcal{B}}[B_D \rightarrow f] = \mathcal{B}[B_D \rightarrow f] \frac{1 + y_D H_f}{1 - y_D^2} \quad (\text{II.4})$$

where y_D is proportional to the width difference $\Delta\Gamma_D$

$$y_D = \frac{\Delta\Gamma_D}{2\Gamma_D} \equiv \frac{\Gamma_D^{\text{L}} - \Gamma_D^{\text{H}}}{\Gamma_D^{\text{L}} + \Gamma_D^{\text{H}}} . \quad (\text{II.5})$$

The CP asymmetry due to nonvanishing width difference,

$$H_f = \frac{R_f^{\text{H}} - R_f^{\text{L}}}{R_f^{\text{H}} + R_f^{\text{L}}} , \quad (\text{II.6})$$

is an independent observable and provides complementary tests of physics beyond the SM. It can be obtained from measurements of effective lifetimes in untagged, but time-dependent rate measurements [17] or together with the mixing-induced CP asymmetry S_f and the direct CP asymmetry $C_f = -\mathcal{A}_{\text{CP}}$ of a time-dependent analysis

$$\mathcal{A}_{\text{CP}}[B_D \rightarrow f](t) = \frac{S_f \sin(\Delta m_D t) - C_f \cos(\Delta m_D t)}{\cosh\left(\frac{\Delta\Gamma_D t}{2}\right) - H_f \sinh\left(\frac{\Delta\Gamma_D t}{2}\right)} , \quad (\text{II.7})$$

where the mass difference of the heavy and light mass eigenstates is denoted as $\Delta m_D = m_D^{\text{H}} - m_D^{\text{L}} > 0$. The three CP asymmetries are not independent of each other, $|S_f|^2 + |C_f|^2 + |H_f|^2 = 1$, and are given in terms of one complex quantity

$$\lambda_f = \frac{q}{p} \frac{\bar{A}_f}{A_f} , \quad (\text{II.8})$$

as follows

$$\begin{aligned}S_f &= \frac{2 \text{Im}(\lambda_f)}{1 + |\lambda_f|^2} , & H_f &= \frac{2 \text{Re}(\lambda_f)}{1 + |\lambda_f|^2} , \\ C_f &= \frac{1 - |\lambda_f|^2}{1 + |\lambda_f|^2} .\end{aligned}\quad (\text{II.9})$$

In Eq. (II.8) $\bar{A}_f = A[\bar{B}_D \rightarrow f]$ and $A_f = A[B_D \rightarrow f]$ denote the decay amplitudes and in Sec. III we review their calculation in QCDF.

In the limit $\Delta\Gamma_D \rightarrow 0$ one obtains $\bar{\mathcal{B}}[B_D \rightarrow f] = \mathcal{B}[B_D \rightarrow f]$. This is the case for $D = d$ to a very good approximation in the SM where $y_{d|\text{SM}} = (0.21 \pm 0.04) \cdot 10^{-2} \ll 1$ [18]. Currently, the precision of experimental results does not yet allow to test the SM prediction. Measurements are available from B -factories $|y_d| = (0.7 \pm 0.9) \cdot 10^{-2}$ [19] and a recent determination of

LHCb from effective lifetimes $y_d = (-2.2 \pm 1.4) \cdot 10^{-2}$ [20], which assumes the SM result for H_f . Model-independent analysis of effects of NP in $\Delta\Gamma_d$ show that there is still room for huge nonstandard contributions [21]. We use the approximation $y_d = 0$ in all our predictions, which is well justified in the SM and also the considered NP scenarios.

On the other hand, $\Delta\Gamma_s$ is not negligible and the current world average from $B_s \rightarrow J/\psi\phi$ analyses alone is [19]

$$y_s = (5.8 \pm 1.0) \cdot 10^{-2}, \quad (\text{II.10})$$

which will be used in our analysis. In general $-1 \leq H_f \leq 1$, and therefore the correction factor on the r.h.s. of Eq. (II.4) can become of $\mathcal{O}(10\%)$ for final states f that are CP eigenstates, as has been found for some cases [16]. Other averages take into account $B_s \rightarrow J/\psi\pi\pi$ angular analysis, the effective lifetime measurement of $B_s \rightarrow K^+K^-$ and flavor-specific B_s lifetime averages, which involve additional assumptions in the potential presence of new physics. They yield a slightly larger value than in Eq. (II.10), $y_s = (6.2 \pm 0.9) \cdot 10^{-2}$ [19], being consistent within the uncertainties.

Besides branching fractions and CP-asymmetries, 2-body decays $B \rightarrow VV$ with subsequent decays $V \rightarrow PP$ provide additional observables in the full angular analysis of the 4-body final state [22]. The decay can be described in terms of three amplitudes, which can be chosen to correspond to definite helicities of the final-state vector mesons $V_{a,h_a} V_{b,h_b}$ with $h_a = h_b = (L, +, -)$ or, as in the following, transversity amplitudes $A_{\parallel,\perp} = (A_+ \pm A_-)/\sqrt{2}$. The three magnitudes and two relative phases of the A_h can be measured in a three-fold angular decay distribution, where we follow the definitions [23]. Hence, five CP-averaged and CP-asymmetric observables can be measured in the case where tagging of the initial B -flavor is possible. There are polarization fractions and relative phases for \bar{B} decays

$$f_h^{\bar{B}} = \frac{|\bar{A}_h|^2}{\sum_h |\bar{A}_h|^2}, \quad \phi_{\parallel,\perp}^{\bar{B}} = \arg \frac{\bar{A}_{\parallel,\perp}}{\bar{A}_L}. \quad (\text{II.11})$$

In view of the normalisation condition $f_L^{\bar{B}} + f_{\parallel}^{\bar{B}} + f_{\perp}^{\bar{B}} = 1$ one uses the branching fraction and two of the polarization fractions. In combination with the same quantities from B decays, replacing $\bar{A}_h \rightarrow A_h$, one has three CP-averaged polarization fractions and three CP-asymmetries

$$f_h = \frac{1}{2} (f_h^{\bar{B}} + f_h^B), \quad \mathcal{A}_{\text{CP}h} = \frac{f_h^{\bar{B}} - f_h^B}{f_h^{\bar{B}} + f_h^B}. \quad (\text{II.12})$$

Concerning the phases, the following two CP averaged and CP violating observables can be constructed for $h = (\parallel, \perp)$

$$\begin{aligned} \phi_h &= \frac{1}{2} (\phi_h^{\bar{B}} + \phi_h^B) \\ &\quad - \pi \operatorname{sgn} (\phi_h^{\bar{B}} + \phi_h^B) \theta (\phi_h^{\bar{B}} - \phi_h^B - \pi), \quad (\text{II.13}) \\ \Delta\phi_h &= \frac{1}{2} (\phi_h^{\bar{B}} - \phi_h^B) - \pi \theta (\phi_h^{\bar{B}} + \phi_h^B). \end{aligned}$$

This convention implies $\phi_h = \Delta\phi_h = 0$ at leading order in QCDF, where all strong phases are zero [23] and might differ for the sign of A_L relative to $A_{\parallel,\perp}$ adopted by experimental collaborations.

In the case of $B_s \rightarrow VV$ decays, again a correction factor Eq. (II.4) due to $y_s \neq 0$ applies, however now

$$\begin{aligned} \bar{\mathcal{B}}[B_D \rightarrow f] &= \sum_{h=L,\parallel,\perp} \mathcal{B}[B_D \rightarrow f_h] \frac{1 + y_D H_{f_h}}{1 - y_D^2}, \\ \bar{f}_h &= \frac{\mathcal{B}[B_D \rightarrow f_h]}{\sum_{h=L,\parallel,\perp} \mathcal{B}[B_D \rightarrow f_h]} \frac{1 + y_D H_{f_h}}{1 - y_D^2}. \end{aligned} \quad (\text{II.14})$$

Here H_{f_h} is defined as in Eq. (II.9) and the quantity λ_f is evaluated with $A_f \rightarrow A_{f_h}$.

Besides these observables, further combinations are considered that involve different types of charged and neutral B , M_a and M_b mesons. They are either ratios of branching fractions or differences of direct CP-asymmetries. The complete set of ratios [15, 31] is

$$\begin{aligned} R_c^B &= 2 \frac{\bar{\mathcal{B}}[B^- \rightarrow M_a^- M_b^0]}{\bar{\mathcal{B}}[B^- \rightarrow M_a^0 M_b^-]}, & R_c^{M_a} &= 2 \frac{\bar{\mathcal{B}}[B^- \rightarrow M_a^- M_b^0]}{\bar{\mathcal{B}}[\bar{B}^0 \rightarrow M_a^- M_b^+]}, & R_c^{M_b} &= \frac{\bar{\mathcal{B}}[B^- \rightarrow M_a^0 M_b^-]}{\bar{\mathcal{B}}[\bar{B}^0 \rightarrow M_a^- M_b^+]}, \\ R_n^B &= \frac{1}{2} \frac{\bar{\mathcal{B}}[\bar{B}^0 \rightarrow M_a^- M_b^+]}{\bar{\mathcal{B}}[\bar{B}^0 \rightarrow M_a^0 M_b^0]}, & R_n^{M_a} &= \frac{1}{2} \frac{\bar{\mathcal{B}}[B^- \rightarrow M_a^0 M_b^-]}{\bar{\mathcal{B}}[\bar{B}^0 \rightarrow M_a^0 M_b^0]}, & R_n^{M_b} &= \frac{\bar{\mathcal{B}}[B^- \rightarrow M_a^- M_b^0]}{\bar{\mathcal{B}}[\bar{B}^0 \rightarrow M_a^0 M_b^0]}, \end{aligned} \quad (\text{II.15})$$

where factors of τ_{B^0}/τ_{B^-} are not included in the definition of $R_{c,n}^{M_a, M_b}$, contrary to [15]. It is anticipated that these ratios are measured directly in experimental analyses, such that common experimental systematic errors cancel. Further, the following two differences of direct CP asymmetries are frequently considered

$$\begin{aligned} -\Delta C &= \Delta\mathcal{A}_{\text{CP}} = \mathcal{A}_{\text{CP}}[B^- \rightarrow M_a^- M_b^0] - \mathcal{A}_{\text{CP}}[\bar{B}^0 \rightarrow M_a^- M_b^+], \\ \Delta\mathcal{A}_{\text{CP}}^0 &= \mathcal{A}_{\text{CP}}[B^- \rightarrow M_a^0 M_b^-] - \mathcal{A}_{\text{CP}}[\bar{B}^0 \rightarrow M_a^0 M_b^0], \end{aligned} \quad (\text{II.16})$$

$b \rightarrow s$					$b \rightarrow d$	
$B \rightarrow K\pi$	$B \rightarrow K\eta$	$B \rightarrow K\eta'$	$B_s \rightarrow KK$ [24]	$B_s \rightarrow \pi\pi$	$B \rightarrow KK$	$B_s \rightarrow K\pi$
$K^0\pi^0 : \mathcal{B}, C, S$	$K^0\eta : \mathcal{B}$	$K^0\eta' : \mathcal{B}, C, S$	$K^+K^- : \mathcal{B}, C, S$	$\pi^+\pi^- : \mathcal{B}$	$K^0\bar{K}^0 : \mathcal{B}$	$K^+\pi^- : \mathcal{B}, C$
$K^+\pi^- : \mathcal{B}, C$	$K^+\eta : \mathcal{B}, C$	$K^+\eta' : \mathcal{B}, C$			$K^+K^- : \mathcal{B}$	
$K^+\pi^0 : \mathcal{B}, C$					$K^+K^0 : \mathcal{B}, C$	
$K^0\pi^+ : \mathcal{B}, C$						

TABLE I: Observables of $B \rightarrow PP$ decays mediated by $b \rightarrow s$ and $b \rightarrow d$ transitions that are used in the fit.

$b \rightarrow s$					
$B \rightarrow K^*\pi$	$B \rightarrow K\rho$	$B \rightarrow K^*\eta$	$B \rightarrow K^*\eta'$	$B \rightarrow K\phi$ [25–28]	$B \rightarrow K\omega$ [29, 30]
$K^{*0}\pi^0 : \mathcal{B}, C$	$K^0\rho^0 : \mathcal{B}, C, S$	$K^{*0}\eta : \mathcal{B}, C$	$K^{*0}\eta' : \mathcal{B}, C$	$K^0\phi : \mathcal{B}, C, S$	$K^0\omega : \mathcal{B}, C, S$
$K^{*+}\pi^- : \mathcal{B}, C$	$K^+\rho^- : \mathcal{B}, C$	$K^{*+}\eta : \mathcal{B}, C$	$K^{*+}\eta' : \mathcal{B}, C$	$K^+\phi : \mathcal{B}, C$	$K^+\omega : \mathcal{B}, C$
$K^{*+}\pi^0 : \mathcal{B}, C$	$K^+\rho^0 : \mathcal{B}, C$				
$K^{*0}\pi^+ : \mathcal{B}, C$	$K^0\rho^+ : \mathcal{B}, C$				

TABLE II: Observables of $B \rightarrow PV$ decays mediated by $b \rightarrow s$ transitions that are used in the fit.

in which in QCDF a cancellation of uncertainties takes place [32].

In order to separate NP effects in decays from those in $B_D\text{--}\bar{B}_D$ mixing in S_f , we define the observables [33, 34]

$$\Delta S_f = -\eta_f S_f - \begin{cases} S(\bar{B}_d \rightarrow J/\psi \bar{K}_S) & D = d \\ S(\bar{B}_s \rightarrow J/\psi \phi) & D = s \end{cases} \quad (\text{II.17})$$

with $\eta_f = \pm 1$ the CP eigenvalue of the final state f . The decays $\bar{B}_d \rightarrow J/\psi \bar{K}_S$ and $\bar{B}_s \rightarrow J/\psi \phi$ are dominated by contributions from charm tree-level operators and CP violation in the decay is both parametrically (CKM) and topologically (loop) suppressed. We expect that the CP-violating phase in $B_D\text{--}\bar{B}_D$ mixing, ϕ_{B_d} and ϕ_{B_s} , can clearly be extract from those decays, even in the presence of most NP scenarios [35]

$$\begin{aligned} \lambda_{J/\psi \bar{K}_S} &\simeq e^{-i\phi_{B_d}}, & S(\bar{B}_d \rightarrow J/\psi \bar{K}_S) &\simeq \sin 2\beta, \\ \lambda_{J/\psi \phi} &\simeq e^{-i\phi_{B_s}}, & S(\bar{B}_s \rightarrow J/\psi \phi) &\simeq \sin 2\beta_s, \end{aligned} \quad (\text{II.18})$$

in which the angles of the CKM unitarity triangle are defined as $\beta = \arg(\lambda_c^d/\lambda_t^d)$ and $\beta_s = \arg(\lambda_t^s/\lambda_c^s)$. This source of CP violation enters the mixing-induced CP asymmetry of most decays that are triggered by $b \rightarrow s$ transition in the same way and can be eliminated by the construction of ΔS_f , which therefore exclusively measures the interference of CP violation in the decay and in mixing.

B. Data

We investigate mainly $B \rightarrow MM$ decays mediated by $b \rightarrow s$ transitions but will consider also some $b \rightarrow d$ examples. The final 2-meson state MM consists either out of two pseudo-scalars ($MM = PP$) or one pseudo-scalar and one vector ($MM = PV$)¹ or two vectors ($MM = VV$), which are listed in Tab. I, Tab. II, and Tab. III, respectively, together with the observables that have been measured. We use the most recent values of branching ratios \mathcal{B} as well as direct and mixing-induced CP asymmetries $\mathcal{A}_{CP} = -C$ and S from the Heavy Flavor Averaging Group (HFAG) 2012 compilation and updates from 2013/2014 on the website [19]. For decays into VV -final states we include also the data of polarization fractions $f_{L,\perp}$, the relative phases $\phi_{\parallel,\perp}$ and CP-asymmetries $C_{L,\perp}$. Meanwhile, some observables had been updated or measured for the first time from individual experiments and not yet included in the HFAG averages. In these cases we do not make use of HFAG averages, but instead all measurements from individual experiments enter the likelihood function in Eq. (B3) as single measurements. The according references are given explicitly in the tables for such cases.

In addition we investigate the complementarity of composed observables, the ratios $R_{c,n}^{B,M_a,M_b}$ (II.15) of branching fractions and differences of CP asymmetries ΔC (II.16). In the future, it is desirable to have direct experimental determinations of the uncertainties for

¹ Here $MM = PV$ stands for both, $MM = PV$ and $MM = VP$.

$b \rightarrow s$					$b \rightarrow d$	
$B \rightarrow K^* \rho$	$B \rightarrow K^* \phi$ [36–38]	$B \rightarrow K^* \omega$	$B_s \rightarrow \phi \phi$	$B_s \rightarrow K^* K^*$ [39]	$B_s \rightarrow K^* \phi$	$B \rightarrow K^* K^*$
$K^{*0} \rho^0 : \mathcal{B}, C, f_L$	$K^{*0} \phi : \mathcal{B}, C, C_{L,\perp},$	$K^{*0} \omega : \mathcal{B}, C, f_L$	$\phi \phi : \mathcal{B}, f_L$	$K^{*0} K^{*0} : \mathcal{B}, f_L$		$K^{*0} K^{*0} : \mathcal{B}, f_L$
$K^{*+} \rho^- : \mathcal{B}, C, f_L$	$f_{L,\perp}, \phi_{\parallel,\perp}$	$K^{*+} \omega : \mathcal{B}, C, f_L$			$K^{*+} \phi : \mathcal{B}, f_L$	$K^{*+} K^{*0} : \mathcal{B}, f_L$
$K^{*+} \rho^0 : \mathcal{B}, C, f_L$	$K^{*+} \phi : \mathcal{B}, C, C_{L,\perp},$					
$K^{*0} \rho^+ : \mathcal{B}, C, f_L$	$f_{L,\perp}, \phi_{\parallel,\perp}$					

TABLE III: Observables of $B \rightarrow VV$ decays mediated by $b \rightarrow s$ and $b \rightarrow d$ transitions that are used in the fit.

these “composed” observables that already account for the cancellation of common experimental systematic uncertainties, which are only accessible to the experimental collaborations themselves. This is important, since usually outsiders are not in the position to account retroactively for cancellations of systematic errors and are restricted to the application of rules of error propagation to the uncertainties of the measurements of the involved components, which then might result in too conservative estimates. Of course such a procedure on the experimental side requires that the according decay modes with charged and neutral initial/final states can be analyzed simultaneously, which is the case for Babar, Belle and also Belle II. In this context it should be noted that ratios of gaussian distributed quantities are not gaussian distributed, although the differences are small as long as the tail regions of the distribution do not contribute. The details of the treatment of Gaussian and ratio of Gaussian distributed experimental probability distributions of the measurements are given in App. B.

The tables Tab. I, Tab. II, and Tab. III show that the decay systems $B \rightarrow K\pi$, $K^*\pi$, $K\rho$, $K^*\rho$ (and $K^*\phi$) are the ones with the most measured observables, allowing to investigate the complementarity of the constraints imposed on the phenomenological parameter of WA by branching fractions versus CP asymmetries versus other observables in VV -final states. In these cases we can also form the ratios of branching fractions Eq. (II.15) and differences of CP asymmetries Eq. (II.16). We will perform fits using two different sets of observables for these systems. In the first, called “Set I”, we will use four branching fractions and four direct CP asymmetries. In the lack of precise experimental data on the mixing-induced CP-asymmetry S , we rather prefer to predict them from the results of the fit then including them in the fit, see App. B 4 for details on the procedure. Such predictions can be tested with measurements of S by Belle II and LHCb in the near future [40–42] and are given for the SM and some NP fits in Tab. VII and Tab. X. The second “Set II” contains the fully independent observables of one branching fraction, three ratios $R_{c,n}^{B,M_a,M_b}$, three direct CP asymmetries C and the difference of CP asymmetries ΔC – see Tab. V for the explicit list of observ-

ables. In summary:

$$\begin{aligned} \text{Set I : } & (4 \times \mathcal{B}) + (4 \times C) \\ \text{Set II : } & (1 \times \mathcal{B}) + (3 \times R_{c,n}) \\ & + (3 \times C) + \Delta C. \end{aligned} \quad (\text{II.19})$$

III. $B \rightarrow MM$ IN QCD FACTORIZATION

Here we revisit the building blocks that arise in QCDF to calculate the final state-dependent corrections needed for a suitable prediction of the decay amplitudes λ_f Eq. (II.8) and details of their treatment in our analysis. Most importantly, the parametrization of the end-point divergences arising in weak-annihilation (WA) and hard-scattering (HS) contributions are given, which will be determined from experimental data in Sec. IV and Sec. V in the framework of the SM and scenarios of NP, respectively. Further, we describe in Sec. IIIB the determination of the relative magnitude of WA amplitudes compared to the leading ones in the SM and NP scenarios, as they are formally of subleading order in $1/m_b$, but chirally enhanced.

In our analysis all decay modes are driven by the same flavor transition $b \rightarrow D$ ($D = d, s$), which is described by the effective Hamiltonian of electroweak interactions. In the SM [2, 3]

$$\begin{aligned} \mathcal{H}_{\text{eff}}^D = & \frac{G_F}{\sqrt{2}} \sum_{p=u,c} \lambda_p^{(D)} \left(C_1 O_1^p + C_2 O_2^p \right. \\ & \left. + \sum_{i=3}^{10} C_i O_i + C_{7\gamma} O_{7\gamma} + C_{8g} O_{8g} \right) + \text{h.c.}, \end{aligned} \quad (\text{III.1})$$

where G_F denotes the Fermi constant and $\lambda_p^{(D)} \equiv V_{pb} V_{pD}^*$ are products of elements of the CKM matrix. The flavor-changing operators are

$$\begin{aligned} O_1^p &= (\bar{D}p)_{V-A} (\bar{p}b)_{V-A}, \\ O_2^p &= (\bar{D}_\alpha p_\beta)_{V-A} (\bar{p}_\beta b_\alpha)_{V-A}, \\ O_{3(5)} &= (\bar{D}b)_{V-A} \sum_q (\bar{q}q)_{V\mp A}, \\ O_{4(6)} &= (\bar{D}_\alpha b_\beta)_{V-A} \sum_q (\bar{q}_\beta q_\alpha)_{V\mp A}, \end{aligned}$$

$$\begin{aligned}
O_{7(9)} &= \frac{3}{2}(\bar{D}b)_{V-A} \sum_q e_q(\bar{q}q)_{V\pm A}, \\
O_{8(10)} &= \frac{3}{2}(\bar{D}_\alpha b_\beta)_{V-A} \sum_q e_q(\bar{q}_\beta q_\alpha)_{V\pm A}, \\
O_{7\gamma} &= -\frac{e m_b}{8\pi^2} (\bar{D} \sigma^{\mu\nu} (1 + \gamma_5) b) F_{\mu\nu}, \\
O_{8g} &= -\frac{g_s m_b}{8\pi^2} (\bar{D}_\alpha \sigma^{\mu\nu} (1 + \gamma_5) T_{\alpha\beta}^a b_\beta) G_{\mu\nu}^a, \quad (\text{III.2})
\end{aligned}$$

where $(\bar{q}_1 q_2)_{V\pm A} = \bar{q}_1 \gamma_\mu (1 \pm \gamma_5) q_2$, the sum is over active quarks $q = (u, d, s, c, b)$, with e_q denoting their electric charge in fractions of $|e|$ and α, β denoting color indices. The Wilson coefficients, C_i , are obtained by a matching calculation at a scale typically of the order $\mathcal{O}(M_W)$ of the W -boson mass and are evolved down to the low energy scale of $\mathcal{O}(m_b)$ of the bottom-quark mass by means of

$$\begin{aligned}
\langle M_1 M_2 | O_i | B \rangle &= \sum_j F_j^{B \rightarrow M_1}(m_2^2) \int_0^1 du T_{ij}^I(u) \Phi_{M_2}(u) + (M_1 \leftrightarrow M_2) \\
&+ \int_0^1 d\xi dv du T_i^{II}(u, v, w) \Phi_B(\xi) \Phi_{M_1}(v) \Phi_{M_2}(u) + \mathcal{O}\left(\frac{\Lambda_{\text{QCD}}}{m_b}\right)
\end{aligned} \quad (\text{III.3})$$

two terms with hard-scattering kernels $T^{I,II}$, which are calculable in perturbation theory to higher orders in the QCD coupling α_s . They are convoluted with light-cone distribution amplitudes (DA) of the light mesons, denoted as Φ_{M_i} , and are multiplied by the corresponding heavy-to-light form factors $F_j^{B \rightarrow M_i}$ in the case of T^I and involve an additional convolution with the B -meson distribution amplitude Φ_B in the case of T^{II} . In Eq. (III.3), the meson M_1 inherits the spectator quark of the decaying B meson, and depending on the final state, the decay amplitude might depend also on matrix elements with $M_1 \leftrightarrow M_2$, see [3, 5] for details.

At leading order in $1/m_b$, the perturbative kernels $T^{I,II}$ have been calculated up to NLO in strong coupling α_s [2, 3] and throughout we will stay within this approximation. Contrary to previous works [3, 5, 15], we employ Wilson coefficients of the weak Hamiltonian evaluated at the scale m_b even in WA and HS contributions, only the strong coupling α_s is evaluated at the semi-hard scale $\mu_h = \sqrt{\Lambda_{\text{QCD}} m_b}$. In the SCET approach this is apparent as a subsequent matching step from QCD to SCET_I taken at $\mu \sim m_b$ such that the Wilson coefficients of the weak Hamiltonian do not run below m_b , whereas α_s does. Equivalent arguments in the framework of QCDF can be found in [43].

The NNLO α_s corrections to $T^{I,II}$ are work in progress and by now the only lacking part are corrections to T^I from QCD- and QED-penguin operators $i = 3, \dots, 10$ as well as the dipole operators $i = 7\gamma, 8g$. These NNLO corrections are especially important for decays under con-

sideration here because strong phases are generated in QCDF only at NLO and higher order corrections might be large, apart from the reduction of renormalization scheme dependences. In the case of the color-allowed and color-suppressed current-current contributions due to $O_{1,2}^p$, the NNLO contributions to T^I cancel in large parts for both, real and imaginary parts, [44–46] with the ones to T^{II} [47–49] in the corresponding amplitudes $\alpha_{1,2}(MM)$ [46, 50] for $MM = \pi\pi, \rho\pi$, leaving them close to NLO predictions. This might not be the case for final states considered here.

A. Weak annihilation in QCDF

As was established by Beneke, Buchalla, Neubert and Sachrajda [2, 3], the matrix elements of the involved operators can be treated systematically in a $1/m_b$ expansion that has become known as QCD factorization (QCDF). At leading order this yields

consideration here because strong phases are generated in QCDF only at NLO and higher order corrections might be large, apart from the reduction of renormalization scheme dependences. In the case of the color-allowed and color-suppressed current-current contributions due to $O_{1,2}^p$, the NNLO contributions to T^I cancel in large parts for both, real and imaginary parts, [44–46] with the ones to T^{II} [47–49] in the corresponding amplitudes $\alpha_{1,2}(MM)$ [46, 50] for $MM = \pi\pi, \rho\pi$, leaving them close to NLO predictions. This might not be the case for final states considered here.

As it is discussed in detail in the literature [3, 5], contributions from HS and WA topologies, which are subleading in $1/m_b$, elude so far from a systematic treatment in QCDF. However, they can be chirally enhanced and contribute sizable corrections in predictions. Due to the ignorance of the respective QCD mechanisms, additional phenomenological parameters were introduced

$$X_k = (1 + \rho_k) \ln \frac{m_b}{\Lambda_{\text{QCD}}}, \quad (\text{III.4})$$

$$\rho_k \equiv |\rho_k| e^{i\phi_k}$$

with the complex parameters ρ_k for $k = A, H$.

In the HS they originate from terms involving twist-3 light-cone DAs $\Phi_{m1}(y)$ with $\Phi_{m1}(y) \neq 0$ for $y \rightarrow 1$ in convolutions

$$\int_0^1 \frac{\Phi_{m1}(y) dy}{1-y} \equiv \Phi_{m1}(1) X_H + \int_0^1 \frac{\Phi_{m1}(y) dy}{[1-y]_+}, \quad (\text{III.5})$$

which are regulated by the introduction of the phenomenological parameter X_H^2 , representing a soft-gluon interaction with the spectator quark. As indicated above, it is expected that $X_H \sim \ln(m_b/\Lambda_{\text{QCD}})$ because it arises in a perturbative calculation of these soft interactions that are regulated in principle latest by a physical scale of order Λ_{QCD} . Neither the adequate degrees of freedom nor their interactions, which should be used in an effective theory below this scale are known. It is also conceivable that factorization might be achieved at some intermediate scale between m_b and Λ_{QCD} . The factor $(1 + \rho_H)$ summarises the remainder of an unknown non-perturbative matrix element, including the possibility of a strong phase, which affects especially the predictions of CP asymmetries. The numerical size of the complex parameter ρ_H is unknown, however too large values will give rise to numerically enhanced subleading $1/m_b$ contributions compared to the formally leading terms putting to question the validity of the $1/m_b$ expansion of QCDF.

WA is entirely subleading in $1/m_b$ and consists in principle of six different building blocks $A_k^{i,f}$ ($k = 1, 2, 3$), which are characterized by gluon emission from the initial (i) and final (f) states and the three possible Dirac structures that are involved: $k = 1$ for $(V-A) \otimes (V-A)$, $k = 2$ for $(V-A) \otimes (V+A)$ and $k = 3$ for $(-2)(S-P) \otimes (S+P)$. They contribute to non-singlet annihilation amplitudes with specific combinations of Wilson coefficients of the 4-quark operators [3, 5]

$$\begin{aligned} b_1 &= \frac{C_F}{N_c^2} C_1 A_1^i, \\ b_2 &= \frac{C_F}{N_c^2} C_2 A_1^i, \\ b_3^p &= \frac{C_F}{N_c^2} [C_3 A_1^i + C_5 (A_3^i + A_3^f) + N_c C_6 A_3^f], \\ b_4^p &= \frac{C_F}{N_c^2} [C_4 A_1^i + C_6 A_2^i], \\ b_{3,\text{EW}}^p &= \frac{C_F}{N_c^2} [C_9 A_1^i + C_7 (A_3^i + A_3^f) + N_c C_8 A_3^f], \\ b_{4,\text{EW}}^p &= \frac{C_F}{N_c^2} [C_{10} A_1^i + C_8 A_2^i], \end{aligned} \quad (\text{III.6})$$

and depend on M_1 and M_2 . Here, $N_c = 3$ denotes the number of colors and the color factor $C_F = 4/3$. In particular, they correspond to the amplitudes due to current-current (b_1, b_2), QCD-penguin (b_3^p, b_4^p) and electroweak penguin ($b_{3,\text{EW}}^p, b_{4,\text{EW}}^p$) annihilation. Below we will frequently refer to WA amplitudes with the normalization

[5]

$$\beta_i^{(p)} = \mathcal{N}_\beta \begin{cases} \frac{b_i^{(p)}}{m_{M_2}} & \text{for } M_1 M_2 = V^\pm V^\pm \\ \frac{b_i^{(p)}}{m_B} & \text{for all others} \end{cases} \quad (\text{III.7})$$

where the argument $M_1 M_2$ has been suppressed and $\mathcal{N}_\beta \equiv f_B f_{M_1} / (m_B F^{B \rightarrow M_1})$ is independent on M_2 . As in the case of HS, the endpoint singularities in WA amplitudes are regulated in a model-dependent fashion. The results are expressed in terms of convolutions of hard-scattering kernels with DAs of twist-2 and chirally enhanced twist-3, involving phenomenological parameters X_A

$$\begin{aligned} \int_0^1 \frac{dy}{y} &\rightarrow X_A, \\ \int_0^1 \frac{\ln y dy}{y} &\rightarrow -\frac{1}{2} (X_A)^2, \end{aligned} \quad (\text{III.8})$$

which in principle are different for each meson and each building block $A_k^{i,f}$. Explicit expressions for $A_k^{i,f}$ in terms of X_A are given for $MM = PP, PV, VP, VV$ in the literature [5, 23, 51], but independently one has $A_{1,2}^f = 0$. As a further simplification, it is assumed in the literature that there is only one phenomenological parameter, independent of meson type and Dirac structure, such that $A_k^{i,f}(X_A)$ are functions of the same parameter. In this context we would like to note that in the most relevant WA amplitude β_3^c the building block A_3^f is parametrically enhanced by N_c and in the SM a large Wilson coefficient. In consequence its contribution dominates over the ones of $A_{1,3}^i$. It should be noted that the WA amplitudes (III.6) in the light-cone sum rule (LCSR) approach exhibit the same dependence on the products of Wilson coefficients and building blocks [52], however in this approach the calculation of $A_k^{i,f}$ does not suffer from endpoint singularities due to different assumptions and approximations. With the latter in mind, a more general approach would be to interpret the building blocks themselves as phenomenological parameters, or equivalently introduce one X_A for each of them. When investigating new-physics effects, it is desirable to keep the explicit dependence on the Wilson coefficients in (III.6) since they depend on NP parameters, including new weak phases. In the case of non-negligible WA contributions, the CP asymmetries and branching fractions will be sensitive to the interference of the new physics phases and the strong phases from X_A .

As already indicated, the phenomenological parameters $X_{A,H}$ are unknown and their size is conventionally adjusted within some range $|\rho_{A,H}| \lesssim 2$ to reproduce data whereas the phase $\phi_{A,H}$ is kept arbitrary and varied freely to estimate the uncertainty in theoretical predictions of observables within QCDF due to WA and HS. This procedure showed the phenomenological importance

² In principle one might introduce a separate X_H for each meson M_1 and M_2 as well as for each operator insertion.

of WA and constitutes a major source of theoretical uncertainty in predictions within the SM [5] and searches beyond [15] and below we will refer to it as “conventional QCDF”.

In this work, we are going to fit ρ_A — and for $B \rightarrow K\pi$ also ρ_H — from data. As a consequence, no predictions will be possible for those observables that are used in the fit, while the fitted values of ρ_A depend on the short-distance model under consideration. Yet, the consistency of the underlying short-distance model can be tested. We perform our fits in the framework of the SM, and further in new physics scenarios simultaneously with the additional NP parameters. In the latter case, the determination of the NP parameters will take into account the uncertainty of the WA contribution when marginalizing over ρ_A .

This procedure is different to conventional QCDF in as much as it assumes one universal parameter ρ_A for all observables in one specific decay mode. Indeed, in conventional QCDF the independent variation of $\rho_{A,H}$ for each observable in a specific decay corresponds to a different WA (and HS) parameter for each observable. However, since in QCDF the parameters $\rho_{A,H}$ are introduced at the level of decay amplitudes one would expect that they are the same for all observables of a specific decay mode. Consequently, conventional QCDF allows for situations where experimental measurements and theory predictions for two observables are in agreement, although for the first observable the agreement is reached for values of $\phi_{A,H}$ that might be much different from those where the agreement is reached for the second observable.

In the lack of precise data for most of the decays, we make the further assumption of a WA parameter that is even universal for decay modes that are related by the exchange of ($u \leftrightarrow d$) quarks. As an example, this allows to combine observables of the four decay channels $\bar{B}^0 \rightarrow \bar{K}^0\pi^0$, $K^-\pi^+$ and $B^- \rightarrow K^-\pi^0$, $\bar{K}^0\pi^-$, to which we refer as “decay system” $B \rightarrow K\pi$. All considered decay systems and the according observables have been listed in Tab. I, Tab. II and Tab. III. This assumption is motivated by the circumstance that the dominant contributions to the amplitude in all considered decays come actually from the linear combination $\hat{\alpha}_4(M_1M_2) = \alpha_4(M_1M_2) + \beta_3(M_1M_2)$, which is due to isospin-conserving QCD penguin operators $O_{3,\dots,6}$ (III.2). The definition of all α_i ’s can be found in [5], whereas β_i ’s are given in Eq. (III.7). Other assumptions have been tested in the literature as for example universal weak annihilation among B_s and B_d decays into final states containing kaons and pions [53].

The procedure reflects the general idea inherent to $1/m_b$ expansions, which aim at a factorization into short-distance and universal nonperturbative quantities, where the latter are determined from data in the lack of first principle determinations. Presently, however, factorization theorems are not yet established at subleading order that would support the existence of such universal quantities. In view of this, our study can affirm at most

experimental evidence against the assumption of one universal parameter per decay system. Therefore a positive affirmation may not be over interpreted. Finally, it must also be noted that contributions of not included NNLO corrections could be sizeable and in our fits they are interpreted as part of the phenomenological WA parameter.

B. Size of power suppressed corrections

In this work, we determine the size of subleading WA (and HS) contributions from data in the framework of the SM and NP scenarios. Due to the chiral enhancement, WA contributions are not necessarily $1/m_b$ suppressed numerically with respect to the leading order amplitudes. Therefore, it is of interest to know the relative magnitude of WA to leading amplitudes for the best fit regions of $\rho_{A(H)}$. For this purpose we introduce the quantities

$$\xi_i^A(\rho_A) = \left| \frac{\beta_i(\rho_A)}{\alpha_{(i+\delta_{i3}),I}} \right|, \quad (\text{III.9})$$

for WA and

$$\xi_i^H(\rho_H) = \left| \frac{\alpha_{i,\text{II}}^{\text{tw}-3}(\rho_H)}{\alpha_{i,I} + \alpha_{i,\text{II}}^{\text{tw}-2}} \right|, \quad (\text{III.10})$$

for HS amplitudes. For the latter, $\alpha_{i,\text{II}}^{\text{tw}-3}$ denotes the subleading, but chirally enhanced, twist-3 contribution, whereas $\alpha_{i,\text{II}}^{\text{tw}-2}$ is the leading HS contribution from twist-2 DAs, which is free of endpoint divergences. The leading amplitudes are splitted into $\alpha_i = \alpha_{i,I} + \alpha_{i,\text{II}}$, with the two contributions from kernel I and II introduced in Eq. (III.3). Note that $\xi_3^A = |\beta_3/\alpha_{4,I}|$. This definition is generalized for the case $MM = VV$, where ξ^A is defined as the mean value of the corresponding ratios for the longitudinal and negative polarized amplitudes $\xi_{i,VV}^A \equiv (\xi_{i,L}^A + \xi_{i,-}^A)/2$.

The most important contribution from power-suppressed corrections are clearly obtained from HS in α_2 , which is enhanced by the large Wilson Coefficient C_1 and from the WA correction β_3 in QCD-penguin dominated decays. Therefore ξ_2^H and ξ_3^A will play an important role in the phenomenological part of this work.

In the SM, the ξ^A -ratios depend exclusively on ρ_A and contour lines of constant ξ^A can be easily obtained in the complex ρ_A -plane. Concerning fits in new-physics scenarios, the ξ^A -ratios depend in addition on new-physics parameters \mathbf{x}^{NP} , where $\dim(\mathbf{x}^{\text{NP}})$ corresponds to their number. The dependence is both, explicit in the Wilson coefficients and implicit on data via the likelihood. In this case one would be interested in the minimal value of $\xi_i^A(\mathbf{x}^{\text{NP}})$ in the 68% credibility regions (CR) of all NP parameters, but marginalized over ρ_A . Since the determination of this CRs requires huge computational efforts when $\dim(\mathbf{x}^{\text{NP}}) > 2$, we proceed differently. In the course of the fit, we histogram in all 2-dimensional subspaces of NP parameters $(x_a^{\text{NP}}, x_b^{\text{NP}})$, with $a \neq b$, those values ξ^A

in each bin $(x_a^{\text{NP}}, x_b^{\text{NP}})$ that belong to the largest likelihood value when sampling the complementary subspace of the remaining NP parameters x_c^{NP} with $c \neq a$ and $c \neq b$. As a result, in each of the 2D-marginalized planes, “labeled” by (a, b) , the 68% CR will contain a smallest and a largest ξ_i^A in one of the bins in $(x_a^{\text{NP}}, x_b^{\text{NP}})$, which all belong to the minimal χ^2 in the subspace of x_c . As the final range we choose the minimum of the smallest values and the maximum of the largest values from all the pairs (a, b) in our NP analyses in Sec. V.

IV. WEAK ANNIHILATION IN THE STANDARD MODEL

In this section we present the results of the determination of the WA parameter ρ_A from data of various QCD-penguin- and WA-dominated nonleptonic charmless $B \rightarrow MM$ decays in the framework of the SM. This includes characteristics of the best-fit regions, the p values at the best-fit point and pull values for observables, as well as the relative amount of the subleading WA contribution needed to explain the data, which we quantify by the ratio ξ_3^A defined in Eq. (III.9).

We start with an extensive discussion of the $B \rightarrow K\pi$ system, which shows the largest deviations from SM predictions for the difference of CP asymmetries $\Delta C(K\pi)$ (see Eq. (II.16)), commonly known in the literature as the “ $\Delta\mathcal{A}_{\text{CP}}$ puzzle” and to a lesser extent in the ratio $R_n^B(K\pi)$. We investigate the “ $\Delta\mathcal{A}_{\text{CP}}$ puzzle” further in a simultaneous fit of the parameter of WA, ρ_A , and HS, ρ_H , and discuss the implications on other CP asymmetries in $B_{d,s} \rightarrow K\pi$.

We turn then to the discussion of the decays $B \rightarrow K\rho$, $K^*\rho$, $K^*\pi$, which allow also for studies of different sets of observables in Set I and Set II due to the rather numerous and quite precise measurements. Subsequently, we discuss shortly the results for other decays listed in Tab. I, Tab. II and Tab. III with some special comments on $B \rightarrow K\omega$ and $B \rightarrow K^*\phi$. For each decay system we present separate constraints from branching fractions, CP asymmetries, polarization fractions and relative phases on the WA parameter ρ_A , besides the combined ones.

Apart from the above listed penguin dominated decays, we also study decays mediated solely by weak annihilation, such as $B \rightarrow K^+K^-$ and $B_s \rightarrow \pi^+\pi^-$. Being independent of β_3 and hence A_3^f , these decay modes are sensitive to a WA contribution from $A_{1,2}^i$ and provide access to different building blocks.

Based on our previous fit results, we discuss finally the assumption of a universal WA for B_d and B_s decays into the same final states and investigate in particular consequences for CP asymmetries in $B_s \rightarrow K\pi$ in view of the “ $\Delta\mathcal{A}_{\text{CP}}$ puzzle” in $B \rightarrow K\pi$.

The statistical procedure used in all fits is described in App. B. In the SM, we deal mostly with the fit of one complex-valued parameter ρ_A except for the $B \rightarrow K\pi$

system, where we also perform a simultaneous fit of ρ_A and ρ_H . When fitted, for both parameters a uniform prior

$$0 \leq |\rho_{A,H}| \leq 8, \quad 0 \leq \phi_{A,H} \leq 2\pi, \quad (\text{IV.1})$$

is assumed and no restriction is imposed on the phases. In comparison, in conventional QCDF the magnitude $|\rho_{A,H}| \leq 2$ is used for uncertainty estimates of theoretical predictions. In the case that ρ_H is not fitted, but treated as a nuisance parameter instead, we use $|\rho_H| = 1$ and vary $0 \leq \phi_H \leq 2\pi$.

Our findings for lower and upper bounds on ρ_A in the 68% CR are summarized in Tab. IV for all considered decay systems. It can be seen that data requires non-zero values of $|\rho_A|$ to be in agreement with QCDF predictions in the SM. In some cases they are much larger compared to the conventionally adapted ranges, allowing thus in principle for a better agreement of theoretical predictions with data. Since we use Wilson coefficients at the scale $\mu \sim m_b$ in WA (and HS) contributions, contrary to [5, 15], our numerical values of $|\rho_A|$ are in general a bit larger compared to the ones known in the literature. Representing the size of a nonperturbative quantity, $|\rho_A|$ is expected naively to be of order one, whereas too large values would put in doubt the convergence of the $1/m_b$ expansion.

Further we list the ratio ξ_3^A of WA amplitudes to leading ones as a measure of the numerical relevance of these formally subleading but chirality enhanced contributions. At the best-fit point of ρ_A the according value is indeed $\xi_3^A < 1$ for many decay systems. Although at the best-fit point ξ_3^A might reach values up to 2 or even 3 for some decay systems, once considering the 68% CR in ρ_A , it is possible to have again $\xi_3^A < 1$ (except for $B_s \rightarrow K^*K^*$) for the price of some tension among data and prediction. Bearing in mind the chirality enhancement, our fits of the data thus do not indicate anomalously huge WA contributions, which put QCDF into question in principle. By definition, there is no ξ_3^A for the two pure WA modes $B_d \rightarrow K^+K^-$ and $B_s \rightarrow \pi^+\pi^-$.

A. Results for $B \rightarrow K\pi$

The $B \rightarrow K\pi$ system offers the most precise measured branching fractions and CP asymmetries (see Tab. I) among the decays considered here. In consequence, we find stringent bounds on the WA parameter $\rho_A^{K\pi}$. This can be seen in Fig. 1a when using the observables in Set I and Fig. 1b for Set II. The allowed regions from both, \mathcal{B} and/or $R_{c,n}^{B,M_a,M_b}$ (blue) as well as C and/or ΔC (green) are very distinct leaving two tiny overlap regions (red) at 68% probability around $\rho_A^{K\pi} \approx 2.1 \exp(i 5.5)$ and $\rho_A^{K\pi} \approx 3.4 \exp(i 2.7)$, which differ only slightly for both Sets I and II. The best-fit points listed in Tab. V fall into the solution with larger $|\rho_A^{K\pi}| \approx 3.4$, but it must be noted that the other solution provides almost equally good fits in terms of χ^2 .

$MM = PP$								
		$B \rightarrow K\pi$	$B \rightarrow K\eta$	$B \rightarrow K\eta'$	$B \rightarrow KK$	$B_s \rightarrow KK$	$B_s \rightarrow \pi\pi$	$B_s \rightarrow K\pi$
ξ_3^A	BFP	0.39	0.08	1.83	0.58	1.83	–	0.96
	68% CR	[0.37; 0.54]	[0.00; –]	[0.18; 3.25]	[0.00; 2.07]	[0.02; 2.09]	–	[0.56; 1.54]
	95% CR	[0.34; 0.69]	[0.00; –]	[0.16; 3.34]	[0.00; 2.10]	[0.00; 2.13]	–	[0.44; 1.83]
$ \rho_A $	lower	> 1.8	> 0	> 0.9	> 0 (0.9)	> 0	> 3.4	> 2.3
	upper	< 3.9	–	< 7.7	< 6.1 (8.6)	< 5.5	< 10.9	< 4.8

$MM = PV$							
		$B \rightarrow K^*\pi$	$B \rightarrow K\rho$	$B \rightarrow K^*\eta$	$B \rightarrow K^*\eta'$	$B \rightarrow K\phi$	$B \rightarrow K\omega$
ξ_3^A	BFP	0.89	0.78	2.74	0.48	0.50	2.7
	68% CR	[0.75; 1.40]	[0.39; 1.55]	[0.71; 3.77]	[0.02; 7.84]	[0.40; 2.41]	[0.63; 2.88]
	95% CR	[0.69; 1.56]	[0.16; 2.18]	[0.64; 5.06]	[0.02; 8.41]	[0.32; 2.54]	[0.57; 2.88]
$ \rho_A $	lower	> 1.4	> 0.8	> 1.1	> 0	> 0.8	> 1.3
	upper	< 3.4	< 3.4	< 4.4	< 6.1	< 3.6	< 4.3

$MM = VV$								
		$B \rightarrow K^*\rho$	$B \rightarrow K^*\phi$	$B_s \rightarrow K^*\phi$	$B \rightarrow K^*K^*$	$B_s \rightarrow K^*K^*$	$B_s \rightarrow \phi\phi$	$B \rightarrow K^*\omega$
ξ_3^A	BFP	1.33	0.38	1.53	1.84	3.01	0.50	0.91
	68% CR	[0.84; 1.94]	[0.31; 0.43]	[0.30; 2.05]	[0.85; 2.68]	[1.94; 3.79]	[0.49; 1.11]	[0.20; 1.39]
	95% CR	[0.56; 2.33]	[0.25; 0.50]	[0.10; 2.15]	[0.09; 2.90]	[0.96; 4.17]	[0.41; 1.38]	[0.09; 1.46]
$ \rho_A $	lower	> 1.0	> 0.6	> 0.3	> 1.2	> 1.6	> 0.7	> 0.3
	upper	< 2.9	< 1.8	< 3.2	< 3.0	< 3.6	< 2.3	< 2.4

TABLE IV: Compilation of the power suppressed ratio ξ_3^A at the best-fit point (BFP) and in the 68% and 95% CRs, as well as lower and upper bounds on the fit parameter $|\rho_A|$ in the 68% CR for all relevant decay systems. For $B \rightarrow (K\pi, K^*\pi, K\rho, K^*\rho)$, values correspond to the fit with the observable Set II. The pure WA decay $B^0 \rightarrow K^+K^-$ is not included in the decay system $B \rightarrow KK$ and ρ_A -bounds are given separately in parenthesis.

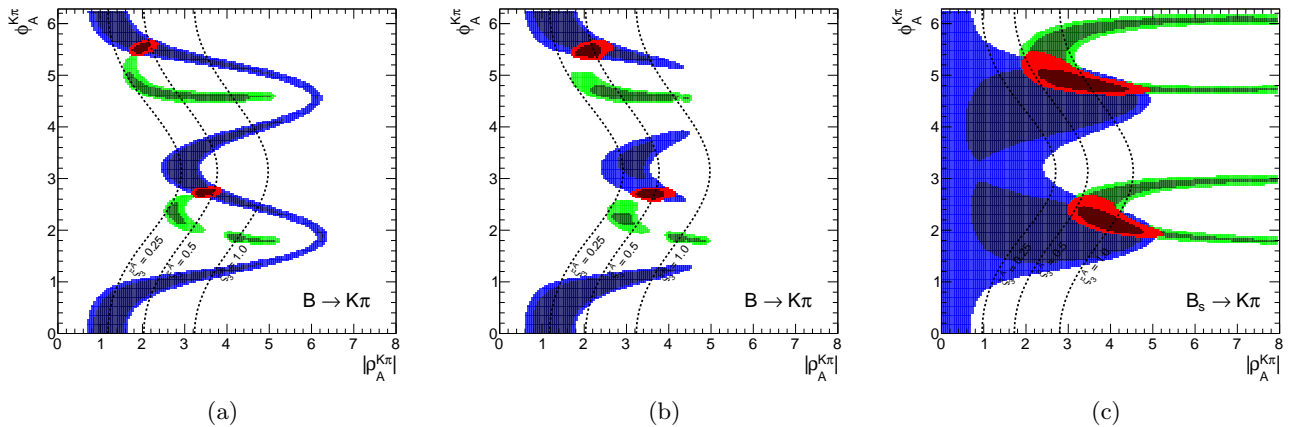


FIG. 1: The 68% (dark) and 95% (bright) CRs of $\rho_A^{M_1 M_2}$ from a fit of observables in the $(B \rightarrow K\pi)$ -system in (a) Set I and (b) Set II, and for comparison in the (c) $(B_s \rightarrow K\pi)$ -system. Allowed regions are shown for B and $R_{n,c}$ (blue), C and ΔC (green) and their combination (red). The dashed lines correspond to constant $\xi_3^A = (0.25, 0.5, 1.0)$ from left to right.

$M_a M_b$ set	$K\pi$		$K^*\pi$		$K\rho$		$K^*\rho$	
	SI	SII	SI	SII	SI	SII	SI	SII
p value	0.44	0.04	0.95	0.90	1	1	1	0.97
best-fit point	3.39; 2.73	3.34; 2.71	1.79; 5.85	1.61; 5.84	2.57; 2.79	2.69; 2.68	2.31; 2.74	1.56; 5.66
$\mathcal{B}(\bar{B}^0 \rightarrow M_a^0 M_b^0)$	$+0.3\sigma$	—	-0.3σ	—	0.0σ	—	0.0σ	—
$\mathcal{B}(\bar{B}^0 \rightarrow M_a^- M_b^+)$	0.0σ	—	0.0σ	—	0.0σ	—	$+0.3\sigma$	$+0.1\sigma$
$\mathcal{B}(B^- \rightarrow M_a^- M_b^0)$	0.0σ	—	$+0.6\sigma$	—	0.0σ	—	0.0σ	—
$\mathcal{B}(B^- \rightarrow M_a^0 M_b^-)$	0.0σ	$+0.2\sigma$	0.0σ	$+0.1\sigma$	0.0σ	$+0.1\sigma$	0.0σ	—
R_c^B	—	—	—	—	—	—	—	-0.5σ
R_n^B	—	-1.9σ	—	$+0.6\sigma$	—	0.0σ	—	$+0.6\sigma$
$R_c^{M_a}$	—	0.0σ	—	$+0.8\sigma$	—	$+0.7\sigma$	—	-0.8σ
$R_c^{M_b}$	—	$+0.9\sigma$	—	0.0σ	—	-0.2σ	—	—
$C(\bar{B}^0 \rightarrow M_a^0 M_b^0)$	0.0σ	0.0σ	$+0.5\sigma$	$+0.4\sigma$	0.0σ	0.0σ	0.0σ	0.0σ
$C(\bar{B}^0 \rightarrow M_a^- M_b^+)$	$+0.7\sigma$	$+0.1\sigma$	$+0.1\sigma$	$+0.1\sigma$	0.0σ	$+0.1\sigma$	$+0.5\sigma$	$+0.6\sigma$
$C(B^- \rightarrow M_a^- M_b^0)$	-2.1σ	—	0.0σ	—	0.0σ	—	$+0.3\sigma$	—
$C(B^- \rightarrow M_a^0 M_b^-)$	$+1.0\sigma$	$+1.0\sigma$	$+0.9\sigma$	$+1.0\sigma$	$+0.7\sigma$	$+0.7\sigma$	$+0.1\sigma$	0.0σ
ΔC	—	-2.8σ	—	-0.1σ	—	0.0σ	—	0.0σ
$f_L(\bar{B}^0 \rightarrow M_a^0 M_b^0)$	—	—	—	—	—	—	0.0σ	0.0σ
$f_L(\bar{B}^0 \rightarrow M_a^- M_b^+)$	—	—	—	—	—	—	-0.6σ	-0.5σ
$f_L(B^- \rightarrow M_a^- M_b^0)$	—	—	—	—	—	—	$+0.7\sigma$	$+0.9\sigma$
$f_L(B^- \rightarrow M_a^0 M_b^-)$	—	—	—	—	—	—	0.0σ	0.0σ

TABLE V: Compilation of p values and pulls of the SM fit, evaluated at the best-fit point of $\rho_A^{M_a M_b}$ for the two different sets of observables Set I and Set II for the decays $B \rightarrow K\pi$, $K^*\pi$, $K\rho$, $K^*\rho$.

As shown in Tab. V, the p values at the best-fit points of the fits of Set I and Set II are very different: 0.44 versus 0.04, respectively. The reason are large pull values of composed observables in Set II at the best-fit point: -2.8σ for $\Delta C(K\pi)$ and -1.9σ for $R_n^B(K\pi)$, compared to Set I: -2.1σ for $C(B^- \rightarrow K^-\pi^0)$, showing the importance and complementarity of composed observables. The large pull values in CP asymmetries arise from the higher statistical weight of the preciselier measured branching fractions in their combined fit, reflecting the “ $\Delta\mathcal{A}_{CP}$ puzzle” in the $B \rightarrow K\pi$ system. The individual pull values of $C(B^- \rightarrow K^-\pi^0)$ and $C(\bar{B}^0 \rightarrow K^-\pi^+)$ in Set I add up to the large pull of $\Delta C(K\pi)$ in Set II.

In the following we will elaborate on the constraints posed by individual observables. For example, the general shape of the contour of branching fractions can be easily understood as follows: The leading contribution of the decay amplitude $\hat{\alpha}_4^c(K\pi) = \alpha_4^c(K\pi) + \beta_3^c(K\pi)$ is given as the sum of the QCD-penguin and the ρ_A -dependent WA amplitudes α_4^c and β_3^c , respectively. The experimental measurement of the branching fraction restricts $\hat{\alpha}_4^c$ to a circle in its imaginary plane

$$\sqrt{\mathcal{B}} \simeq \lambda_c^{(s)} F_0^{B \rightarrow \pi} f_K |\hat{\alpha}_4^c| (1 + \mathcal{O}(r_i)) \quad (\text{IV.2})$$

where the $r_i = (r_T, r_T^C, r_{EW}, r_{EW}^C, r_{EW}^A)$ ’s [15] are numerically small, mode-dependent corrections, normalized

to $\hat{\alpha}_4^c$. Consequently, $\beta_3^c(\rho_A^2, \rho_A)$ can interfere constructively or destructively with α_4^c depending on the phase of $\rho_A^{K\pi}$. For $\phi_A^{K\pi} \sim 0, \pi$, the WA contribution is mainly real and contributes constructively to α_4^c . However, the contributions to β_3^c that are linear and quadratic in ρ_A also interfere with each other either constructively ($\phi_A^{K\pi} \sim 0$) leading to small $|\rho_A^{K\pi}| \sim 2.0$ or destructively ($\phi_A^{K\pi} \sim \pi$), leading to larger $|\rho_A^{K\pi}| \sim 3.4$. On the other hand, large values $|\rho_A^{K\pi}| \sim 6.0$ are required for $\phi_A^{K\pi} \sim \pi/2, (3\pi/2)$ where β_3^c becomes purely imaginary and interferes destructively with α_4^c . In summary, the four branching fraction measurements in Set I of the $B \rightarrow K\pi$ system can be described by a single universal ρ_A and by themselves they do not exclude any value of the phase and allow up to $|\rho_A^{K\pi}| \lesssim 6$.

Whereas the branching fractions fix the modulus of

$$\hat{\alpha}_4^c = |\hat{\alpha}_4^c| \exp(i\hat{\phi}_4^c), \quad (\text{IV.3})$$

the ratios of branching fractions (see Eq. (II.15)) depend strongly on the real part of $\hat{\alpha}_4^c$, i.e., are sensitive to the phase $\hat{\phi}_4^c$

$$R_{c,n}^{B,K,\pi} \simeq 1 + \cos \hat{\phi}_4^c \sum_i c_i \text{Re}(r_i) + \dots \quad (\text{IV.4})$$

Here the c_i denote proportionality factors and terms proportional to $\text{Im}(r_i)$ are denoted by dots. The latter become numerically important only in the vicinity

of $\hat{\phi}_4^c \sim \pi/2, (3\pi/2)$, and are fully included in the fits. Hence these ratios are sensitive to flips of $\hat{\phi}_4^c$ by π . As can be seen in Fig. 1b, the data disfavors and excludes to a large extent the scenario of large WA when using observable Set II, i.e., purely imaginary β_3^c that would interfere destructively with α_4^c . There is no need for anomalously large WA contributions to describe $B \rightarrow K\pi$ data of branching fractions and their ratios in QCDF within the SM. Moreover, at 68% probability the largest portion of allowed $\rho_A^{K\pi}$ parameter space is within $\xi_3^A(K\pi) < 0.5$.

We provide also separately the constraints from direct CP asymmetries. In QCDF the strong phase, necessary for CP violation, arises at $\mathcal{O}(\alpha_s)$, respectively $\mathcal{O}(1/m_b)$, and is thus included only to leading order in our numerical evaluations. Currently, CP asymmetries with neutral kaons in the final state are measured to be small with large errors, whereas the ones with charged kaons are observed to be large and with a relative opposite sign. For the latter decays, the leading terms to the CP asymmetries are from color-allowed, r_T , and color-suppressed, r_T^C , penguin-to-tree ratios [15],

$$\begin{aligned} C(B^- \rightarrow K^- \pi^0) &\approx 2 \text{Im}(r_T + r_T^C) \sin \gamma \\ &= (-4.0 \pm 2.1)\%, \\ C(\bar{B}^0 \rightarrow K^- \pi^+) &\approx 2 \text{Im}(r_T) \sin \gamma \\ &= (+8.2 \pm 0.6)\%, \end{aligned} \quad (\text{IV.5})$$

where the measured values are taken from [19], and γ denotes the angle of the CKM unitarity triangle. Their difference is dominated by the color-suppressed tree amplitude

$$\Delta C \simeq 2 \text{Im}(r_T^C) \sin \gamma \simeq (-12.2 \pm 2.2)\%. \quad (\text{IV.6})$$

In QCDF, one has

$$\begin{aligned} \text{Im}(r_T) &\propto -\frac{\text{Re}(\alpha_1)}{|\hat{\alpha}_4^c|} \sin \hat{\phi}_4^c + \frac{\text{Im}(\alpha_1)}{|\hat{\alpha}_4^c|} \cos \hat{\phi}_4^c, \\ \text{Im}(r_T^C) &\propto -\frac{\text{Re}(\alpha_2)}{|\hat{\alpha}_4^c|} \sin \hat{\phi}_4^c + \frac{\text{Im}(\alpha_2)}{|\hat{\alpha}_4^c|} \cos \hat{\phi}_4^c, \end{aligned} \quad (\text{IV.7})$$

where $\hat{\alpha}_4^c$ depends on ρ_A . The numerical values for

$$\begin{aligned} 100 \cdot \frac{\alpha_1}{|\hat{\alpha}_4^c|} &\approx -17.4_{-0.9}^{+1.0} - i 0.4_{-0.5}^{+0.6}, \\ 100 \cdot \frac{\alpha_2}{|\hat{\alpha}_4^c|} &\approx -5.8_{-3.4}^{+1.1} + i 1.5_{-0.5}^{+0.3} - 2.1_{-1.2}^{+0.3} \rho_H^{K\pi}, \end{aligned} \quad (\text{IV.8})$$

hold for the central values as well as the variation of theory parameters and $\rho_A^{K\pi}$ at the best-fit point of Set II listed in Tab. V. We kept explicitly the dependence of r_T^C on the HS parameter $\rho_H^{K\pi}$, which is numerically irrelevant for r_T . It can be seen that r_T^C can be enhanced if $\text{Re}(\rho_H^{K\pi}) > 0$ and $\text{Im}(\rho_H^{K\pi}) < 0$ — see later discussion concerning Fig. 2a.

The allowed regions obtained from a fit of only CP asymmetries in Fig. 1a and Fig. 1b (shown in green) are similar for Set I and Set II. The best-fit point is at

$\rho_A^{K\pi} \approx 4.1 \exp(i1.8)$, along the branch of $\phi_A^{K\pi} \sim \pi/2$ that gives rise to strong cancellations in destructive interference of α_4^c and β_3^c and leads to large theoretical uncertainties, which in turn allows for good agreement with the data. Apart from the fact that branching fraction measurements would become incompatible at more than 30σ , neglected higher order perturbative and power corrections would become important in these regions of parameter space putting into doubt the reliability of the prediction. However, there are substantial parts of the 68% CRs with $\xi^A(K\pi) < 0.5$ and the size of WA contributions can be as low as 0.25, for which these comments do not apply.

The very same figures (Fig. 1a and Fig. 1b) show also that there is no or hardly any overlap at 95% probability of the allowed regions from branching fractions (blue) and those from CP asymmetries (green). In our approach, the so-called “ $\Delta\mathcal{A}_{\text{CP}}$ puzzle” manifests itself only in the combined fit of branching fractions and CP asymmetries, where then large pull values arise for ΔC (Set II), or equivalently also $C(B^- \rightarrow K^- \pi^0)$ (Set I). These pull values are shown in Tab. V and caused by the higher statistical weight of the branching fraction measurements. So one might wonder, how previous QCDF analyses, for example [15, 54], arrived at a “ $\Delta\mathcal{A}_{\text{CP}}$ puzzle” based on the conventional approach, where ρ_A is varied independently for each observable? The answer is rather simple: there the uncertainty of an observable is determined by the spread of values obtained in a scan of ρ_A with $|\rho_A^{K\pi}| \approx 1$ and arbitrary phase $\phi_A^{K\pi}$. Moreover, the central value of the observable is usually assigned by definition to $\phi_A^{K\pi} = 0$. This corresponds in Fig. 1a and Fig. 1b to a line of constant $|\rho_A^{K\pi}| = 1$, which yields only consistent results for branching fractions, but never for the combination of CP-asymmetries, i.e. those CP asymmetries which dominate statistically over the ones with large experimental errors. In the conventional approach there will be no “ $\Delta\mathcal{A}_{\text{CP}}$ puzzle” once larger values of $|\rho_A^{K\pi}| \lesssim 2$ and a fine stepsize for the variation of $\phi_A^{K\pi}$ are permitted in the scan, implying of course larger $\xi^A(K\pi) \lesssim 0.5$ and increased theoretical uncertainties. We note that $C(B^- \rightarrow K^0 \pi^-)$ almost vanishes in QCDF and even in the presence of large power corrections it is difficult to increase the predictions beyond 1%, such that the current pull of 1σ (see Tab. V) can hardly be reduced. We emphasize again the different assumptions underlying our approach, i.e., WA parameters are universal among decays related by ($u \leftrightarrow d$) quark exchange, but need not be small and are determined from data, contrary to the conventional approach, i.e., WA parameters are scanned over a rather small range and the resulting errors correspond to non-universal parameters.

The results of the combined fit of branching fractions and CP asymmetries had been already discussed at the beginning of this section. Whereas CP asymmetries involved in the “ $\Delta\mathcal{A}_{\text{CP}}$ puzzle” exhibit larger pull values for both sets of observables Set I and Set II, predictions of branching fractions are in good agreement with the cor-

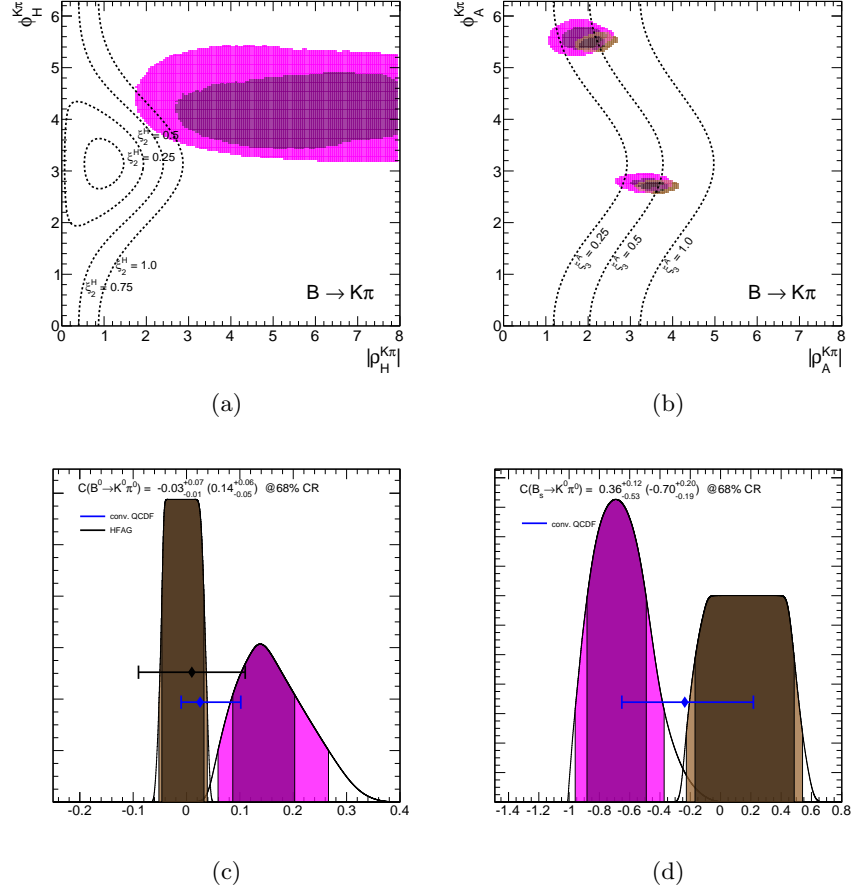


FIG. 2: The 68% (dark) and 95% (bright) CRs of $\rho_H^{K\pi}$ (upper left) and $\rho_A^{K\pi}$ (upper right), obtained from a fit with partial (see text) observable Set II for $B \rightarrow K\pi$ decays, treating $\rho_H^{K\pi}$ either as a fit parameter (purple) or nuisance parameter as described in App. B 1 (brown). The dashed lines correspond to constant $\xi_2^H(K\pi) = (0.25, 0.5, 0.75, 1.0)$ and $\xi_3^A(K\pi) = (0.25, 0.5, 1.0)$, respectively. The lower panels show the predictions for $C(B_d \rightarrow K^0\pi^0)$ (left) and $C(B_s \rightarrow K^0\pi^0)$ (right). The available experimental results are shown with 1σ errors and a prediction from QCDF with the conventional uncertainty estimate is labeled “conv. QCDF”. The 68% credibility intervals for the predictions are given on the top of both panels for conventional ρ_H (brown) and in brackets for fitted ρ_H (purple).

responding measurements, in part also due to large form factor uncertainties. The latter parametric dependence cancels to a large extent in ratios of branching fractions and yields a large pull value of -1.9σ for $R_n^B(K\pi)$ in Set II, which contributes also to the problematic p value of 0.04. In a fit of Set II without CP asymmetries we obtain pull values of -1.2σ for $R_n^B(K\pi)$, 0.4σ for $R_c^K(K\pi)$ and 0.6σ for $R_c^K(K\pi)$, which can be compared to the pull in Tab. V when including CP asymmetries. This can be also seen in Fig. 1b where the solution of the combined fit (red) at $\rho_A \sim 3.3 \exp(2.7i)$ does neither overlap with the 68% CRs from $\mathcal{B}/R_{n,c}$ (blue) nor from $C/\Delta C$ (green).

Finally, we explore in more detail the discrepancy in ΔC , departing from the conventional error estimate of power corrections of HS contributions that had been used until now, see App. A. As previously mentioned in Eq. (IV.6), the color-suppressed tree amplitude α_2^u de-

termines the magnitude of $r_T^C \propto |\lambda_u^{(s)}/\lambda_c^{(s)}| \alpha_2^u/\hat{\alpha}_4^c$. Possible large NNLO corrections might relax the tension in the case of destructive interference to the real and constructive interference to the imaginary part. For $\pi\pi$ -final states, however, such NNLO vertex corrections are cancelled by the NLO HS corrections [44–46, 50], which might not necessarily takes place to the same extent in $K\pi$ final states. Nevertheless, in the following we will assume no large perturbative higher order corrections and fit instead the phenomenological parameter $\rho_H^{K\pi}$ in addition to $\rho_A^{K\pi}$. We point out that ΔC depends on the sum $\alpha_{2,I} + \alpha_{2,II}^{\text{tw}-2} + \alpha_{2,II}^{\text{tw}-3}(\rho_H) + \beta_2(\rho_A^i)$, where β_2 is dominated by building block A_1^i and the corresponding WA parameter ρ_A^i — see Eq. (III.6). The contribution of β_2 is always much smaller than $\alpha_{2,II}^{\text{tw}-3}$ unless $\rho_H \ll \rho_A^i$. Hence we prefer to fit ρ_H and assume $\rho_A^i = \rho_A$, the common

WA parameter of all building blocks $A_{1,2,3}^{i,f}$. Only for a rather large $\rho_A^i \gtrsim 4$ will the β_2 contribution be comparable to the theory uncertainties of the leading amplitudes in ΔC .

The results of a fit to the partial observable Set II for the parameters $\rho_H^{K\pi}$ and $\rho_A^{K\pi}$ is shown in purple in Fig. 2a and Fig. 2b, respectively. We have removed the CP asymmetry $C(B_d \rightarrow K^0\pi^0)$ that is very sensitive to HS, but its current measurement does not provide any constraints, making it an ideal candidate for a prediction. In contrast, $R_n^B(K\pi)$ is not very sensitive to HS, but its large pull value would force $\rho_H^{K\pi}$ to large values, which might not be necessary to explain ΔC . For comparison we depict as brown contours also the ones from Fig. 1b and provide contour lines of constant $\xi_2^H(K\pi)$ and $\xi_3^A(K\pi)$.

We find that the prediction of $\Delta C = -0.11_{-0.02}^{+0.04}$ at the best-fit point $\rho_H^{K\pi} = 3.3 \exp(3.7i)$ coincides, within experimental uncertainties, with the measurement Eq. (IV.6). The preferred phase of $\phi_H^{K\pi} \sim (3\pi/2)$ implies that HS contributions to $\alpha_2^u(K\pi)$ are mainly imaginary and interfere constructively with the imaginary part of the vertex corrections. At the best-fit point, all observables have zero pull values except for a 0.8σ pull in $C(B^- \rightarrow \bar{K}^0\pi^-)$ and R_n^B which had been discarded from the fit.

As can be seen in Fig. 2a, the contours of constant $\xi_2^H(K\pi)$ exhibit a different dependence on $\rho_H^{K\pi}$ as compared to ξ_3^A for $\rho_A^{K\pi}$. Already in the conventional approach ($|\rho_H^{K\pi}| = 1.0$), $\xi_2^H(K\pi) = 1$ is admitted in estimates of theoretical uncertainties, which is a remnant artefact of the parametrization $X_H \sim (1 + \rho_H^{K\pi})$. In the fit this contour line lies within the 95% CR for $1.8 \lesssim |\rho_H^{K\pi}| \lesssim 2.8$ and for the smallest $|\rho_H^{K\pi}| = 1.8$ at $\phi_H^{K\pi} = 4.6$, the pull of ΔC decreases, to -1.0σ , compared to 2.8σ in the SM. Concerning the WA corrections shown in Fig. 2b, $|\rho_A^{K\pi}|$ is shifted towards lower values compared to Fig. 1b, which allows also for smaller $\xi_3^A(K\pi)$. The fit shows that these lower values of $|\rho_A^{K\pi}|$ are correlated with large values of $|\rho_H^{K\pi}|$.

Assuming that HS corrections are in fact responsible for the observed discrepancy in ΔC , similar effects should be observed for related decays, as for example in CP asymmetries $B_d \rightarrow K^0\pi^0$ and analogously $B_s \rightarrow K^0\pi^0$. In the latter decay, such effects should be enhanced due to a different hierarchy of CKM elements $|\lambda_u^{(s)}/\lambda_c^{(s)}| \ll |\lambda_u^{(d)}/\lambda_c^{(d)}|$. The predictions of both CP asymmetries are shown in Fig. 2c and Fig. 2d, respectively, with color coding as in Fig. 2a and Fig. 2b. Once measured, respectively measured with higher precision, both will allow to test the assumption of large HS contributions to $B_{d,s} \rightarrow K\pi$ decays

$$\begin{aligned} C(B_d \rightarrow K^0\pi^0)^{\text{fit } \rho_H} &= +0.14_{-0.05}^{+0.06}, \\ C(B_d \rightarrow K^0\pi^0)^{\text{scan } \rho_H} &\in [-0.04, 0.04], \end{aligned} \quad (\text{IV.9})$$

and

$$\begin{aligned} C(B_s \rightarrow K^0\pi^0)^{\text{fit } \rho_H} &= -0.70_{-0.19}^{+0.20}, \\ C(B_s \rightarrow K^0\pi^0)^{\text{scan } \rho_H} &\in [-0.17, 0.48]. \end{aligned} \quad (\text{IV.10})$$

The predictions labeled “fit ρ_H ” and “scan ρ_H ” are shown in purple and brown respectively, whereas the QCDF prediction for the conventional approach (with scanned ρ_A) are labeled “QCDF” in Fig. 2c and Fig. 2d. At the current stage, the measurement of $C(B_d \rightarrow K^0\pi^0)$ prefers smaller HS contributions although the uncertainty is still too large to draw a definite conclusion.

A similar analysis of enhanced HS contributions [55] has found a best-fit point at $\rho_H^{K\pi} = 4.9 \exp(4.9i)$. Bearing in mind that different numerical input, e.g. $\lambda_B = 0.35$ GeV, has been used, their result lies in the ballpark of our 68% CR. The very recent work [56] also deals with fits of WA and HS parameters $\rho_{A,H}$ in $B \rightarrow PP$ decays ($PP = \pi\pi, K\pi, KK$) in the SM in the framework of QCDF. In our study one $\rho_A^{M_1M_2}$ is considered for each of the three decay systems separately. Instead, in [56] one ρ_A for building block A_3^f (see Eq. (III.6)), ρ_A^f , and one for building blocks $A_1^i \approx A_2^i$, ρ_A^i , are used simultaneously, neglecting thus $SU(3)$ -breaking corrections for all three $b \rightarrow d$ and $b \rightarrow s$ decay systems. Also in this case one finds that ρ_A^f is rather strongly constrained with two solutions similar to the ones shown in Fig. 1. Concerning ρ_H , similar regions are found as in our Fig. 2a in scenario III of [56].

B. Results for $B \rightarrow K\rho, K^*\pi, K^*\rho$

In this section we discuss decay systems obtained from the replacement of a pseudoscalar in $B \rightarrow K\pi$ by its vector meson equivalent $\pi \leftrightarrow \rho$ and $K \leftrightarrow K^*$. Indeed, QCDF implies some qualitative differences when changing the spin of the final state particles, but since the parametrization of the decay amplitudes of all four decay systems is equal, one might expect the discussed features of the $B \rightarrow K\pi$ system to appear also in $B \rightarrow K^*\pi$ (PV), $B \rightarrow K\rho$ (VP)³ and $B \rightarrow K^*\rho$ (VV). Currently the experimental measurements are not as precise as for $B \rightarrow K\pi$, and no striking tensions are found as can be seen from the p values and pulls of observables in Tab. V.

The allowed regions of $\rho_A^{M_1M_2}$ are shown in Fig. 3 for the observable Set I (upper panels) and Set II (lower panels). As before, the 68% and 95% CRs allowed by fits from only $\mathcal{B}/R_{c,n}$ or only $C/\Delta C$ and in addition for $M_1M_2 = VV$ also only f_L are color coded as blue,

³ The classification of decays into $M_1M_2 = PV$ and VP refers to the amplitude $\alpha_4^c(M_1M_2)$, which indeed exclusively occurs in that combination in all decay amplitudes of both decay systems. Nevertheless, some other α_i with $i \neq 4$ also contain contributions in which the pseudoscalar and vector mesons are interchanged.

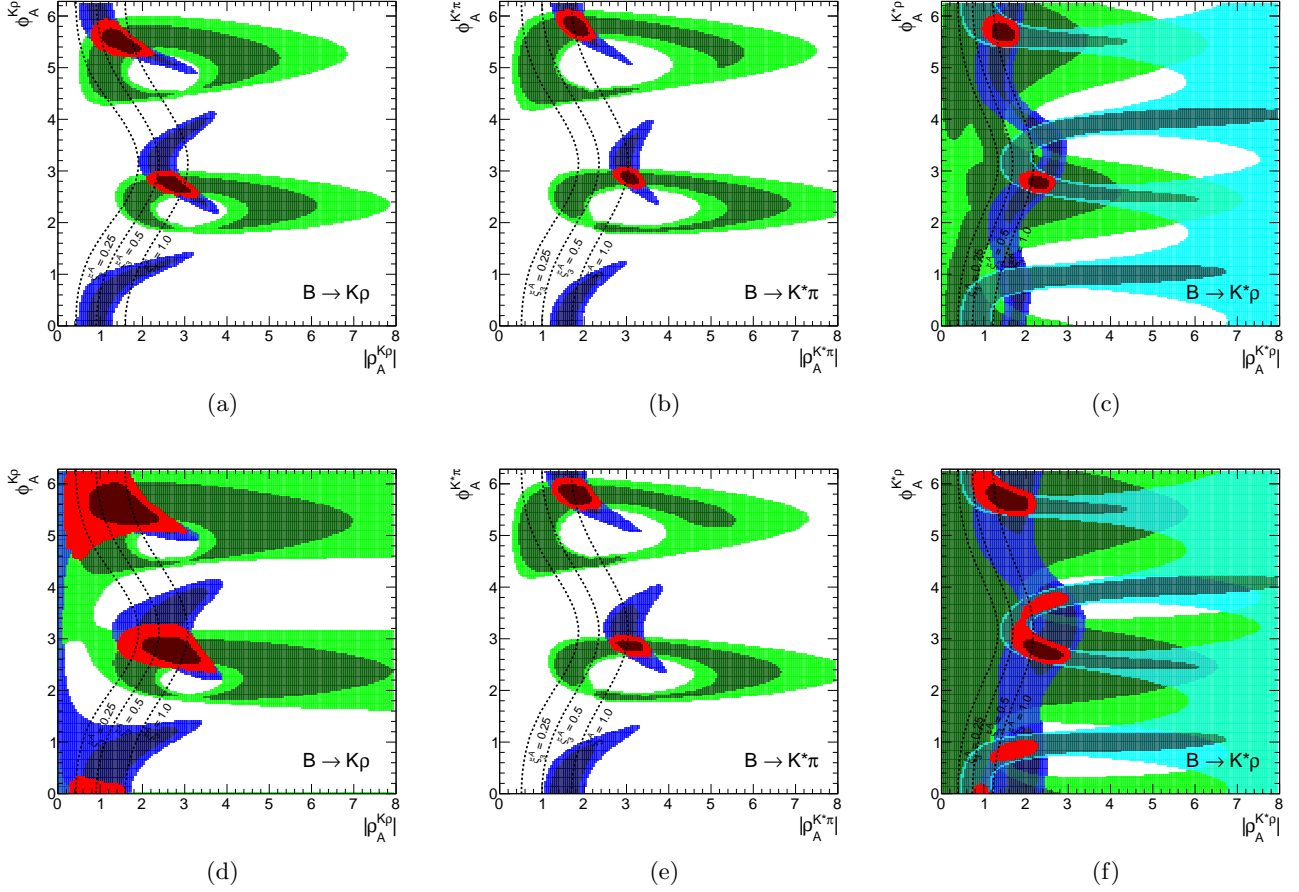


FIG. 3: The 68% (dark) and 95% (bright) CRs of $\rho_A^{M_1 M_2}$ from a fit of observables in Set I (upper) and Set II (lower) of $B \rightarrow K\rho$ (left), $B \rightarrow K^*\pi$ (middle), and $B \rightarrow K^*\rho$ (right). Allowed regions are shown for B and $R_{n,c}$ (blue), C and ΔC (green), f_L (cyan) and their combination (red). The dashed lines correspond to constant $\xi_3^A = (0.25, 0.5, 1.0)$ from left to right.

green and cyan, whereas the combined regions are depicted in red. As in the case of $B \rightarrow K\pi$, the combined constraints on $\rho_A^{M_1 M_2}$ from Set I and Set II observables are compatible with each other, but more stringent from Set I, especially for $B \rightarrow K\rho$ and $B \rightarrow K^*\rho$. Remarkably, the data of all four decay systems $M_1 M_2 = K\pi, K^*\pi, K\rho, K^*\rho$ prefers the same regions of $\phi_A^{M_1 M_2} \sim \pi, 2\pi$, excluding large destructive interference of $\alpha_4^c(M_1 M_2)$ and $\beta_3^c(M_1 M_2)$. There is overlap at the 68% probability level for all three systems for the solution $\phi_A \sim 2\pi$ and at 95% probability for $\phi_A \sim \pi$. This is also supported by the data of f_L in $B \rightarrow K^*\rho$, where the measurements of CP asymmetries are not very precise yet and otherwise no stringent constraints on $\rho_A^{K^*\rho}$ could have been obtained from branching fraction measurements alone.

The relative amount of power corrections to the leading contribution for PV, VP and VV final states is collected in Tab. IV and indicated in Fig. 3 by contour lines of constant $\xi_3^A(M_1 M_2) = 0.25, 0.5, 1.0$. It is typically larger by a factor of 2–3 compared to the PP final state

in $B \rightarrow K\pi$, which is a qualitative feature of QCDF. The leading QCD-penguin flavor amplitude is a linear combination of the vector amplitude, a_4 , and the chirally enhanced scalar QCD-penguin amplitude, a_6 , [5]

$$\alpha_4(M_1 M_2) = a_4(M_1 M_2) \pm r_\chi^{M_2} a_6(M_1 M_2) \quad (\text{IV.11})$$

where the “+” sign applies to $M_1 M_2 = PP, PV$ and the “−” sign to $M_1 M_2 = VP, VV$ final states. The two contributions interfere destructively in the case $M_1 M_2 = VP$ leading to smaller QCD-penguin amplitudes than for $M_1 M_2 = PP$. Further, the tree level contribution to $a_6(M_1 M_2)$ vanishes for $M_2 = V$, again reducing α_4 in $M_1 M_2 = PV, VV$ compared to $M_1 M_2 = PP$ giving implicitly rise to larger ratios $\xi_3^A(M_1 M_2)$. Values as low as $\xi_3^A(K\rho) = 0.50$, $\xi_3^A(K^*\pi) = 0.82$ and $\xi_3^A(K^*\rho) = 0.93$ can be reached within the 68 % CRs of Set I observables, whereas even smaller values are allowed from Set II, see Tab. IV. Concerning decays with K^* in the final state, the largish values of ξ_3^A are required mainly by measurements of branching fractions, whereas CP asymmetries

and polarization fractions f_L would allow for smaller values of ξ_3^A , see Fig. 3b and Fig. 3c.

The largest pull values arise for CP asymmetries $C(B^- \rightarrow \bar{K}^{*0}\pi^-)$ with $+1.0\sigma$ and $C(B^- \rightarrow \bar{K}^0\rho^-)$ with $+0.7\sigma$. As in the case of $C(B^- \rightarrow \bar{K}^0\pi^-)$, these CP asymmetries almost vanish in QCDF and it is difficult to increase the predictions beyond 1%, even in the presence of large power corrections.

The advantage of observable Set II strongly depends on cancellation of theory uncertainties, as for example the form factors in the ratios of branching fractions. Especially in cases where WA contributions are large compared to the leading amplitude, i.e., large ξ_3^A , the reduction of uncertainties is less effective and there is no unambiguous preference for the use of either Set I nor Set II. Furthermore, the outcome of fits of Set I and Set II might differ depending strongly on the experimental measurements. Apart from that we are not aware of a specific reason for the qualitative differences between fits of Set I and Set II for the $B \rightarrow K\pi$, $K^*\pi$ systems compared to $B \rightarrow K\rho$, $K^*\rho$ systems. As can be seen from Tab. V, pull values from Set II are in general slightly larger than from Set I.

C. Other decays and comments on $B \rightarrow K\omega$, $K^*\phi$

We tested our assumption of universal WA also with data listed in Tab. I, Tab. II and Tab. III for other QCD-penguin dominated decay modes mediated by $b \rightarrow (d, s)$ transitions. For these decays, the analysis is restricted to observable Set I, where in most cases the experimental accuracy is poorer than for previously studied $B \rightarrow K\pi$, $K\rho$, $K^*\pi$, $K^*\rho$ systems. The ranges for the ratios $\xi_3^A(M_1M_2)$ that are required by data are listed in Tab. IV, which have been commented previously. For all systems, again preferred regions appear for $\phi_A^{M_aM_b} \sim \pi$, 2π , and in some cases also $\phi_A^{M_aM_b} \sim \pi/2$, $(3\pi/2)$ is still allowed.

The allowed regions for $B \rightarrow PP$ systems $B \rightarrow KK$, $K\eta'$ and $B_s \rightarrow KK$ are shown in Fig. 4 and for $B_s \rightarrow K^-\pi^+$ in Fig. 1c. We do not show $B \rightarrow K\eta$ for which the data is even less constraining. Except for $B_s \rightarrow K^-\pi^+$, the measurements of CP asymmetries are very poor and provide only little additional constraints to the ones of branching fractions. The preferred regions of WA contributions for $B_{d,s} \rightarrow KK$ look very alike supporting the assumption of universal WA for B_d and B_s decays into same final states, entertained in Sec. IV E. In comparison, for $B_{d,s} \rightarrow K\pi$ (Fig. 1a and Fig. 1c) this might not seem the case, however here one should compare the result of the fit to $B_d \rightarrow K^-\pi^+$ only rather than the combination of all $B \rightarrow K\pi$ decays shown in Fig. 1a and Fig. 1b.

In Fig. 5 the allowed regions for $B \rightarrow VP$ systems $B \rightarrow K\omega$, $K\phi$, $K^*\eta'$ are shown, whereas $B \rightarrow K^*\eta'$ has been omitted due to the poor constraints from the respective data. The measurements of branching frac-

tions provide in all three cases already appreciable constraints. Concerning $B \rightarrow K\omega$, no tensions are observed. In case of $C(\bar{B}^0 \rightarrow \bar{K}^0\omega^0)$, we included the HFAG average of the two incompatible measurements of Belle: $C = 0.36 \pm 0.19 \pm 0.05$ [29] and BaBar: $C = -0.52^{+0.22}_{-0.20} \pm 0.03$ [57], which differ by 2.9σ . The HFAG value $C = -0.04 \pm 0.14$ [19] indeed coincides with the theory prediction at the best-fit point ($C = -0.02 \pm 0.08$). One might hope that improved measurements at Belle II will settle this problem. As $\Delta C(K\pi)$, this CP asymmetry is sensitive to the analogous color-suppressed tree amplitude $\alpha_2^u(K\omega)$ and might provide further tests of large HS contributions, which would be clearly visible. As in fact the largest uncertainty in the theory prediction is due to $\rho_H^{K\omega}$. It must be noted that although the best-fit point at $\rho_A^{K\omega} = 4.2 \exp(i1.7)$ corresponds to a large $\xi_3^A(K\omega) = 2.7$, other solutions at 68% probability with $\xi_3^A(K\omega) \lesssim 1$ provide equally vanishing pulls of observables.

Finally, the allowed regions for $B \rightarrow VV$ systems $B \rightarrow K^*K^*$, $K^*\phi$, $K^*\omega$ and $B_s \rightarrow K^*K^*$, $K^*\phi$, $\phi\phi$ are shown in Fig. 6. For $MM = K^*K^*$ final states the measurements of branching fractions require rather large WA contributions, contrary to the other considered VV final states. In all cases, the polarization fractions provide orthogonal constraints, which prefer $\phi_A^{M_aM_b} \sim \pi$, 2π , except for $B \rightarrow K^*K^*$. For the moment measurements of CP asymmetries are only available for $B \rightarrow K^*\omega$ and the very recent LHCb measurements for $B \rightarrow K^*\phi$ [38]. They are compatible with zero and do not provide constraints yet since the theory predicts also rather small values.

Concerning $B \rightarrow K^*\phi$, we include in addition also available measurements of relative amplitude phases $\phi_{\perp,\parallel}$ (purple). The combined allowed region from all observables does not overlap with regions from only branching fractions nor only amplitude phases at 68% probability, giving rise to large pull values of the branching fraction $\mathcal{B}(B^0 \rightarrow K^{*0}\phi)$: 1.7σ from BaBar [36] and 2.6σ from Belle [37]; for $C_L(B^- \rightarrow K^{*-}\phi)$ of -1.5σ from HFAG [19]; for $C_{\perp}(\bar{B}^0 \rightarrow \bar{K}^{*0}\phi)$ of 1.2σ from Belle [37], but not for BaBar (0.2σ) and LHCb (-0.6σ); and for $\phi_{\perp}(\bar{B}^0 \rightarrow \bar{K}^{*0}\phi)$ of 1.1σ from LHCb [38], but not for BaBar and Belle (both 0.0σ). However, the p value of 0.95 of the fit is very high as we include many other measurements that are described consistently in the fit.

Due to a hierarchy of the helicity amplitudes in QCDF $A_L : A^- : A^+ = 1 : 1/m_b : 1/m_b^2$ [23] for the SM operator basis Eq. (III.2) the following relation should hold

$$\phi_{\perp} = \phi_{\parallel}. \quad (\text{IV.12})$$

The experimental situation supports this within current errors. Since the hierarchy of helicity amplitudes does not hold in the presence of chirality-flipped operators beyond the SM, the measurement provides strong constraints on such scenarios. Further, QCDF predicts only small differences for neutral and charged decay modes such that one expects similar predictions for observables in both

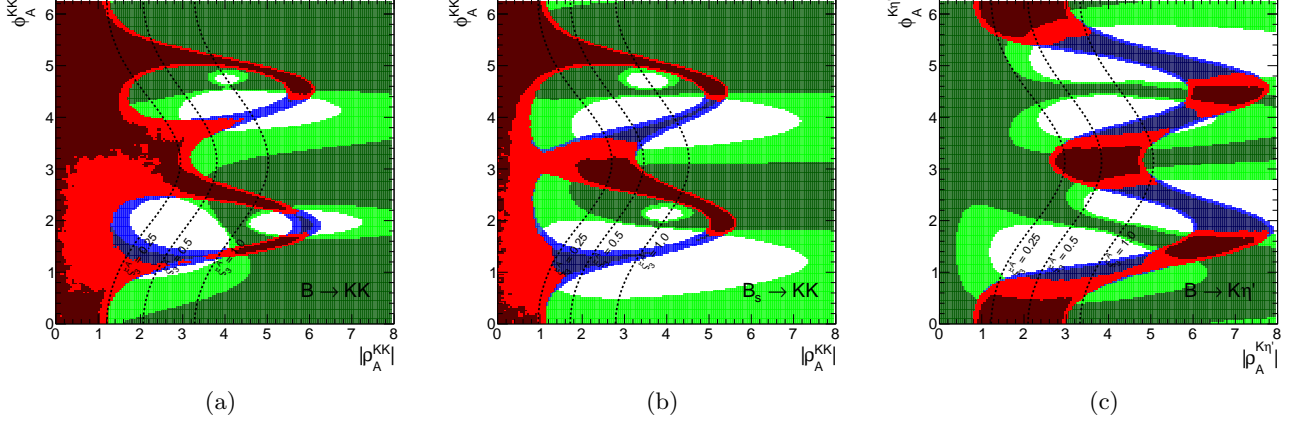


FIG. 4: The 68% (dark) and 95% (bright) CRs of $\rho_A^{M_1 M_2}$ from a fit of observables in $B \rightarrow PP$: (a) $B \rightarrow KK$ (penguin dominated), (b) $B_s \rightarrow KK$ and (c) $B \rightarrow K\eta'$. Allowed regions are shown for \mathcal{B} (blue), \mathcal{C} (green) and their combination (red). The dashed lines correspond to constant $\xi_3^A = (0.25, 0.5, 1.0)$.

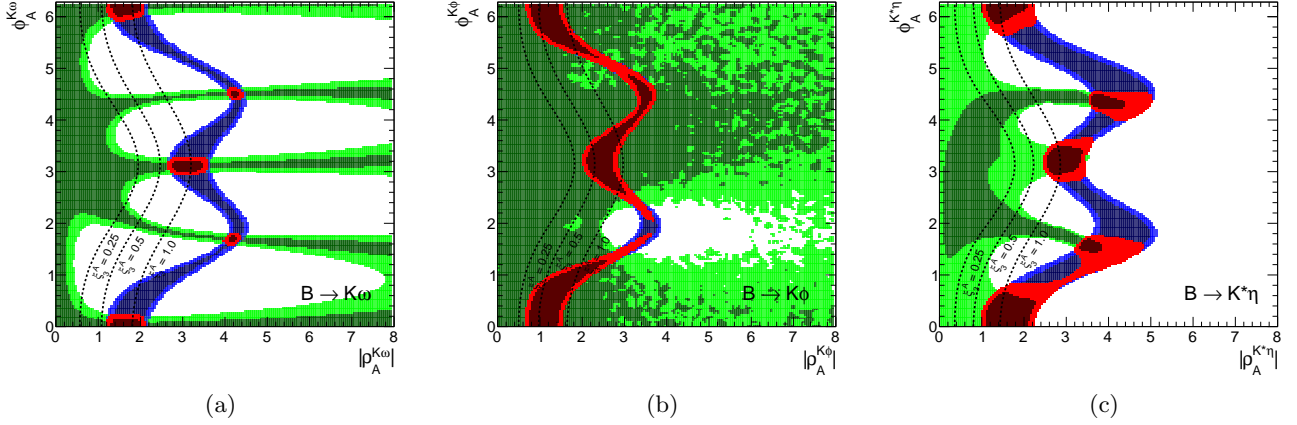


FIG. 5: The 68% (dark) and 95% (bright) CRs of $\rho_A^{M_1 M_2}$ from a fit of observables in $B \rightarrow PV$: (a) $B \rightarrow K\omega$, (b) $B \rightarrow K\phi$ and (c) $B \rightarrow K^*\eta$. Allowed regions are shown for \mathcal{B} (blue), \mathcal{C} (green) and their combination (red). The dashed lines correspond to constant $\xi_3^A = (0.25, 0.5, 1.0)$.

modes, even in the presence of NP contributions.

D. WA dominated $B \rightarrow K^+ K^-$ and $B_s \rightarrow \pi^+ \pi^-$

So far we discussed decays that are dominated by QCD-penguin topologies. They share the feature that leading WA contributions $\beta_3^S(M_1 M_2)$ are dominated by the building block A_3^f (see Eq. (III.6)), which originates from gluon emission off the quark current in the final state. Furthermore, we grouped the decays that are related by $(u \leftrightarrow d)$ -quark exchange, and assumed for each group one universal WA parameter ρ_A .

Now we are interested in decay modes that are governed solely by WA topologies. The only measured systems are so far $B \rightarrow K^+ K^-$ and $B_s \rightarrow \pi^+ \pi^-$. Their

amplitudes are given by

$$\begin{aligned} \mathcal{A}(B \rightarrow K^+ K^-) &\simeq f_{B_d} f_K^2 \sum_p \lambda_p^{(d)} B_{K^+ K^-}^p, \\ \mathcal{A}(B_s \rightarrow \pi^+ \pi^-) &\simeq f_{B_s} f_\pi^2 \sum_p \lambda_p^{(s)} B_{\pi^+ \pi^-}^p, \end{aligned} \quad (\text{IV.13})$$

with

$$B_{M_1 M_2}^p = \left(\delta_{pu} b_1 + 2b_4^p + \frac{1}{2} b_{4,\text{EW}}^p \right). \quad (\text{IV.14})$$

Since they are independent of quantities like form factors and the inverse moment of the B -meson DA, which cause usually large uncertainties, the precision of the determination of $\rho_A^{M_1 M_2}$ from the fit is mainly dictated by the experimental precision. The involved coefficients $b_i(M_1 M_2)$

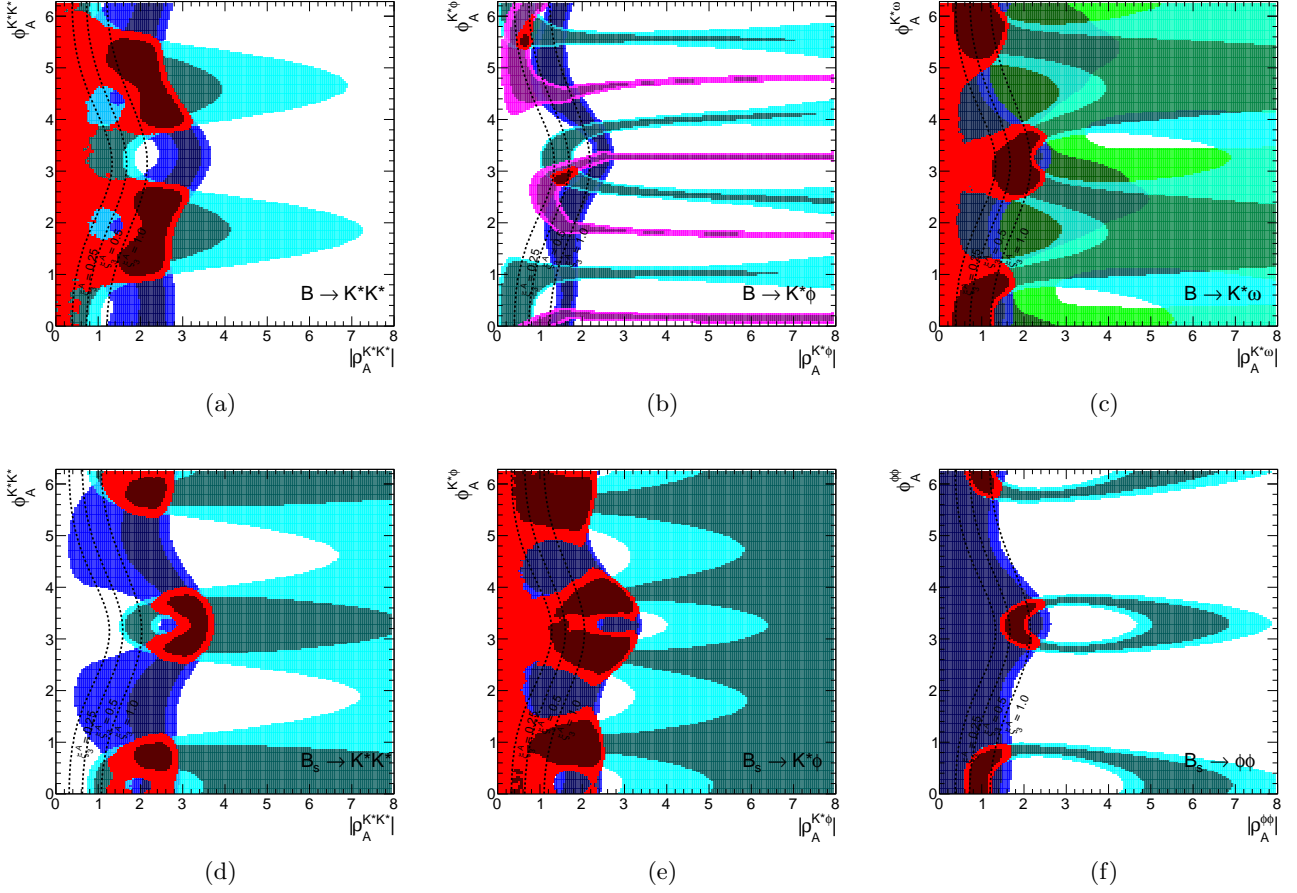


FIG. 6: The 68% (dark) and 95% (bright) CRs of $\rho_A^{M_1 M_2}$ from a fit of observables in $B \rightarrow VV$: (a) $B \rightarrow K^* K^*$, (b) $B \rightarrow K^* \phi$, (c) $B \rightarrow K^* \omega$ and (d) $B_s \rightarrow K^* K^*$, (e) $B_s \rightarrow K^* \phi$, (f) $B_s \rightarrow \phi \phi$. Allowed regions are shown for \mathcal{B} (blue), C_h (green), f_h (cyan), ϕ_h (purple) and their combination (red). The dashed lines correspond to constant $\xi_3^A = (0.25, 0.5, 1.0)$ from left to right.

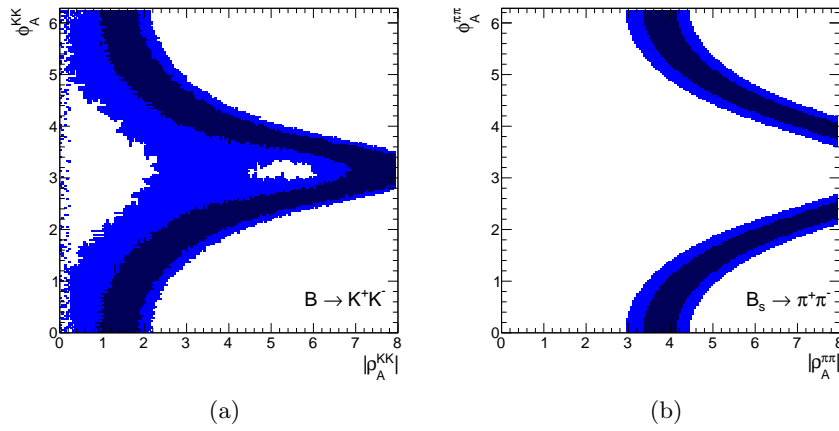


FIG. 7: The 68% (dark) and 95% (bright) CRs for $\rho_A^{M_1 M_2}$ obtained from the branching fraction of WA dominated decays (a) $B \rightarrow K^+ K^-$ and (b) $B_s \rightarrow \pi^+ \pi^-$.

depend exclusively on the building blocks $A_{1,2}^i(M_1M_2)$ (see Eq. (III.6)) where the gluon is emitted off the quark current of the initial state, and are thus in principle different from A_3^f that dominates the penguin-dominated decays. Moreover, $A_1^i \approx A_2^i$ for $MM = PP$ final states when restricting to the asymptotic forms of the light-meson DAs [5].

The contours of $\rho_A^{K^+K^-}$ and $\rho_A^{\pi^+\pi^-}$ from the branching fraction measurement are shown in Fig. 7a and Fig. 7b, respectively. Contrary to the penguin-dominated decays, the shape of the contour from the branching fractions is different, reaching large values $|\rho_A^{M_1M_2}|$ for phases $\phi_A^{M_1M_2} \sim \pi$, whereas for $\phi_A^{M_1M_2} \sim 0$ the absolute value can be restricted: $|\rho_A^{K^+K^-}| \in [0.9, 1.9]$ and $|\rho_A^{\pi^+\pi^-}| \in [3.4, 4.1]$ at 68% probability. While it is possible to have $|\rho_A^{K^+K^-}| \lesssim 2$ for small phases, as is the case for the previously considered penguin-dominated decays, the data requires $|\rho_A^{\pi^+\pi^-}| \gtrsim 3$ for any value of $\phi_A^{\pi^+\pi^-}$, and indeed, the contours of $\rho_A^{K^+K^-}$ and $\rho_A^{\pi^+\pi^-}$ do not overlap within the 95% CR. Our results are in agreement with similar fits [58].

Apart from the mismatch of WA contributions for different initial and final states, there might be another interesting aspect, which can be studied in these decays. Namely, the amplitudes Eq. (IV.13) are proportional to one overall CP conserving strong phase due to the fact that the single amplitudes $b_i^p(M_1M_2)$ (see Eq. (III.6)) depend on the same CP-conserving strong phase of A_1^i due to the aforementioned relation $A_1^i \approx A_2^i$. Hence Eq. (IV.14) becomes

$$B_{PP}^p \approx \frac{C_F}{N_c^2} A_1^i \left(\delta_{pu} C_1 + 2(C_4 + C_6) + \frac{C_{10} + C_8}{2} \right). \quad (\text{IV.15})$$

This is contrary to the requirement of at least one relative strong phase between the CP conserving and CP violating part of the amplitude in order to have a non-vanishing CP asymmetry. Since QCDF predicts vanishing CP asymmetries, up to even further suppressed power corrections, no complementary information can be gained on the phases ϕ_A apart from the one of the branching fractions. An observation of direct CP violation would put into question the regularization of endpoint divergences Eq. (III.8) introduced in QCDF.

The measurement of other WA dominated decay modes with PV and VV final states can help to further scrutinize WA contributions. For example for $M_1M_2 = PV$, one has $A_1^i \approx -A_2^i$ [5] yielding

$$B_{PV}^p \approx \frac{C_F}{N_c^2} A_1^i \left(\delta_{pu} C_1 + 2(C_4 - C_6) + \frac{C_{10} - C_8}{2} \right), \quad (\text{IV.16})$$

whereas for $MM = VV$ final states $A_1^{i,h} \approx A_2^{i,h}$ ($h = L, +, -$) [23]. In the SM, the Wilson coefficients interfere destructively for $MM = PV$ and constructively in

$MM = (PP, VV)$ decay modes. These decays are in principal sensitive to physics beyond the SM in O_1 and the color-octet operators $O_{4,6,8,10}$.

E. Universal WA for B_d and B_s decays to same final states

So far, we have assumed one universal parameter for WA contributions of QCD-penguin dominated decays that are related by ($u \leftrightarrow d$)-quark exchange, i.e., those groups of decays gathered in Tab. I, Tab. II and Tab. III. For the purpose of this section, we will study effects which arise from the additional assumption of a universal WA parameter ρ_A for decays into same final states mediated by the same quark currents at the weak interaction vertex. This implies in general relations between $|\Delta S| = 1$ and $|\Delta D| = 1$ decays.

In QCDF this assumption might be justified bearing in mind that WA contributions in QCD-penguin dominated decay amplitudes are numerically dominated by topologies in which the gluon is emitted from the quark current that hadronizes into the final states, namely A_3^f in Eq. (III.6). In this case the momentum transfer from the initial B meson is solely present at the weak interaction vertex, rendering the final-state hadronization independent of the flavor of the initial-state spectator quark. Therefore, one can expect that the difference between WA amplitudes in $B_d \rightarrow M_a M_b$ and $B_s \rightarrow M_a M_b$ decays might be of the order $\sim (m_{B_s} - m_{B_d})/m_{B_s} \approx m_s/m_b$. Similar arguments had been presented for the decays $B_d \rightarrow K^+\pi^-$ and $B_s \rightarrow K^+\pi^-$ in [59].

Currently experimental information is limited for B_s decays to final states $M_a M_b = K\pi, KK, K^*\phi, K^*K^*$, whereas for $M_a M_b = \phi\phi$ the corresponding measurements for the B_d is lacking. We do not consider $B_s \rightarrow \pi^+\pi^-$, which is WA-dominated and was discussed in Sec. IV D, and further the corresponding $B_d \rightarrow \pi^+\pi^-$ decay is tree-dominated. For $B_{d,s} \rightarrow KK$, the 68% CRs overlap nicely as can be seen from the comparison of Fig. 4a and Fig. 4b. In the case of $B_{d,s} \rightarrow K^*K^*$, branching-fraction measurements are compatible, but regions from polarization-fraction measurements that are favored for B_d decays are excluded for B_s decays as shown in Fig. 6a and Fig. 6d. In consequence, 68% CRs in $B_{d,s} \rightarrow K^*K^*$ overlap only marginally.

This leaves us mainly with the final state system $K\pi$ to explore in more detail the consequences of the assumption of universal WA in decays with same final states, since for $K^*\phi$ the experimental information for the B_s decay is not yet accurate enough to derive conclusive insights on this assumption. Especially we would like to test whether the CP asymmetry $C(B_s \rightarrow K^+\pi^-)$, which had been measured recently by CDF [60] and LHCb [61], can be predicted correctly from WA contributions determined in $B \rightarrow K\pi$ decays.

As discussed before in Sec. IV A, the fit for $B \rightarrow K\pi$ does not allow for a simultaneous explanation of the two

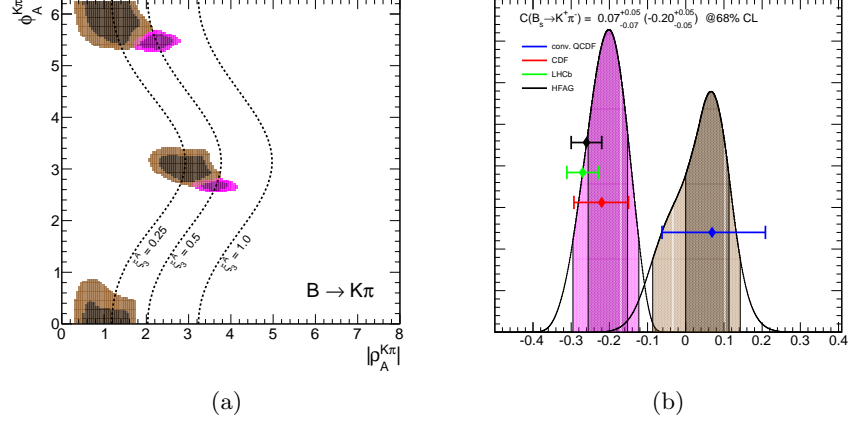


FIG. 8: The 68% (dark) and 95% (bright) CRs for $\rho_A^{K\pi}$ (left), obtained from a fit with the reduced observable set for $B^- \rightarrow K^- \pi^0$ (brown) and $B_d \rightarrow K^+ \pi^-$ (purple) (see text) assuming the SM. The dashed lines correspond to constant $\xi_3^A(K\pi) = (0.25, 0.5, 1.0)$. The right panel shows the predictions for the direct CP asymmetry $C(B_s \rightarrow K^+ \pi^-)$ for the two fit regions of $\rho_A^{K\pi}$ in the left panel using the same color-coding. Experimental results are shown with 1σ errors and the prediction from QCDf with conventional uncertainty estimates is labeled “QCDf”.

CP asymmetries $C(B^- \rightarrow K^- \pi^0)$ and $C(\bar{B}^0 \rightarrow K^- \pi^+)$. For this purpose we determine $\rho_A^{K\pi}$ separately from the combination of the branching fraction and CP asymmetry for each of the two contradicting decays. In addition we used $R_c^K(K\pi)$ to suppress solutions from the large WA scenario. The best-fit regions of $\rho_A^{K\pi}$ are shown in Fig. 8a where the contour from $\bar{B}^0 \rightarrow K^- \pi^+$ coincides nicely with the one in Fig. 1b, where all constraints had been combined, due to the higher statistical weight of $C(\bar{B}^0 \rightarrow K^- \pi^+)$. We note that $|\rho_A^{K\pi}| > 1$ does originate from the precise measurement of $C(\bar{B}^0 \rightarrow K^- \pi^+)$, contrary to $C(B^- \rightarrow K^- \pi^0)$ that allows also smaller values of $|\rho_A^{K\pi}|$ as can be seen in Fig. 8a.

Based on our assumption, we predict from both fits the CP asymmetry $C(B_s \rightarrow K^+ \pi^-)$, see App. B 4 for details. As shown in Fig. 8b, the measurements agree with the prediction from the $(K^- \pi^+)$ -fit whereas it fails at more than 4σ for the $(K^- \pi^0)$ -fit. In this case data supports the assumption that WA might be universal for decays with the same final states. It will be interesting to test these assumption further against improved measurements in the future. On the other hand this result shows that giving up the universality of the WA parameter for final states related by $(u \leftrightarrow d)$ exchange, but still insisting on a universal parameter for same final states would also resolve the “ $\Delta\mathcal{A}_{CP}$ puzzle”.

V. NEW PHYSICS SCENARIOS

In the framework of the SM, our analysis in the previous Sec. IV has shown that the data of all investigated systems can be described with one universal WA parameter per system of decays that are related by $(u \leftrightarrow d)$ quark exchange, apart from stronger tensions

in $B \rightarrow K\pi$ and in $B \rightarrow K^* \phi$. This section is devoted to the attempt to constrain new-physics parameters in fits of the data simultaneously with the determination of one universal WA parameter per system using data from $B \rightarrow K\pi$, $K\rho$, $K^* \pi$, $K^* \rho$, and $K^* \phi$, i.e., in total five WA parameters $\rho_A^{M_a M_b}$. In the presence of additional degrees of freedom of the NP parameters, one can expect that tensions present in the SM fit will be relaxed and the size of power corrections (ξ_3^A) can be decreased further.

We choose a model-independent approach, assuming NP contributions to Wilson coefficients of operators present in the SM operator basis Eq. (III.1) and their chirality-flipped counterparts obtained by $(1 - \gamma_5) \leftrightarrow (1 + \gamma_5)$ interchange. The $B \rightarrow M_1 M_2$ matrix elements of the chirality-flipped operators can be obtained from the non-flipped ones via parity transformations [62]

$$\langle M_1 M_2 | O'_i | B \rangle = -\eta_{M_1 M_2} \langle M_1 M_2 | O_i | B \rangle \quad (\text{V.1})$$

with $\eta_{M_1 M_2} = +1$ for $M_1 M_2 = PP, VV$ final states and $\eta_{M_1 M_2} = -1$ for $M_1 M_2 = PV, VP$ final states. In this case $b'_i(M_1 M_2) = b_i(M_1 M_2)[C_i \rightarrow C'_i]$, see Eq. (III.6), and analogous relations hold for $a'_i(M_1 M_2)$. In the case of positive/negative polarized final states, form factors and decay amplitudes have to be replaced by their helicity-flipped counterpart e.g., $F_\pm \leftrightarrow F_\mp$ and $A_\pm(M_1 M_2) \leftrightarrow A_\mp(M_1 M_2)$.

In Sec. V A we explore new physics contributions to the Wilson coefficients of color-singlet QED-penguin Wilson coefficients $C_{7,9}$ and their chirality-flipped counterparts $C'_{7,9}$. They are well-known solutions of the “ $\Delta\mathcal{A}_{CP}$ puzzle” in $B \rightarrow K\pi$ [63, 64] and here we further investigate the compatibility of such NP contributions with data of the four other aforementioned decay systems. As a second model-independent scenario we consider NP contributions in the Wilson coefficients of the tree-level

$b \rightarrow s \bar{u}u$ operators in Sec. VB. In the SM, they are doubly Cabibbo-suppressed $\sim \lambda_u^{(s)}/\lambda_c^{(s)}$ in all CP-averaged observables in $b \rightarrow s$ transitions, but give leading contributions to CP asymmetries. The investigation of further scenarios that involve also complementary constraints from exclusive $b \rightarrow s(\gamma, \ell\ell)$ decays are given in [65].

A. NP in QED penguins

The QED-penguin operators $O_{7,\dots,10}$, see Eq. (III.1), and their chirality-flipped counterparts $O'_{7,\dots,10}$ are isospin-violating. Compared to the SM, NP contributions can relax the encountered tensions in $\Delta C(K\pi)$ and $R_n^B(K\pi)$ and here we combine $B \rightarrow K\pi$ data with additional measurements from the aforementioned decay systems. We will focus on the color-singlet operators $i = 7, 7', 9, 9'$ since the matching contributions to Wilson coefficients of the color-octet operators $i = 8, 8', 10, 10'$ are suppressed by the strong coupling α_s . Moreover, in the SM the chirality structure yields very small C_7 and large C_9 , which must not be the case for NP scenarios. Depending on the final state, the two linear combinations $\bar{C}_i \equiv (C_i + C'_i)$ and $\Delta C_i \equiv (C_i - C'_i)$ can be tested in $MM = PV$ and $MM = PP$, $V_L V_L$, respectively.

We introduce NP contributions to the Wilson coefficients at the matching scale $\mu_0 = M_W$ that we set to the mass of the W -boson and for practical purposes we rescale them with the SM value $C_9^{\text{SM}}(\mu_0) = -1.01\alpha_e$

$$C_i(\mu_0) = C_i^{\text{SM}}(\mu_0) + |C_9^{\text{SM}}(\mu_0)| \mathcal{C}_i \quad (\text{V.2})$$

for $i = 7, 7', 9, 9'$. We consider several sub-scenarios

- single operator dominance
Sc- i : $C_i \neq 0$ and $C_{j \neq i} = 0$ for $i = 7, 7', 9, 9'$
- parity (anti-)symmetric scenario
Sc-77' : $C_{7,7'} \neq 0$ and $C_{9,9'} = 0$
Sc-99' : $C_{9,9'} \neq 0$ and $C_{7,7'} = 0$
- (axial-)vector coupling scenario
Sc-79 : $C_{7,9} \neq 0$ and $C_{7',9'} = 0$
Sc-7'9' : $C_{7',9'} \neq 0$ and $C_{7,9} = 0$
- generic scenario
Sc-77'99' : $C_i \neq 0$

with complex-valued \mathcal{C}_i . Although we introduce a NP parameterization at the matching scale, RG evolution will not lead to mixing of QED penguin operators into QCD and tree-level operators $i = 1, \dots, 6$ at the order considered here. Thus NP contributions will not modify the leading amplitude $\hat{\alpha}_4^c$, but only $\alpha_{3(4),\text{EW}}^p$ and the WA amplitudes $\beta_{3(4),\text{EW}}^p$. Consequently, branching fractions will become modified only slightly, whereas CP asymmetries can deviate substantially from their SM predictions for nonzero CP violating phases.

As long as NP contributions do not become very large compared to $\hat{\alpha}_4^c$ one might still employ the expansion in small mode-dependent ratios

$$r_i = r_{i,\text{SM}} + \sum_j r_{i,j} \bar{\mathcal{C}}_j, \quad (\text{V.3})$$

see Eq. (IV.2), in which the NP contributions r_i depend linearly on the complex NP parameters $\mathcal{C}_j \equiv |\mathcal{C}_j| e^{i\delta_j}$. In particular [15]

$$\begin{aligned} C(B^- \rightarrow \bar{K}^0 \pi^-) &\simeq \sum_{j=7,9} \text{Im} \left(\frac{2}{3} r_{\text{EW},j}^{\text{C}} - \frac{4}{3} r_{\text{EW},j}^{\text{A}} \right) \text{Im} \bar{\mathcal{C}}_j, \\ \Delta C - \Delta C^{\text{SM}} &\simeq \sum_{j=7,9} \text{Im} (-2r_{\text{EW},j} - 2r_{\text{EW},j}^{\text{A}}) \text{Im} \bar{\mathcal{C}}_j. \end{aligned} \quad (\text{V.4})$$

Numerically one has approximately

$\text{Im}(r_{i,j}) \times 10^2$	$j = 7$	$j = 9$
$i = \text{EW}$	$2.0^{+0.7}_{-0.8}$	$-2.0^{+0.8}_{-0.7}$
$i = \text{EW,C}$	$-1.7^{+0.6}_{-0.5}$	$0.3^{+1.2}_{-1.2}$
$i = \text{EW,A} (\rho_A^{\text{fit}})$	$6.5^{+0.5}_{-0.5}$	-0.06 ± 0.04
$i = \text{EW,A} (\rho_A^{\text{scan}})$	$0.8^{+5.4}_{-7.4}$	$0.1^{+0.9}_{-0.9}$

(V.5)

in which we used the best-fit point of $\rho_A^{K\pi}$ that was obtained from the SM fit with Set II in the case of $i \in (\text{EW}; \text{EW,C})$ and no variation of $\phi_A^{K\pi}$ is included in the determination of theory uncertainties. The case of $r_{\text{EW},j}^{\text{A}}$ is more involved due to the explicit dependence on the WA parameter and we provide two points: *i*) for $\rho_A^{K\pi}$ obtained from the SM fit as above, denoted as ρ_A^{fit} in Eq. (V.5) and *ii*) for $\phi_A^{K\pi} = 0$, denoted as ρ_A^{scan} in Eq. (V.5), as usually chosen in conventional QCDF as central value including the variation of $\phi_A^{K\pi}$ into the error estimation. Several observations can be made:

1. Given that $\text{Im} \bar{\mathcal{C}}_{7,9} \sim \mathcal{O}(1)$, the numerical coefficients imply that the total amount of CP violation from $r_{i,j}$ of $i \in (\text{EW}; \text{EW,C})$ does not exceed 3.5%, whereas $r_{\text{EW},9}^{\text{C}}$ is numerically negligible.
2. An accidental cancellation can be observed in $(r_{\text{EW},7} + r_{\text{EW},7}^{\text{C}})$ as well as in $(r_{\text{EW},7} + r_{\text{EW},9})$ if $\text{Im} \bar{\mathcal{C}}_7 \approx \text{Im} \bar{\mathcal{C}}_9$.
3. The amount of CP violation from $\text{Im} \bar{\mathcal{C}}_9$ to r_{EW}^{A} can be neglected in both cases *i*) and *ii*), whereas the contribution of $\text{Im} \bar{\mathcal{C}}_7$ can indeed become large.
4. Since the measurement of $C(B^- \rightarrow \bar{K}^0 \pi^-) = (1.5 \pm 1.9)\%$ is rather accurate, it forbids too large CP-violating contributions from $\text{Im} \bar{\mathcal{C}}_7$ if ρ_A is fitted.

We start the discussion of our results with the confrontation of our procedure of fitting simultaneously NP and WA parameters, with the conventional QCDF approach, where only NP parameters are fitted and WA

	$\text{Re}(\mathcal{C}_i^{(\prime)})$ $\text{Im}(\mathcal{C}_i^{(\prime)})$	$\Delta C(K\pi)$	$R_n^B(K\pi)$	$C_L(K^{*-}\phi)$	$\mathcal{B}(\bar{K}^{*0}\phi)$	$f_L(K^{*-}\rho^0)$	$R_n^B(K^*\pi)$	$R_n^B(K^*\rho)$	$\Delta\chi^2(\text{SM})$
SM		-2.8σ	-1.9σ	-1.5σ	$1.7/2.6\sigma$	0.9σ	0.6σ	0.6σ	
Sc-7	1.01, -0.04	-0.7σ	-0.8σ	-1.6σ	$0.3/1.2\sigma$	1.0σ	0.0σ	1.1σ	18.7
Sc-7'	-0.95, 0.02	-0.8σ	-0.8σ	-1.6σ	$1.2/2.1\sigma$	1.2σ	0.0σ	0.9σ	12.8
Sc-9	0.28, 0.19	-2.7σ	0.0σ	-1.3σ	$1.7/2.6\sigma$	1.0σ	1.1σ	0.7σ	1.5
Sc-9'	-0.40, -0.27	-2.6σ	0.0σ	-1.2σ	$1.6/2.5\sigma$	1.1σ	0.0σ	0.6σ	3.6
Sc-77'	1.94, 0.12 -1.65, 0.03	0.0σ	0.0σ	-1.5σ	$0.0/0.0\sigma$	0.8σ	0.3σ	1.6σ	23.9
Sc-99'	-0.05, 2.15 -0.42, 1.64	-2.2σ	0.0σ	-0.6σ	$1.6/2.5\sigma$	0.9σ	1.6σ	0.7σ	9.7
Sc-79	1.02, -0.02 0.06, 0.13	-0.9σ	-0.6σ	-1.6σ	$0.3/1.2\sigma$	0.9σ	0.0σ	1.2σ	19.0
Sc-7'9'	-1.75, -0.02 -0.93, 0.28	-0.4σ	0.3σ	-1.6σ	$0.0/0.3\sigma$	2.3σ	1.0σ	1.6σ	18.0
Sc-77'99'	1.61, 0.24 -0.87, 0.11 0.31, 1.65 -0.60, 1.59	-0.1σ	0.0σ	-1.2σ	$0.0/0.0\sigma$	0.6σ	0.7σ	1.5σ	31.2

TABLE VI: Compilation of best-fit points and pull values with $|\delta| \geq 1.6$ for the model-independent fits of scenarios with NP in QED-penguin operators. $C(\bar{K}^{*0}\phi)$ and $\mathcal{B}(\bar{K}^{*0}\phi)$ are for experimental values [37].

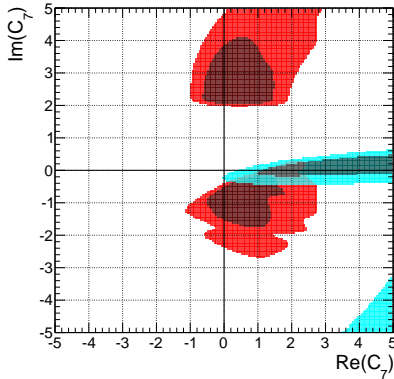


FIG. 9: The 68% (dark) and 95% (bright) CRs for \mathcal{C}_7 in scenario Sc-7, obtained from a fit of observable Set II of the $B \rightarrow K\pi$ system when treating $\rho_A^{K\pi}$ either as a fit parameter (cyan) or as a nuisance parameter (red).

parameters are treated as nuisance parameters. As an example, Fig. 9 provides the allowed regions of $\text{Re } \mathcal{C}_7$ versus $\text{Im } \mathcal{C}_7$ in the scenario Sc-7 from the observable Set II of the $B \rightarrow K\pi$ system. We emphasize again that both fits underly very different assumptions, in fact treating $\rho_A^{K\pi}$ as a nuisance parameter implies that it can be different for each decay as well as each observable, whereas fitting it imposes one universal parameter for all observ-

ables in the $B \rightarrow K\pi$ system. It can be seen that both approaches yield rather different results that overlap only for a very small part of the considered parameter space. The contour from conventional QCDF (red) allows $\text{Im } \mathcal{C}_7$ to be rather large and even its sign is not dictated by the data. Contrary to that the corresponding contour that we obtain from a simultaneous fit of NP and WA parameters (cyan) becomes strongly constrained and fixes \mathcal{C}_7 to be almost purely real. The different outcomes due to the two treatments of ρ_A originate from $r_{\text{EW},7}^A$, which is in both cases the leading NP contribution to ΔC and $C(B^- \rightarrow \bar{K}^0\pi^-)$ in Eq. (V.4). However, for case *ii*), $r_{\text{EW},7}^A$ is assigned with an approximately vanishing central value and huge symmetric uncertainties, whereas for *i*) the central value of $r_{\text{EW},7}^A$ is large and uncertainties are small. The former implies that both CP asymmetries in Eq. (V.4) can be explained simultaneously due to large uncertainties, which depend linearly on $\text{Im } \bar{\mathcal{C}}_7$ and enter the determination of the individual observables uncorrelated. The latter case however implies that a significant modification of one of the two CP asymmetries inevitably induces a similar large contribution to the other. Since $C(B^- \rightarrow \bar{K}^0\pi^-)$ is measured rather accurately and consistent with its value at the best-fit point of the SM fit, large contributions to $\text{Im } \bar{\mathcal{C}}_7$ are consequently forbidden (see 4). This shows that the bounds on a NP parameter space strongly depend on the treatment of ρ_A .

Bounds on the complex-valued Wilson coefficients

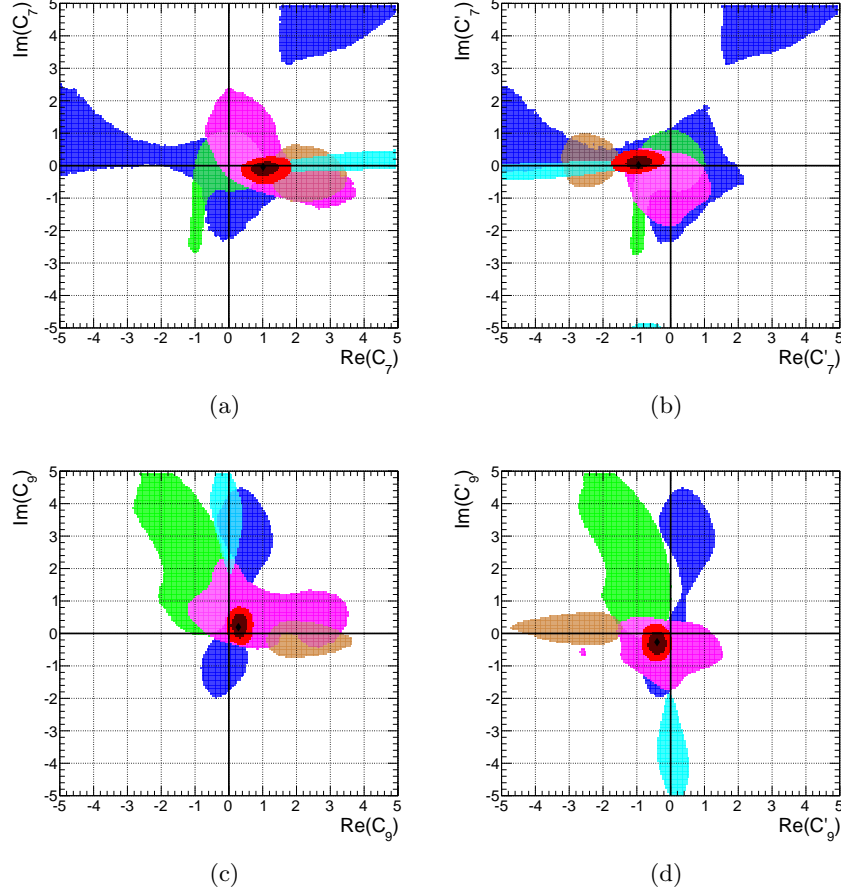


FIG. 10: 68% CR for the complex Wilson coefficients $\mathcal{C}_{7,9}^{(n)}$ in the scenarios Sc-7, 7', 9, 9'. Constraints are obtained from the decay systems $B \rightarrow K\pi$ (cyan), $B \rightarrow K\rho$ (blue), $B \rightarrow K^*\pi$ (green), $B \rightarrow K^*\rho$ (purple), and $B \rightarrow K^*\phi$ (brown). The combined contour (red) is shown for a probability of 68% and 95%. The \blacklozenge corresponds to the best-fit point of the combined fit.

$\mathcal{C}_i^{(n)}$ from fits in scenarios of single operator dominance are shown in Fig. 10 for each of the decay systems $B \rightarrow K\pi, K\rho, K^*\pi, K^*\rho, K^*\phi$ at 68% and their combination at 68% and 95% probability. Due to the different dependence of the spin of the final states on chirality-flipped operators, see Eq. (V.1) and comments below, the contours for $B \rightarrow PP, V_L V_L$ systems are mirrored at the origin, whereas for $B \rightarrow PV$ systems they remain invariant, when considering scenarios that are related by $\mathcal{C}_i \leftrightarrow \mathcal{C}_i'$.

As can be expected from the pull values of the SM fit, shown in Tab. V, the allowed regions from $B \rightarrow K\rho, K^*\rho$ contain the SM, whereas some small pulls in $B \rightarrow K^*\pi$ can be reduced with non-SM values of $\mathcal{C}_{9,9'}$. Concerning $B \rightarrow K\pi$, the data prefers NP contributions that are almost purely real for Sc-7, 7' and imaginary for Sc-9, 9', excluding the SM with a probability of more than 95%. As already explained above, experimental data of $C(B^- \rightarrow \bar{K}^0 \pi^-)$ forbids large contributions to $\text{Im}\bar{\mathcal{C}}_7$, implying also small ΔC in the approximation of

small $r_{i,j}$ as used in Eq. (V.4). Nevertheless, in our approach $r_{\text{EW},7}^A$ can become rather large, see Eq. (V.5), such that second order interference terms $\propto r_T r_{\text{EW},7}^A \text{Re}\bar{\mathcal{C}}_7$, which do not exactly cancel in ΔC , can provide better agreement with the data. The improvement of the tension is quantified in Tab. VI at the best-fit point of the combination of all five decay systems. For example, scenarios Sc-7, 7' allow to reduce the pull of ΔC of -2.8σ in the SM below -1σ , and similarly for $R_n^B(K\pi)$. In scenarios Sc-9, 9' the solution to the “ $\Delta\mathcal{A}_{\text{CP}}$ puzzle” proceeds via $r_{\text{EW},9}$, see Eq. (V.5), requiring large values of $\text{Im}\Delta\mathcal{C}_9$, which are strongly disfavored by measurements of direct CP asymmetries in $B \rightarrow K^*\phi$. In consequence of this strong tension, Sc-9, 9' cannot really improve existing pulls of the SM, except for $R_n^B(K\pi)$, which results in a very small improvement of $\Delta\chi^2(\text{SM})$, shown in Tab. VI. Contrary, Sc-7, 7' exhibits a large improvement of $\Delta\chi^2(\text{SM})$ since here the allowed region of the Wilson coefficient from $B \rightarrow K^*\phi$ is compatible with the one from $B \rightarrow K\pi$.

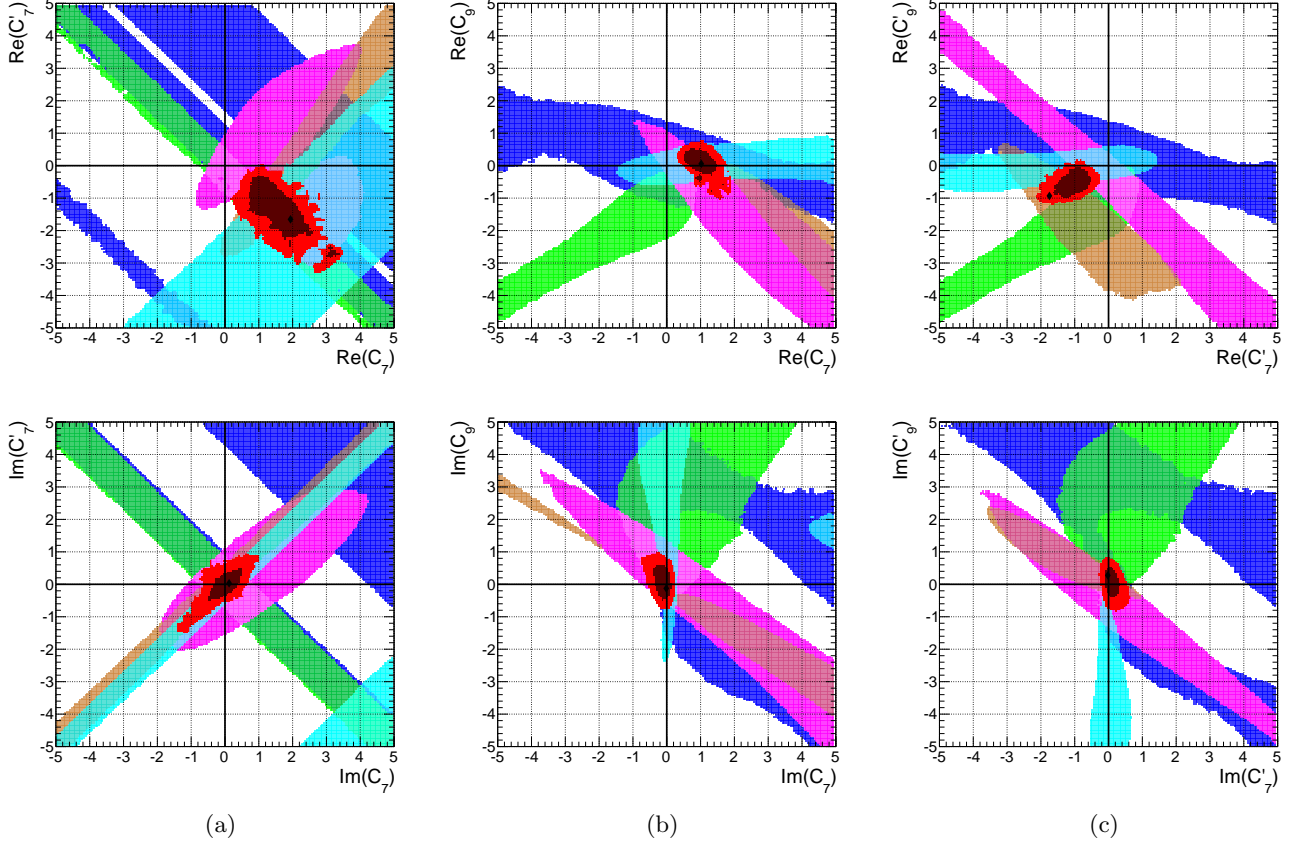


FIG. 11: 68% CR for the complex Wilson Coefficients $\mathcal{C}_{7,9}^{(j)}$ in the scenarios Sc-77' (left), Sc-79 (middle), and Sc-7'9' (right). Constraints are obtained from the decay systems $B \rightarrow K\pi$ (cyan), $B \rightarrow K\rho$ (blue), $B \rightarrow K^*\pi$ (green), $B \rightarrow K^*\rho$ (purple), and $B \rightarrow K^*\phi$ (brown). The combined contour (red) is shown for 68% and 95% CRs. The \blacklozenge corresponds to the best-fit point of the combined fit.

The analysis of scenarios that are dominated by single operators has shown that NP in QED-penguin operators is suitable to sufficiently address all tensions present in the SM, though not all in one particular scenario. The benefits of each single scenario combines in the generalized scenarios, as is evident from the improvement of $\Delta\chi(\text{SM})$ in Tab. VI. In fact, the most general considered Sc-77'99' has greatly reduced pull values compared to the SM and largest $\Delta\chi(\text{SM})$. Concerning models that allow for NP in two Wilson coefficients, only Sc-99' cannot resolve tensions in $B \rightarrow K\pi$, $K^*\pi$, $K^*\phi$, showing that NP is required in \mathcal{C}_7 , respectively \mathcal{C}_7' . In Fig. 11, we show the contours for $\text{Re}\mathcal{C}_i$ versus $\text{Re}\mathcal{C}_j$ and $\text{Im}\mathcal{C}_i$ versus $\text{Im}\mathcal{C}_j$ of the fits of Sc-77', Sc-79, and Sc-7'9'. The features of Fig. 10 are present again, namely large imaginary parts for the Wilson coefficients are excluded, whereas for $\mathcal{C}_7^{(j)}$ non-SM values for the real parts are allowed, disfavoring the SM by more than 95% probability in all three scenarios. On the other hand large imaginary parts for $\mathcal{C}_9^{(j)}$ can only arise in Sc-99' and Sc-77'99', since only $\text{Im}\bar{\mathcal{C}}_9$ is bound to be close to zero by the combination of $B \rightarrow K^*\rho$, $K^*\phi$.

Measurements of the mixing-induced CP asymmetries ΔS_f only exist for two out of the five considered decay systems: $\bar{B}^0 \rightarrow \bar{K}^0\pi^0$ and $\bar{B}^0 \rightarrow \bar{K}^0\rho^0$. Since these are rather imprecisely measured, we omit ΔS_f as constraint from the fit and instead give predictions for each scenario of single operator dominance together with the SM prediction in Tab. VII. In the case of the SM, we observed that the mixing-induced CP asymmetries are insensitive to the residual ρ_A parameter space that is allowed from constraints of branching fractions and direct CP asymmetries. As a consequence, the SM predictions are dictated by error estimation of the nuisance parameters and therefore quoted as interval. We have seen from the fits that CP-violating NP contributions to $\mathcal{C}_7^{(j)}$ are strongly disfavored and to $\mathcal{C}_9^{(j)}$ tightly constrained. Although $\text{Im}\mathcal{C}_9'$ could still become large if \mathcal{C}_9 and \mathcal{C}_9' are modified, such scenarios do not significantly increase the quality of the fit. Hence, mixing-induced CP asymmetries are not strongly affected in the case of single operator dominance and in most cases the central values of NP predictions coincide with the SM interval. Ratios of branching fractions, respectively branching

fractions are more sensitive to, for example, large real-valued $C_7^{(\prime)}$. In particular, the purely isospin-breaking branching fractions $B_s \rightarrow \phi\pi, \phi\rho$ as well as $R_n^{B_s}(KK)$, which predictions are also accumulated in Tab. VI, are sensitive to NP in QED-penguin operators. Indeed, all four considered scenarios, except for the branching fraction of $B_s \rightarrow \phi\pi$ in Sc-7 and Sc-9', predict a further suppression of $\mathcal{B}(B_s \rightarrow \phi\pi, \phi\rho)$, which would unfortunately demand even more experimental effort to observe these very rare decays. On the contrary, the prediction of $R_n^{B_s}(KK)$ remains unchanged within Sc-9', whereas it largely deviates within Sc-7' compared to the SM.

Apart from the NP parameters discussed so far, we simultaneously fitted one universal WA parameter per decay system. The comparison of the best-fit points of these parameters with the SM fit is summarized in Tab. VIII for each of the considered scenarios. These best-fit points lie in the solutions that were singled out by the SM fit, owing to the fact that NP in QED-penguin operators does not modify the numerically leading decay amplitude $\hat{\alpha}_4^c$. We further provide ranges for the ratios ξ_3^A at 68% probability that quantify the relative size of subleading WA amplitudes, which have been determined according to the procedure given in Sec. IIIB. The presence of NP always allows for smaller values of ξ_3^A than in the SM fit. In the most general scenario Sc-77'99' the size of power corrections can be lower than 15% for all considered decay systems. Especially for $B \rightarrow K\rho, K^*\rho$ also simpler NP scenarios already lead to a significant reduction. On the other hand the presence of NP might allow also for very large values of ξ_3^A in most systems, except for $B \rightarrow K\pi (K^*\phi)$, where $\xi_3^A \lesssim 1.5$ (1.2).

B. NP in tree-transitions $b \rightarrow s\bar{u}u$

In the case of the SM, isospin-breaking contributions to hadronic B decays occur either through QED-penguin operators, which were investigated in the previous section, or through tree-level operators with an up-quark current. The latter operators occur in the SM in a color-singlet, O_1^u , and -octet, O_2^u , configuration and are the only source of CP violation in the SM for flavor-violating $b \rightarrow s$ transitions of B mesons. Hence, these operators seem to be suitable to address the tensions of the SM in both $\Delta C(K\pi)$ as well as $R_n^B(K\pi)$ if they can be enhanced. We also encountered some discrepancy in the branching fraction of $B \rightarrow K^{*0}\phi$, but these decays do not directly depend on either of the two tree-level operators, leaving their explanation, at least in the context of the following discussion, due to statistical fluctuation or underestimated theory uncertainties. Due to the strong CKM hierarchy in $b \rightarrow s$ transitions, $b \rightarrow s\bar{u}u$ operators give only numerically important contributions to CP asymmetries, contrary to $b \rightarrow d\bar{u}u$ operators, which are constrained by well-measured branching fractions and CP asymmetries in tree-dominated decays $B \rightarrow \pi\pi, \rho\rho, \rho\pi$ [21].

We introduce the following NP contribution to the Hamiltonian of Eq. (III.1)

$$C_{1,2}^u(\mu_0) = C_{1,2}^{u,SM}(\mu_0) + C_{1,2}^u, \quad (\text{V.6})$$

where we choose $\mu_0 = M_W$ as before. Although $C_{1,2}^u$ mix into Wilson coefficients of all other SM operators, this contribution is doubly Cabibbo-suppressed compared to $C_{1,2}^c$ and numerically negligible in all amplitudes, except for r_T, r_T^C . As discussed in Eq. (V.4), in the SM the latter two are the dominant contributions in CP asymmetries for decay systems considered below.

In connection with the SM, we already discussed in Sec. IV A the possibility of large hard scattering solution to the $\mathcal{A}_{CP}(K\pi)$ problem, see also [55]. Here we show that the assumption of NP in $b \rightarrow s\bar{u}u$ operators provide qualitatively different solutions to large hard scattering. For this purpose we remind of the dependence of CP asymmetries and ratios of branching fractions Eq. (II.15) on the tree amplitudes:

$$\begin{aligned} C &\propto 2 \operatorname{Im}(r_T^{(C)}) \sin \gamma + 2 \operatorname{Im}(r_{T,j}^{(C)}) \operatorname{Im}(C_j e^{-i\gamma}), \\ S &\propto 2 \operatorname{Re}(r_T^{(C)}) \sin \gamma + 2 \operatorname{Re}(r_{T,j}^{(C)}) \operatorname{Im}(C_j e^{-i\gamma}), \\ R &\propto 2 \operatorname{Re}(r_T^{(C)}) \cos \gamma + 2 \operatorname{Re}(r_{T,j}^{(C)}) \operatorname{Re}(C_j e^{-i\gamma}) + \dots, \end{aligned} \quad (\text{V.7})$$

when utilising the expansion in small r_i and the dots stand for contributions of further r_i that are not affected from NP in the considered scenarios. Hard scattering enters only the r_i , especially r_T^C . Hence, direct and mixing-induced CP asymmetries become correlated through their common dependence on $\operatorname{Im}(C_j e^{-i\gamma})$, whereas they depend differently on hard scattering. Analogous, qualitative differences exist among CP asymmetries and the ratios R . In consequence, when mixing-induced CP asymmetries become more precisely measured, it will be possible to distinguish both scenarios.

We investigate the effects of the complex-valued Wilson coefficients $C_j = |C_j|e^{i\delta_j}$ separately and in combination in the three scenarios:

- single operator dominance
Sc- i : $C_i^u \neq 0$ and $C_{j \neq i}^u = 0$ for $i = 1, 2$
- combined scenario
Sc-12 : $C_{1,2}^u \neq 0$

Fig. 12 shows the individual contours for C_1^u (left) and C_2^u (right) that were obtained from a fit of each decay systems $B \rightarrow K\pi, K\rho, K^*\pi, K^*\rho$ within the scenarios of a single operator dominance. In the case of new physics contribution to the color-singlet operator, the fit prefers a real-valued C_1^u with a significant contribution of the order of its SM value. Due to the parameterization of the effective weak Hamiltonian in Eq. (III.1) and of the NP contribution in Eq. (V.6), such a solution implies that the CP violating phase of a particular NP model has to be aligned with the one of the SM. Hence, the

	$\Delta S(K\pi)$	$\Delta S(K\rho)$	$\Delta S(K^*\pi)$	$\Delta S_L(K^*\rho)$	$\Delta S(K\eta')$	$\Delta S(K\omega)$	$\Delta S(K\phi)$	$\Delta S_L(K^*\phi)$	$\mathcal{B}(\phi\pi)$	$\mathcal{B}(\phi\rho)$	$R_n^{B_s}(KK)$
HFAG	$-0.11^{+0.17}_{-0.17}$	$-0.14^{+0.18}_{-0.21}$	—	—	$-0.05^{+0.06}_{-0.06}$	$0.03^{+0.21}_{-0.21}$	$0.06^{+0.11}_{-0.13}$	—	—	—	—
SM	[0.05, 0.13]	[-0.19, -0.04]	[0.06, 0.17]	[-0.15, 0.09]	[-0.01, 0.04]	[0.09, 0.17]	[0.01, 0.05]	[0.01, 0.04]	$0.24^{+0.07}_{-0.04}$	$0.68^{+0.19}_{-0.10}$	$0.99^{+0.01}_{-0.08}$
Sc-7	$0.13^{+0.02}_{-0.13}$	$-0.18^{+0.11}_{-0.10}$	$0.07^{+0.09}_{-0.07}$	$0.08^{+0.07}_{-0.13}$	$0.03^{+0.04}_{-0.09}$	$0.15^{+0.04}_{-0.31}$	$0.04^{+0.05}_{-0.08}$	$0.03^{+0.06}_{-0.08}$	$0.91^{+0.28}_{-0.22}$	$0.35^{+0.14}_{-0.07}$	$0.80^{+0.04}_{-0.06}$
Sc-7'	$0.13^{+0.02}_{-0.13}$	$-0.08^{+0.07}_{-0.10}$	$0.10^{+0.09}_{-0.07}$	$0.10^{+0.09}_{-0.12}$	$0.02^{+0.06}_{-0.08}$	$0.12^{+0.06}_{-0.08}$	$-0.01^{+0.06}_{-0.07}$	$0.05^{+0.06}_{-0.07}$	$0.06^{+0.05}_{-0.04}$	$0.26^{+0.12}_{-0.08}$	$0.87^{+0.06}_{-0.06}$
Sc-9	$0.06^{+0.06}_{-0.08}$	$-0.04^{+0.09}_{-0.10}$	$0.05^{+0.07}_{-0.09}$	$-0.01^{+0.10}_{-0.18}$	$0.00^{+0.06}_{-0.07}$	$0.09^{+0.09}_{-0.07}$	$-0.04^{+0.07}_{-0.07}$	$-0.08^{+0.11}_{-0.06}$	$0.11^{+0.06}_{-0.04}$	$0.40^{+0.13}_{-0.10}$	$0.94^{+0.03}_{-0.06}$
Sc-9'	$0.05^{+0.06}_{-0.08}$	$-0.20^{+0.10}_{-0.11}$	$0.17^{+0.05}_{-0.07}$	$-0.05^{+0.13}_{-0.15}$	$-0.02^{+0.08}_{-0.05}$	$0.16^{+0.03}_{-0.11}$	$0.06^{+0.03}_{-0.10}$	$-0.03^{+0.09}_{-0.12}$	$0.49^{+0.14}_{-0.12}$	$0.32^{+0.15}_{-0.10}$	$0.93^{+0.05}_{-0.04}$

TABLE VII: Predictions for the mixing-induced CP asymmetry of diverse B_d decays and for the purely isospin-breaking branching ratios $\mathcal{B}(\bar{B}_s \rightarrow \phi\pi, \phi\rho)$ within the single dominant operator scenarios and the SM.

	$K\pi$		$K^*\pi$		$K\rho$		$K^*\rho$		$K^*\phi$	
	$ \rho_A , \phi_A$	ξ_3^A	$ \rho_A , \phi_A$	ξ_3^A	$ \rho_A , \phi_A$	ξ_3^A	$ \rho_A , \phi_A$	ξ_3^A	$ \rho_A , \phi_A$	ξ_3^A
SM	3.34, 2.71	0.39	1.61, 5.84	0.89	2.69, 2.68	0.78	1.56, 5.66	1.33	1.50, 2.82	0.38
Sc-7	2.14, 5.45 [0.38, 0.60]		1.80, 5.90 [0.86, 1.39]		1.88, 5.58 [0.39, 1.64]		1.41, 5.66 [0.70, 1.81]		1.53, 2.85 [0.29, 0.65]	
Sc-7'	3.61, 2.68 [0.34, 0.64]		3.73, 1.84 [0.72, 2.72]		2.14, 5.36 [0.54, 1.46]		1.29, 5.64 [0.57, 1.75]		0.71, 5.64 [0.38, 0.59]	
Sc-9	1.86, 5.49 [0.35, 0.60]		1.63, 5.87 [0.78, 1.49]		1.52, 5.44 [0.41, 1.38]		1.54, 5.63 [0.62, 1.97]		1.53, 2.83 [0.35, 0.52]	
Sc-9'	1.85, 5.49 [0.35, 0.62]		2.99, 2.91 [0.76, 1.55]		2.71, 2.68 [0.41, 1.49]		1.53, 5.62 [0.62, 1.91]		1.55, 2.84 [0.36, 0.53]	
Sc-77'	2.45, 5.69 [0.34, 1.18]		3.03, 2.91 [0.71, 2.98]		1.51, 5.44 [0.00, 1.61]		1.71, 6.00 [0.51, 2.37]		0.95, 6.00 [0.30, 0.88]	
Sc-99'	2.39, 5.40 [0.33, 0.71]		3.34, 2.99 [0.68, 3.24]		1.44, 0.04 [0.01, 2.78]		2.31, 2.74 [0.40, 2.28]		1.54, 2.84 [0.26, 0.71]	
Sc-79	3.59, 2.68 [0.23, 0.70]		1.80, 5.90 [0.78, 1.70]		1.95, 5.60 [0.24, 2.40]		2.19, 2.79 [0.31, 2.06]		1.53, 2.86 [0.17, 0.68]	
Sc-7'9'	2.17, 5.53 [0.30, 0.66]		2.89, 2.77 [0.56, 2.74]		2.19, 5.27 [0.65, 1.84]		2.43, 2.87 [0.43, 1.92]		0.99, 6.01 [0.31, 0.83]	
Sc-77'99'	2.24, 5.56 [0.08, 1.49]		1.65, 6.07 [0.11, 3.58]		1.45, 6.28 [0.00, 2.64]		1.81, 5.89 [0.12, 2.83]		0.90, 5.93 [0.01, 1.02]	

TABLE VIII: Compilation of best-fit points for ρ_A and ξ_3^A at 68% probability. The results are given for the considered decay systems and scenarios Sc- i . As explained in Sec. IIIB, the interval of $\xi_3^A(\text{NP})$ should be compared to $\xi_3^A(\text{SM})$ at the best-fit point of ρ_A , listed in the first row.

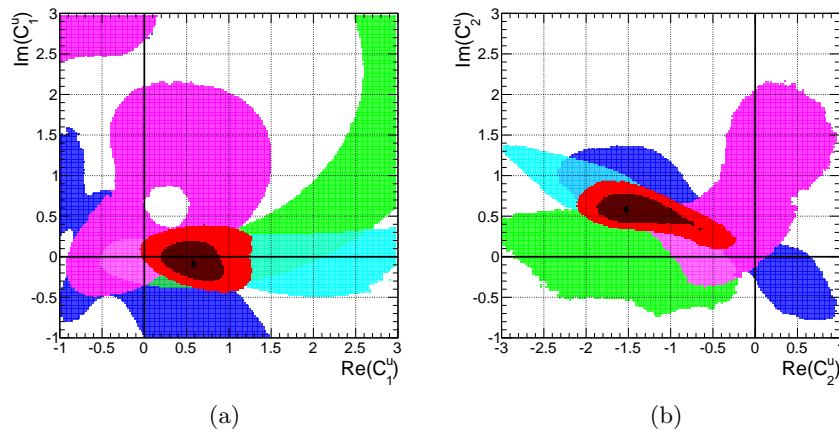


FIG. 12: 68% CR for the complex Wilson Coefficients $C_{1,2}^u$ in the scenarios Sc-1 (left) and Sc-2 (right).

Constraints are obtained from the decay systems $B \rightarrow K\pi$ (cyan), $B \rightarrow K\rho$ (blue), $B \rightarrow K^*\pi$ (green), and $B \rightarrow K^*\rho$ (purple). The combined contour (red) is shown for 68% and 95% CRs. The \blacklozenge corresponds to the best-fit point of the combined fit.

	$\text{Re}(C_i^u), \text{Im}(C_i^u)$	$\Delta C(K\pi)$	$R_n^B(K\pi)$	$R_n^B(K^*\pi)$	$\Delta\chi^2(SM)$
SM		-2.8σ	-1.9σ	0.6σ	
Sc-1	0.58, -0.09	-0.9σ	0.0σ	0.2σ	9.2
Sc-2	-1.53 , 0.58	0.0σ	-0.3σ	1.6σ	12.4
Sc-12	1.47, 0.03	0.0σ	-0.5σ	1.1σ	15.6
	-2.25 , 0.38				

TABLE IX: Compilation of best-fit points and pull values, with $|\delta| \geq 1.6$, for the model-independent fits of $b \rightarrow s \bar{u}u$ operators.

	$\Delta S(K\pi)$	$\Delta S(K\rho)$	$\Delta S(K^*\pi)$	$\Delta S_L(K^*\rho)$	$\Delta S(K\eta')$	$\Delta S(K\omega)$	$\Delta S(K\phi)$	$\Delta S_L(K^*\phi)$	$\mathcal{B}(\phi\pi)$	$\mathcal{B}(\phi\rho)$	$R_n^{B_s}(KK)$
HFAG	$-0.11^{+0.17}_{-0.17}$	$-0.14^{+0.18}_{-0.21}$	—	—	$-0.05^{+0.06}_{-0.06}$	$0.03^{+0.21}_{-0.21}$	$0.06^{+0.11}_{-0.13}$	—	—	—	—
SM	[0.05, 0.13]	[-0.19 , -0.04]	[0.06, 0.17]	[-0.15 , 0.09]	[-0.01 , 0.04]	[0.09, 0.17]	[0.01, 0.05]	[0.01, 0.04]	$0.24^{+0.07}_{-0.04}$	$0.68^{+0.19}_{-0.10}$	$0.99^{+0.01}_{-0.08}$
Sc-1	$0.13^{+0.07}_{-0.07}$	$-0.10^{+0.06}_{-0.22}$	$0.12^{+0.11}_{-0.06}$	$-0.06^{+0.16}_{-0.32}$	$0.01^{+0.07}_{-0.06}$	$0.20^{+0.06}_{-0.09}$	$0.09^{+0.02}_{-0.11}$	$0.09^{+0.02}_{-0.11}$	$0.27^{+0.06}_{-0.07}$	$0.73^{+0.17}_{-0.17}$	$0.92^{+0.08}_{-0.09}$
Sc-2	$-0.30^{+0.11}_{-0.12}$	$0.26^{+0.01}_{-0.09}$	$-0.66^{+0.20}_{-0.19}$	$-1.05^{+0.30}_{-0.28}$	$0.06^{+0.05}_{-0.05}$	$-0.55^{+0.25}_{-0.22}$	$0.09^{+0.02}_{-0.11}$	$0.09^{+0.01}_{-0.11}$	$1.36^{+0.74}_{-0.54}$	$3.94^{+1.77}_{-1.40}$	$0.91^{+0.04}_{-0.03}$
Sc-12	$-0.42^{+0.15}_{-0.20}$	$0.18^{+0.09}_{-0.25}$	$-0.93^{+0.29}_{-0.29}$	$-1.59^{+0.43}_{-0.11}$	$0.07^{+0.06}_{-0.05}$	$-0.51^{+0.21}_{-0.43}$	$0.06^{+0.05}_{-0.06}$	$0.04^{+0.06}_{-0.04}$	$2.74^{+1.59}_{-1.21}$	$8.78^{+3.74}_{-3.67}$	$0.85^{+0.11}_{-0.09}$

TABLE X: Predictions for the mixing-induced CP asymmetry of diverse B_d decays and for the purely isospin-breaking branching ratios $\mathcal{B}(\bar{B}_s \rightarrow \phi\pi, \phi\rho)$ within the Sc-1, 2 scenarios and the SM.

Wilson coefficient is enhanced from $C_1^u(M_W) = 0.98$ in the SM to $C_1^u(M_W) = |0.98 + (0.58 - i0.09)| \approx 1.56$ at the best-fit point, tabulated in Tab. IX, whereas its weak phase γ receives only marginal corrections from $\delta_1 \approx -8.8^\circ$. Since all contours from the individual decay systems nicely overlap with each other, we expect to resolve the discrepancy that are present for the SM in $B \rightarrow K\pi$ without introducing new tensions in the data of other decay systems. This is confirmed from the pull values listed in Tab. IX. It can also be seen from the table that the tensions in $\Delta C(K\pi)$ and $R_n^B(K\pi)$ can be well explained within Sc-2 and Sc-12 when tolerating a rising tension in $R_n^B(K^*\pi)$ of 1.6σ , respectively 1.1σ .

The corresponding contours of C_2^u are displayed in Fig. 12b. The combined contour reduces to a common area of the allowed regions for the decay systems $B \rightarrow K\pi, K\rho, K^*\rho$, whereas the green contour from $B \rightarrow K^*\pi$ is slightly separated from the combination. The SM value of the color-octet Wilson coefficient, $C_2^{u,SM}(M_W) = 0.05$, is strongly suppressed compared to its color-singlet counterpart, but the preferred values that were obtained from our fits shift $C_2^u(M_W) = |0.05 + (-1.53 + i0.58)| \approx 1.58$ — competitive to $C_1^u(M_W)$. In contrast to Sc-1, the weak phase of C_2^u is not aligned with the SM, but rather receives a significant phase shift of $\delta_2 \approx 159^\circ$.

The pattern that were obtained from the single operator dominance scenarios is also observed for the combined scenario: $C_{1,2}^u$ becomes further enhanced by $|0.98 + (1.47 + i0.03)| \approx 2.45$, respectively $|0.05 + (-2.25 + i0.38)| \approx 2.23$ and $\delta_1 \sim 1^\circ$, whereas δ_2 further tend to 170° .

As in the previous analysis of the QED-penguin operators, we quote in Tab. X predictions for several mixing-

induced CP asymmetries as well as for the isospin-sensitive branching fractions of $B_s \rightarrow \phi\pi, \phi\rho$ and for $R_n^{B_s}(KK)$. The impact from an enhanced C_1^u on these observables is small and rather challenging to isolate from the SM background, which is not the case for NP in C_2^u . Especially the predictions of the mixing-induced CP asymmetries of the decays $B \rightarrow K\pi, K\rho, K^*\pi, K^*\rho$ and $B \rightarrow K\omega$ are visibly different compared to the SM, making these observables an ideal probe of NP in the color-octet operator. The same is true for the branching fractions of $B_s \rightarrow \phi\pi, \phi\rho$, which we found to be enhanced by a factor of 5–6 for Sc-2 and by more than a factor of 10 in the case of Sc-12. Although these predictions largely deviate from the one of the SM, existing measurements do not contradict NP in C_2^u due to lacking precision.

As before, the NP contributions to the Wilson coefficients have been fitted simultaneously with WA parameters ρ_A for each decay system in all considered scenarios. Since NP in $b \rightarrow s \bar{u}u$ operators do not contribute directly to the leading decay amplitude \hat{a}_4^c but rather indirectly through the common dependence on the likelihood function, we expect moderate changes of WA compared to the results of the SM fit. The best-fit points of the individual ρ_A as well as the 68% probability intervals of ξ_3^A are summarized in Tab. XI for each of the three scenarios. We observe that almost all best-fit points of ρ_A lie within the contour regions of the SM fit. The only exceptions are $\rho_A^{K\rho}$ in Sc-12 and $\rho_A^{K\pi}$ for all considered scenarios. For the latter, the most likely values of $|\rho_A^{K\pi}|$ in the case of Sc-1 and Sc-2 are significantly reduced compared to the SM, whereas $\phi_A^{K\pi}$ tends towards smaller strong phases in the combined scenario. Due to the additional degrees of freedom, it is possible that the relative amount

	$K\pi$		$K^*\pi$		$K\rho$		$K^*\rho$	
	ρ_A	ξ_3^A	ρ_A	ξ_3^A	ρ_A	ξ_3^A	ρ_A	ξ_3^A
SM	3.34, 2.71	0.39	1.61, 5.84	0.89	2.69, 2.68	0.78	1.56, 5.66	1.33
Sc-1	1.54, 5.58 [0.29, 0.50]		1.65, 5.87 [0.73, 1.33]		3.03, 2.81 [0.53, 1.32]		1.39, 5.90 [0.83, 1.72]	
Sc-2	1.54, 5.58 [0.26, 0.77]		1.60, 5.92 [0.75, 1.33]		1.11, 0.19 [0.33, 1.00]		2.63, 3.76 [0.92, 2.32]	
Sc-12	2.05, 5.80 [0.13, 0.88]		1.52, 5.90 [0.54, 1.47]		3.76, 4.56 [0.22, 3.17]		1.96, 3.38 [0.27, 2.61]	

TABLE XI: Compilation of best-fit points for ρ_A and ξ_3^A at 68% probability. The results are given for the considered decay systems and scenarios Sc- i . As explained in Sec. IIIB, the interval of $\xi_3^A(\text{NP})$ should be compared to $\xi_3^A(\text{SM})$ at the best-fit point of ρ_A , listed in the first row.

of power-suppressed corrections can be reduced. In general ξ_3^A is most strongly affected in the combined scenario, for which we find lower bounds on $\xi_3^A(K\pi) \gtrsim 0.13$, $\xi_3^A(K\rho) \gtrsim 0.22$, and $\xi_3^A(K^*\rho) \gtrsim 0.27$. The potential suppression of ξ_3^A for $B \rightarrow K^*\pi$ is less effective and a relative amount of power-suppressed contribution of at least 0.54 is required in any case. It is worth to notice that the large WA scenario is still disfavored for $B \rightarrow K\pi$, which is in general not true for all other decay modes.

VI. CONCLUSION

In this work we have carried out a phenomenological study of QCD- and QED-penguin dominated charmless 2-body B -meson decays in the framework of QCD factorization (QCDF). In particular we investigated whether data supports the assumption of one universal parameter, ρ_A , in weak annihilation (WA) contributions for decay channels related by ($u \leftrightarrow d$) quark exchange in $B_{u,d,s}$ meson decays to PP , VP and VV final states, while the remaining theory uncertainties are incorporated in an uncorrelated manner.

We analyse the decay systems of $B_{u,d}$ decays into $PP = K\pi, K\eta^{(\prime)}, KK$ or $PV = K\rho, K\phi, K\omega, K^*\pi, K^*\eta^{(\prime)}$ or $VV = K^*\rho, K^*\phi, K^*\omega, K^*K^*$, and further B_s decays into $PP = \pi\pi, KK, K\pi$ or $VV = \phi\phi, K^*\phi, K^*K^*$ final states and employ the available data (see Tab. I, II, III) on branching fractions, direct CP asymmetries and for VV final states also polarization fractions and relative phases between polarization amplitudes.

Within the standard model (SM), the data can be described using one universal WA parameter for each decay system. The only exception is the $B \rightarrow K\pi$ system when using Set II of observables, as specified in Sec. IIB, which includes $\Delta\mathcal{A}_{\text{CP}}$ and R_n^B , as a manifestation of the “ $\Delta\mathcal{A}_{\text{CP}}$ puzzle” in our framework. The only other noticeable pull value of 2.6σ (1.7σ) arises for the measurement of $\mathcal{B}(\bar{B}^0 \rightarrow \bar{K}^{*0}\phi)$ from Belle (BaBar). For each system, there are at least two allowed regions at 68% CR with the best fit solution residing in one of them (see Tab. IV). These two regions correspond to phases close to π and 2π , outside of regions of large destructive in-

terference of WA amplitudes with leading amplitudes. Moreover the ratio of the magnitudes of WA amplitudes to leading amplitudes, ξ_3^A (see Tab. IV), is similar in size in both regions and within the 68% CR it is possible to have $\xi_3^A < 1$ (except for $B_s \rightarrow K^*K^*$) and for the majority even $\xi_3^A < 0.5$. QCDF can thus describe the current data without the need of anomalously large WA contributions.

We emphasize that in our analysis the “ $\Delta\mathcal{A}_{\text{CP}}$ puzzle” is only present if we assume a universal WA parameter that can be fitted from data. If we lift this assumption the anomaly would only reappear if we restrict our analysis to rather small WA parameters ρ_A . Without such a restriction, however the non-linear dependence of ξ_3^A on ρ_A still permits reasonably small ξ_3^A , which are not larger as currently accepted in the literature.

We studied also ratios of branching fractions and differences of CP asymmetries (Set II) for the decay systems $B \rightarrow K\pi, K^*\pi, K\rho, K^*\rho$. They are less sensitive to form-factor and CKM uncertainties or are especially sensitive to numerically suppressed contributions from tree topologies. The according results listed in Tab. V show that currently both sets yield good fits to the data, except for $B \rightarrow K\pi$, where Set II has a p -value of only 4%. The data of ratios of branching fractions and differences of CP asymmetries have been obtained by ourselves from measurements of observables in Set I. This neglects correlations and potential cancellations of systematic uncertainties accessible only in the experimental analyses. In this regard, future analysis would benefit from the direct experimental determination of these composed observables.

In view of the large pull value of 2.8σ for $\Delta\mathcal{A}_{\text{CP}}$ in $B \rightarrow K\pi$, we performed also a simultaneous fit of the WA and hard-scattering (HS) phenomenological parameters in the SM. The HS contribution necessary to lower the pull value of $\Delta\mathcal{A}_{\text{CP}}$ to 1.0σ is not larger than typically considered in conventional error estimates in the literature — $\xi_2^H = 1.0$. A better description of the data can be achieved with even larger HS contributions. A preciser measurement of $C(B_d \rightarrow K^0\pi^0)$ in the future could be helpful to test a “large HS”-scenario. Further, larger HS contributions allow for smaller WA contributions.

We investigate the feasibility to constrain new-physics

(NP) scenarios in view of the aforementioned tensions in the SM. Within our framework this requires the fit of WA phenomenological parameters simultaneously with NP parameters from data. In contrast to the conventional handling of WA contributions within QCDF, we find that the assumption of one universal parameter per decay system yields stronger constraints on new-physics parameters for the considered scenarios. We have studied model-independent scenarios of NP in QED-penguin operators as possible solutions to the “ $\Delta\mathcal{A}_{\text{CP}}$ puzzle” in $B \rightarrow K\pi$ and tensions in $B \rightarrow K^*\phi$, taking into account also data from the systems $B \rightarrow K\rho$, $K^*\pi$, $K^*\rho$. As a second possible solution to the “ $\Delta\mathcal{A}_{\text{CP}}$ puzzle” we investigated NP in $b \rightarrow s\bar{u}u$ current-current operators including again data from $B \rightarrow K\rho$, $K^*\pi$, $K^*\rho$. For each scenario we provide the best fit regions of the NP contributions to the according Wilson coefficients, reduction of χ^2 compared to the SM fit, the pull values of observables, and predictions of mixing-induced CP asymmetries, as well as branching fractions of $B_s \rightarrow \phi\pi$, $\phi\rho$.

In both classes of NP scenarios there is no direct contribution to the numerically leading amplitude of QCD-penguin operators, since we consider only new isospin-violating contributions. In consequence, the allowed regions of WA parameters do not differ qualitatively from those of the SM fit. Yet, the combined fit of NP and WA allows for smaller ξ_3^A in all scenarios compared to the SM.

It is conceivable that one day factorization theorems will be established even for WA contributions involving then new nonperturbative quantities. Our studies suggest that it will be possible to extract these new quantities also from data in the lack of first principle nonperturbative methods of their calculation. It will be important to have access to more accurate measurements of the involved observables which should become available from Belle II and LHCb within the next decade.

ACKNOWLEDGMENTS

We thank Martin Beneke, Gerhard Buchalla and Yuming Wang for helpful discussions and Yuming Wang for comments on the manuscript. We would like to thank Frederik Beaujean for his support on BAT [66]. C.B. received support from the ERC Advanced Grant project “FLAVOUR” (267104). M.G. acknowledges partial support by the UK Science & Technology Facilities Council (STFC) under grant number ST/G00062X/1.

Appendix A: Numerical input

Here we collect the numerical input used in our analysis in Tab. XII. We list two sets of CKM parameters. The first, denoted by “SM”, is obtained in a global CKM fit in the framework of the SM [67] and is used throughout our SM analyses Sec. IV. The second, denoted by “NP”,

is obtained from a global fit that includes only tree-level mediated observables [67] and which we use throughout the analysis of scenarios beyond the SM in Sec. V. Further, for B_s decays we use the value of y_s Eq. (II.10) as an additional source of error in Eq. (II.4). Throughout we vary the renormalization scale $\mu_b \in [m_b/2, 2m_b]$ for the central value of $\mu_b = 4.2$ GeV. The uncertainty from endpoint divergences in subleading hard-scattering contributions is determined by varying $\phi_H \in [0, 2\pi]$ for fixed $|\rho_H| = 1$, as frequently done in the literature.

Appendix B: Statistical procedure

This appendix summarizes the statistical methods that are used in order to obtain probability regions for the parameters of interest, pull values of theory predictions and corresponding measurements of observables, and p -values as a measure of the goodness of fit. Further, we describe the determination of probability distributions of predictions for observables that were not included in the fit.

1. Probability regions

For the purpose of parameter inference we use Bayes theorem to determine the posterior probability distribution, $P(\boldsymbol{\theta}|M, D)$, of the parameters of interest, $\boldsymbol{\theta} = (\theta_1, \theta_2, \dots)$, given a model M and data D . Parameters of interest in our analysis are *i*) the phenomenological parameters of weak annihilation $\rho_A^{M_1 M_2}$ and *ii*) parameters of new physics scenarios. Bayes theorem relates the posterior probability to the likelihood $\mathcal{L}(\boldsymbol{\theta}) = P(D|M, \boldsymbol{\theta})$, which is the probability of the data given the model M with parameter values $\boldsymbol{\theta}$ and the prior distributions, $P(M, \boldsymbol{\theta})$, which are the probability of model M with parameter values $\boldsymbol{\theta}$

$$P(\boldsymbol{\theta}|M, D) = \frac{P(D|M, \boldsymbol{\theta}) P(M, \boldsymbol{\theta})}{Z}. \quad (\text{B1})$$

Here, the model-dependent normalization factor

$$Z \equiv \int P(D|M, \boldsymbol{\theta}) P(M, \boldsymbol{\theta}) d\boldsymbol{\theta} \quad (\text{B2})$$

is known as “evidence” or “marginal likelihood” that plays an important role in model comparison within the Bayesian approach. Throughout, the priors of the $\boldsymbol{\theta}$ are chosen as uniform within a certain interval.

It is common to introduce the likelihood function $\mathcal{L}(\boldsymbol{\theta})$ as the product of the probabilities $p(O_i = O_i^{\text{th}}(\boldsymbol{\theta}))$ that each observable O_i in the data set takes the particular value $O_i^{\text{th}}(\boldsymbol{\theta})$ predicted at the value of $\boldsymbol{\theta}$

$$\begin{aligned} \mathcal{L}(\boldsymbol{\theta}) &= \prod_{i \in \text{data}} p(O_i = O_i^{\text{th}}(\boldsymbol{\theta})) \\ &\sim \exp \left[-\frac{1}{2} \sum_{i \in \text{data}} \left(\chi_i(\boldsymbol{\theta}) \right)^2 \right]. \end{aligned} \quad (\text{B3})$$

Electroweak input					
$G_F[10^{-5} \text{ GeV}^{-2}]$	$\Lambda_{\overline{\text{MS}}}^{(5)}[\text{GeV}]$	$M_Z[\text{GeV}]$	$\alpha_s^{(5)}(M_Z)$	$\alpha_e^{(5)}(m_b)$	
1.16638	0.213	91.1876	0.1184	1/132	[68] [69]
quark masses [GeV]					
m_t^{pole}	$m_b(m_b)$	$m_c(m_b)$	m_s	m_q/m_s	
(173.2 ± 0.9)	4.2	(1.3 ± 0.2)	(0.095 ± 0.005)	0.0370	[5] [68] [70]
CKM elements					
	λ	$ V_{cb} $	$\bar{\rho}$	$\bar{\eta}$	
SM	0.22535 ± 0.00065	0.04172 ± 0.00056	0.127 ± 0.023	0.353 ± 0.014	[67]
NP	0.2253 ± 0.0006	0.04061 ± 0.00097	0.147 ± 0.045	0.368 ± 0.048	
B-meson input					
	B_u	B_d	B_s		
$f_B[\text{MeV}]$	190.5 ± 4.2		227.7 ± 4.5		[71]
$\lambda_B[\text{MeV}]$	200^{+250}_{-0}				
$\tau_B[\text{ps}^{-1}]$	1.641	1.519	1.516		[68]
$M_B[\text{MeV}]$	5279.25	5279.58	5366.77		
Hadronic input – pseudoscalar mesons					
	K	π	η	η'	
$f_P[\text{MeV}]$	160	131	$(1.07 \pm 0.02)f_\pi$	$(1.34 \pm 0.06)f_\pi$	[4] [5]
$F_0^{B \rightarrow P}$	$0.33 \pm 0.04^\dagger$	0.26 ± 0.02	0.23 ± 0.05	0.19 ± 0.12	[4] [72] [73]
$F^{B_s \rightarrow P}$	$0.30^{+0.04}_{-0.03}$	–	–	–	[74]
$\alpha_1(P)$	0.05 ± 0.02	0.00	0.00	0.00	[4] [75]
$\alpha_2(P)$	0.17 ± 0.10	0.17 ± 0.10	0.00 ± 0.3	0.00 ± 0.3	
Hadronic input – vector mesons					
	K^*	ρ	ϕ	ω	
$f_V[\text{MeV}]$	218 ± 4	209 ± 1	221 ± 3	187 ± 3	[5]
$f_V^\perp[\text{MeV}]$	175 ± 10	156 ± 9	175 ± 9	142 ± 9	[76]
$A_0^{B \rightarrow V}$	0.34 ± 0.03	0.30 ± 0.03	–	0.28 ± 0.03	[77]
$F_-^{B \rightarrow V}$	0.62 ± 0.05	0.58 ± 0.04	–	0.55 ± 0.04	
$F_+^{B \rightarrow V}$	0.00 ± 0.06	0.00 ± 0.06	–	0.00 ± 0.06	[23]
$A_0^{B_s \rightarrow V}$	0.39 ± 0.03	–	0.47 ± 0.04	–	[77]
$F_-^{B_s \rightarrow V}$	0.59 ± 0.04	–	0.72 ± 0.04	–	
$F_+^{B_s \rightarrow V}$	0.00 ± 0.06	–	0.00 ± 0.06	–	[23]
$\alpha_1(V)$	0.02 ± 0.02	0.00	0.00	0.00	[78]
$\alpha_1^\perp(V)$	0.03 ± 0.03	0.00	0.00	0.00	
$\alpha_2(V)$	0.08 ± 0.06	0.10 ± 0.05	0.13 ± 0.06	0.10 ± 0.05	
$\alpha_2^\perp(V)$	0.08 ± 0.06	0.11 ± 0.05	0.11 ± 0.05	0.11 ± 0.05	

TABLE XII: Numerical input used for our analysis. Form factors are given at zero momentum transfer $q^2 = 0$.

Other scale dependent quantities are quoted at the scale $\mu = 2 \text{ GeV}$. † For the $B \rightarrow K$ form factor we used $\alpha_4^K(2.2 \text{ GeV}) = -0.0089$ [72] as additional input.

The probabilities p are given by the measured probability density functions $\text{pdf}[O_i]$ of each observable O_i and the second part \sim of (B3) indicates the special case of gaussian distributed pdf's permitting to define a $\chi_i(\theta)$.

The expression of $\mathcal{L}(\theta)$ does not yet include the uncertainties due to nuisance parameters, $\nu = (\nu_1, \nu_2, \dots)$, which enter theoretical predictions of $B \rightarrow M_1 M_2$ decays. In this case, the nuisance parameters give rise to an inter-

val for the theory prediction $[O_i^{\text{th}} - \Delta_i^-, O_i^{\text{th}} + \Delta_i^+]$ with possibly asymmetric uncertainties Δ_i^\pm around the central value O_i^{th} that is obtained for central values of all nuisance parameters. Here, the theoretical uncertainty Δ_i^\pm is determined by adding in quadrature the uncertainties due to each nuisance parameter ν_a

$$\Delta_i^\pm = \sqrt{\sum_a (\Delta_{i,a}^\pm)^2}, \quad (\text{B4})$$

which arises from the minimal, central and maximal values ν_a^{min} , ν_a^{cen} and ν_a^{max} , respectively,

$$\Delta_{i,a}^{+(-)} = |O_i^{\text{th}}(\nu_a^{\text{max}(\text{min})}) - O_i^{\text{th}}(\nu_a^{\text{cen}})|, \quad (\text{B5})$$

while keeping all others at their central values. Clearly, this is an approximation that neglects more compli-

cated interdependences of observables on several parameters and also possible correlations among different nuisance parameters. The nuisance parameters are listed in Tab. XII.

In the presence of nuisance parameters, we will adopt the simple procedure to use the maximal value of the pdf inside the interval of the theory prediction, hence replacing in (B3)

$$\begin{aligned} \text{pdf}(O_i = O_i^{\text{th}}(\boldsymbol{\theta})) &\rightarrow \\ \max \left(\text{pdf}(O_i) \mid O_i \in [O_i^{\text{th}} - \Delta_i^-, O_i^{\text{th}} + \Delta_i^+] \right), \end{aligned} \quad (\text{B6})$$

where the dependence of O_i^{th} and Δ_i^\pm on $\boldsymbol{\theta}$ and $\boldsymbol{\nu}$ is not explicitly shown. This procedure is implemented easily for gaussian distributed pdf's by the modification of the definition of

$$\chi_i(\boldsymbol{\theta}, \boldsymbol{\nu}) = \begin{cases} \frac{|O_i^{\text{th}}(\boldsymbol{\theta}, \boldsymbol{\nu}) - O_i^{\text{exp}}| - \Delta_i^+(\boldsymbol{\theta}, \boldsymbol{\nu})}{\sigma_i^-} & \text{if } O_i^{\text{exp}} \geq O_i^{\text{th}} + \Delta_i^+ \\ \frac{|O_i^{\text{th}}(\boldsymbol{\theta}, \boldsymbol{\nu}) - O_i^{\text{exp}}| - \Delta_i^-(\boldsymbol{\theta}, \boldsymbol{\nu})}{\sigma_i^+} & \text{if } O_i^{\text{exp}} \leq O_i^{\text{th}} - \Delta_i^- \\ 0 & \text{else} \end{cases} \quad (\text{B7})$$

where O_i^{exp} and σ_i^\pm denote the central value and the left and right standard deviation of the pdf $[O_i]$, respectively. The central value of the theoretical prediction O_i^{th} is obtained at the particular value of the parameters of interest $\boldsymbol{\theta}$, and the $\boldsymbol{\nu}$ are set to their central values.

Obviously, the modification (B7) is tailored to gaussian pdf's, which is our interpretation of experimental world averages given by the Particle Data Group (PDG) [68] or HFAG [19]. However, the ratios of gaussian distributed observables – like the ones defined in Eq. (II.15): $R = \mathcal{B}_1/\mathcal{B}_2$ – follow a gaussian ratio distribution. In the absence of experimental results of these ratios, one has to resort to the combination of the two gaussian distributions of numerator and denominator. In all relevant cases, the \mathcal{B}_i are gaussian distributed with symmetric errors (from HFAG) and assuming that their errors are uncorrelated, the analytical expression of $p(R)$ is known [79]. Since it is monotonly rising till its maximum at $R^{\text{exp}} \equiv \mathcal{B}_1^{\text{exp}}/\mathcal{B}_2^{\text{exp}}$ and then monotonly falling, the maximal value of the probability in the theory interval can be easily found by evaluating $p(R)$ at

$$R = \begin{cases} R_i^{\text{th}} + \Delta_i^+ & \text{if } R^{\text{exp}} \geq R_i^{\text{th}} + \Delta_i^+ \\ R_i^{\text{th}} - \Delta_i^- & \text{if } R^{\text{exp}} \leq R_i^{\text{th}} - \Delta_i^- \\ R^{\text{exp}} & \text{else} \end{cases} \quad (\text{B8})$$

The probability value is converted to $\chi = -2 \log p(R)$. Let us finally note that the difference between the gaussian ratio distribution and a gaussian distribution with central value R and $\sigma(R)$ determined from simple uncertainty propagation calculus, is numerically negligible unless large deviations of experimental and theoretical values probe the tails of the distributions, which are “heavier” for the gaussian ratio distribution.

Concerning the evaluation of the posterior probability, it is determined numerically with the help of the Markov Chain Monte Carlo (MCMC) implementation of the Bayesian Analysis Tool (BAT) [66]. One and two-dimensional posterior distributions are obtained in turn by marginalization over the remaining parameters of interest. The best fit points are identified with the help of Minuit that is initialized with the point of the highest posterior found during the MCMC run.

2. Pull value

The deviation of a single measurement of an observable O_i from its prediction $O_i^{\text{th}} \pm \Delta_i^\pm$ for a particular value of the parameters of interest $\boldsymbol{\theta}_*$ will be given in terms of the pull-value, accounting for theoretical uncertainties. Here, we define the pull value, δ , as the integral over those regions of the pdf $[O_i]$, which have higher

probability as the maximal probability value p^{\max} appearing in the interval spanned by the theory prediction $[O_i^{\text{th}} - \Delta_i^-, O_i^{\text{th}} + \Delta_i^+]$ evaluated at θ_* and varying the nuisance parameters, i.e.,

$$\delta = \int_{-\infty}^{+\infty} dO_i p(O_i) \theta[p(O_i) - p^{\max}] \quad (\text{B9})$$

where $\theta(x)$ denotes the step function. Consequently, the pull value is zero if the maximum of the pdf is inside this theory interval. In the case of a normally distributed pdf (with $\sigma_i^+ = \sigma_i^-$), a non-zero pull implies a symmetric integration interval around the central value O_i^{exp} of the distribution and the integrated fraction of probability can be converted into the distance between the lower or upper boundary of the theory uncertainty interval to O_i^{exp} in terms of its standard deviation σ_i depending on whether the theory prediction is above or below O_i^{exp} . In the case of non-gaussian pdf's, the pull value gives a measure of the probability fraction that corresponds to those values of O_i that have higher experimental probability than the ones contained in the interval of the theory prediction⁴. The pull value is simply calculated by drawing values for O_i that are distributed according to the pdf $[O_i]$ and taking the ratio of the cases in which $p(O_i) > p^{\max}$ and the total number of draws.

3. p Value

As a measure of the goodness of fit, we will use p values in order to compare within the same theoretical model at some point θ_* – usually the best fit point(s) – the quality of the fit for different sets of data Set I and Set II. For this purpose we will assume the model with the specific choice θ_* , allowing us to produce frequencies of possible outcomes within the model. We will use two ways to calculate p values.

The common definition is used as a first possibility, assuming the validity of normal and all independent pdf's. It consists in the evaluation of the cumulative of the χ^2 -distribution – the latter denoted by $f(x, N_{\text{dof}})$, with N_{dof} number of degrees of freedom – starting from the value $\chi_*^2 = -2 \log \mathcal{L}(\theta_*)$

$$p = \int_{\chi_*^2}^{\infty} dx f(x, N_{\text{dof}}), \quad (\text{B10})$$

and corresponds to the probability of observing a test statistic at least as extreme in a χ^2 distribution with N_{dof} . Values of $p < 5\%$ are usually referred to as “statistical significant” deviation from the null hypothesis, i.e., the validity of the model with parameters θ_* . As usual, the number of degrees of freedom is given as $N_{\text{dof}} = (N_{\text{meas}} - \dim(\theta))$, with N_{meas} denoting the number of measurements.

As a second possibility we calculate the p value defining a test statistics based on the likelihood [80]. The according frequency distribution is determined from 10^6 pseudo experiments in the lack of raw data and experimental efficiency corrections that require dedicated detector simulations. For this purpose, the pdf of each observable O_i is shifted such that the position of its maximum at $O_i = O_i^{\text{exp}}$ coincides with the prediction $O_i^{\text{th}}(\theta_*)$ at the point θ_* of interest. In this way, the uncertainties of the measurement with central value O_i^{exp} are adopted for $O_i^{\text{th}}(\theta_*)$, neglecting possibly different experimental efficiency corrections. In each pseudo experiment, possible experimental outcomes are drawn for all measurements in the data set from the shifted pdf's and the likelihood value is compared to that of the observed data set, determining this way the fraction of pseudo experiments with smaller likelihood values. The p value is identified with this fraction, however for the number of degrees of freedom that corresponds to the number of measurements N_{meas} in the data set. Subsequently, we correct the p value by converting it to a χ^2 value with the help of the inverse cumulative distribution with N_{meas} degrees of freedom and recalculate it for the actual N_{dof} [81] using (B10).

4. Probability distributions of observables

If certain observables are not yet measured or despite an existing measurement are not included in the data set D of the fit, one might obtain a prediction of its probability distribution given the data D and model M [80]. We calculate the considered observables at each point of the Markov Chain for the current value of θ and determine the interval of the theory uncertainty $[O_i^{\text{th}} - \Delta_i^-, O_i^{\text{th}} + \Delta_i^+]$ due to nuisance parameters as described in App. B1. The obtained intervals are used to fill a histogram that is normalized eventually to obtain a probability distribution.

⁴ For very non-gaussian pdf's with several disconnected regions of probability, the pull value might give rise to misleading interpretations, however, all measurements at hand are gaussian or gaussian ratio distributed.

-
- [1] M. Beneke, G. Buchalla, M. Neubert, and C. T. Sachrajda, Phys.Rev.Lett. **83**, 1914 (1999), arXiv:hep-ph/9905312 [hep-ph].
 - [2] M. Beneke, G. Buchalla, M. Neubert, and C. T. Sachrajda, Nucl.Phys. **B591**, 313 (2000), arXiv:hep-ph/0006124 [hep-ph].
 - [3] M. Beneke, G. Buchalla, M. Neubert, and C. T. Sachrajda, Nucl.Phys. **B606**, 245 (2001), arXiv:hep-ph/0104110

- [hep-ph].
- [4] M. Beneke and M. Neubert, Nucl.Phys. **B651**, 225 (2003), arXiv:hep-ph/0210085 [hep-ph].
 - [5] M. Beneke and M. Neubert, Nucl.Phys. **B675**, 333 (2003), arXiv:hep-ph/0308039 [hep-ph].
 - [6] M. Beneke, G. Buchalla, M. Neubert, and C. Sachrajda, Phys.Rev. **D72**, 098501 (2005), arXiv:hep-ph/0411171 [hep-ph].
 - [7] J. Chay and C. Kim, Nucl.Phys. **B680**, 302 (2004), arXiv:hep-ph/0301262 [hep-ph].
 - [8] C. W. Bauer, D. Pirjol, I. Z. Rothstein, and I. W. Stewart, Phys.Rev. **D70**, 054015 (2004), arXiv:hep-ph/0401188 [hep-ph].
 - [9] C. W. Bauer, I. Z. Rothstein, and I. W. Stewart, Phys.Rev. **D74**, 034010 (2006), arXiv:hep-ph/0510241 [hep-ph].
 - [10] A. R. Williamson and J. Zupan, Phys.Rev. **D74**, 014003 (2006), arXiv:hep-ph/0601214 [hep-ph].
 - [11] Y.-Y. Keum, H.-n. Li, and A. Sanda, Phys.Lett. **B504**, 6 (2001), arXiv:hep-ph/0004004 [hep-ph].
 - [12] Y. Keum, H.-N. Li, and A. Sanda, Phys.Rev. **D63**, 054008 (2001), arXiv:hep-ph/0004173 [hep-ph].
 - [13] C.-D. Lu, K. Ukai, and M.-Z. Yang, Phys.Rev. **D63**, 074009 (2001), arXiv:hep-ph/0004213 [hep-ph].
 - [14] A. Ali, G. Kramer, Y. Li, C.-D. Lu, Y.-L. Shen, *et al.*, Phys.Rev. **D76**, 074018 (2007), arXiv:hep-ph/0703162 [hep-ph].
 - [15] L. Hofer, D. Scherer, and L. Vernazza, JHEP **1102**, 080 (2011), arXiv:1011.6319 [hep-ph].
 - [16] K. De Bruyn, R. Fleischer, R. Knegjens, P. Koppenburg, M. Merk, *et al.*, Phys.Rev. **D86**, 014027 (2012), arXiv:1204.1735 [hep-ph].
 - [17] R. Fleischer and R. Knegjens, Eur.Phys.J. **C71**, 1532 (2011), arXiv:1011.1096 [hep-ph].
 - [18] A. Lenz and U. Nierste, arXiv:1102.4274 [hep-ph].
 - [19] Y. Amhis *et al.* (Heavy Flavor Averaging Group), arXiv:1207.1158 [hep-ex].
 - [20] R. Aaij *et al.* (LHCb collaboration), JHEP **1404**, 114 (2014), arXiv:1402.2554 [hep-ex].
 - [21] C. Bobeth, U. Haisch, A. Lenz, B. Pecjak, and G. Tetlalmatzi-Xolocotzi, JHEP **1406**, 040 (2014), arXiv:1404.2531 [hep-ph].
 - [22] J. Korner and G. R. Goldstein, Phys.Lett. **B89**, 105 (1979).
 - [23] M. Beneke, J. Rohrer, and D. Yang, Nucl.Phys. **B774**, 64 (2007), arXiv:hep-ph/0612290 [hep-ph].
 - [24] R. Aaij *et al.* (LHCb), JHEP **1310**, 183 (2013), arXiv:1308.1428 [hep-ex].
 - [25] K. Chen *et al.* (Belle Collaboration), Phys.Rev.Lett. **91**, 201801 (2003), arXiv:hep-ex/0307014 [hep-ex].
 - [26] D. Acosta *et al.* (CDF Collaboration), Phys.Rev.Lett. **95**, 031801 (2005), arXiv:hep-ex/0502044 [hep-ex].
 - [27] J. Lees *et al.* (BaBar Collaboration), Phys.Rev. **D85**, 112010 (2012), arXiv:1201.5897 [hep-ex].
 - [28] R. Aaij *et al.* (LHCb collaboration), Phys.Lett. **B728**, 85 (2014), arXiv:1309.3742 [hep-ex].
 - [29] V. Chobanova *et al.* (Belle Collaboration), Phys.Rev. **D90**, 012002 (2014), arXiv:1311.6666 [hep-ex].
 - [30] B. Aubert *et al.* (BaBar Collaboration), Phys.Rev. **D76**, 031103 (2007), arXiv:0706.3893 [hep-ex].
 - [31] R. Fleischer and T. Mannel, Phys.Rev. **D57**, 2752 (1998), arXiv:hep-ph/9704423 [hep-ph].
 - [32] E. Lunghi and A. Soni, JHEP **0709**, 053 (2007), arXiv:0707.0212 [hep-ph].
 - [33] M. Beneke, Phys.Lett. **B620**, 143 (2005), arXiv:hep-ph/0505075 [hep-ph].
 - [34] G. Buchalla, G. Hiller, Y. Nir, and G. Raz, JHEP **0509**, 074 (2005), arXiv:hep-ph/0503151 [hep-ph].
 - [35] Y. Nir, arXiv:hep-ph/0510413 [hep-ph].
 - [36] B. Aubert *et al.* (BaBar Collaboration), Phys.Rev. **D78**, 092008 (2008), arXiv:0808.3586 [hep-ex].
 - [37] M. Prim *et al.* (Belle Collaboration), Phys.Rev. **D88**, 072004 (2013), arXiv:1308.1830 [hep-ex].
 - [38] R. Aaij *et al.* (LHCb collaboration), JHEP **1405**, 069 (2014), arXiv:1403.2888 [hep-ex].
 - [39] R. Aaij *et al.* (LHCb Collaboration), Phys.Lett. **B709**, 50 (2012), arXiv:1111.4183 [hep-ex].
 - [40] T. Abe (Belle II Collaboration), arXiv:1011.0352 [physics.ins-det].
 - [41] B. Meadows, M. Blanke, A. Stocchi, A. Drutskoy, A. Cervelli, *et al.*, arXiv:1109.5028 [hep-ex].
 - [42] R. Aaij *et al.* (LHCb Collaboration), Eur.Phys.J. **C73**, 2373 (2013), arXiv:1208.3355 [hep-ex].
 - [43] M. Beneke, T. Feldmann, and D. Seidel, Eur.Phys.J. **C41**, 173 (2005), arXiv:hep-ph/0412400 [hep-ph].
 - [44] G. Bell, Nucl.Phys. **B795**, 1 (2008), arXiv:0705.3127 [hep-ph].
 - [45] G. Bell, Nucl.Phys. **B822**, 172 (2009), arXiv:0902.1915 [hep-ph].
 - [46] M. Beneke, T. Huber, and X.-Q. Li, Nucl.Phys. **B832**, 109 (2010), arXiv:0911.3655 [hep-ph].
 - [47] M. Beneke and S. Jäger, Nucl.Phys. **B751**, 160 (2006), arXiv:hep-ph/0512351 [hep-ph].
 - [48] N. Kivel, JHEP **0705**, 019 (2007), arXiv:hep-ph/0608291 [hep-ph].
 - [49] V. Pilipp, Nucl.Phys. **B794**, 154 (2008), arXiv:0709.3214 [hep-ph].
 - [50] G. Bell and V. Pilipp, Phys.Rev. **D80**, 054024 (2009), arXiv:0907.1016 [hep-ph].
 - [51] M. Bartsch, G. Buchalla, and C. Kraus, arXiv:0810.0249 [hep-ph].
 - [52] A. Khodjamirian, T. Mannel, M. Melcher, and B. Melic, Phys.Rev. **D72**, 094012 (2005), arXiv:hep-ph/0509049 [hep-ph].
 - [53] Q. Chang, X.-W. Cui, L. Han, and Y.-D. Yang, Phys.Rev. **D86**, 054016 (2012), arXiv:1205.4325 [hep-ph].
 - [54] L. Hofer and L. Vernazza, arXiv:1212.4785 [hep-ph].
 - [55] H.-Y. Cheng and C.-K. Chua, Phys.Rev. **D80**, 074031 (2009), arXiv:0908.3506 [hep-ph].
 - [56] Q. Chang, J. Sun, Y. Yang, and X. Li, (2014), arXiv:1409.1322 [hep-ph].
 - [57] B. Aubert *et al.* (BaBar Collaboration), Phys.Rev. **D79**, 052003 (2009), arXiv:0809.1174 [hep-ex].
 - [58] K. Wang and G. Zhu, Phys.Rev. **D88**, 014043 (2013), arXiv:1304.7438 [hep-ph].
 - [59] H. J. Lipkin, Phys.Lett. **B621**, 126 (2005), arXiv:hep-ph/0503022 [hep-ph].
 - [60] T. A. Aaltonen *et al.* (CDF Collaboration), arXiv:1403.5586 [hep-ex].
 - [61] R. Aaij *et al.* (LHCb collaboration), Phys.Rev.Lett. **110**, 221601 (2013), arXiv:1304.6173 [hep-ex].
 - [62] A. L. Kagan, arXiv:hep-ph/0407076 [hep-ph].
 - [63] A. J. Buras, R. Fleischer, S. Recksiegel, and F. Schwab, Phys.Rev.Lett. **92**, 101804 (2004), arXiv:hep-ph/0312259 [hep-ph].
 - [64] A. J. Buras, R. Fleischer, S. Recksiegel, and F. Schwab, Nucl.Phys. **B697**, 133 (2004), arXiv:hep-ph/0402112

- [hep-ph].
- [65] S. Vickers, TU Munich, PhD thesis (2014).
 - [66] A. Caldwell, D. Kollar, and K. Kroninger, *Comput.Phys.Comm.* **180**, 2197 (2009), arXiv:0808.2552 [physics.data-an].
 - [67] M. Bona *et al.* (UTFit Collaboration), Fit results from Summer 2013 available from <http://www.utfit.org>.
 - [68] J. Beringer *et al.* (Particle Data Group), *Phys. Rev.* **D86**, 010001 and 2013 partial update for the 2014 edition (2012).
 - [69] S. Bethke, *Eur.Phys.J.* **C64**, 689 (2009), arXiv:0908.1135 [hep-ph].
 - [70] T. Aaltonen *et al.* (CDF Collaboration, D0 Collaboration), *Phys.Rev.* **D86**, 092003 (2012), arXiv:1207.1069 [hep-ex].
 - [71] M. Beneke and S. Jäger, *Nucl.Phys.* **B768**, 51 (2007), arXiv:hep-ph/0610322 [hep-ph].
 - [72] P. Ball and R. Zwicky, *Phys.Rev.* **D71**, 014015 (2005), arXiv:hep-ph/0406232 [hep-ph].
 - [73] A. Bharucha, *JHEP* **1205**, 092 (2012), arXiv:1203.1359 [hep-ph].
 - [74] G. Duplancic and B. Melic, *Phys.Rev.* **D78**, 054015 (2008), arXiv:0805.4170 [hep-ph].
 - [75] P. Ball, V. Braun, and A. Lenz, *JHEP* **0605**, 004 (2006), arXiv:hep-ph/0603063 [hep-ph].
 - [76] P. Ball, G. W. Jones, and R. Zwicky, *Phys.Rev.* **D75**, 054004 (2007), arXiv:hep-ph/0612081 [hep-ph].
 - [77] P. Ball and R. Zwicky, *Phys.Rev.* **D71**, 014029 (2005), arXiv:hep-ph/0412079 [hep-ph].
 - [78] P. Ball, V. Braun, and A. Lenz, *JHEP* **0708**, 090 (2007), arXiv:0707.1201 [hep-ph].
 - [79] D. V. Hinkley, *Biometrika* **56**, 635 (1969).
 - [80] F. Beaujean, C. Bobeth, D. van Dyk, and C. Wacker, *JHEP* **1208**, 030 (2012), arXiv:1205.1838 [hep-ph].
 - [81] F. Beaujean, A. Caldwell, D. Kollar, and K. Kroninger, *Phys.Rev.* **D83**, 012004 (2011), arXiv:1011.1674 [physics.data-an].